

A PERFORMANCE EVALUATION OF VORTEX-INDUCED VIBRATION
SUPPRESSION DEVICES FOR MARINE APPLICATIONS

by

Junghan Lee

B.S., Seoul National University, 1980

Submitted to the Department of Ocean
Engineering in partial fulfillment of
the requirements for the degree of

OCEAN ENGINEER

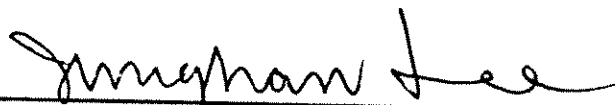
at the

MASSACHUSETTS INSTITUTE OF TECHNOLOGY

May 1987

Copyright (c) 1987 Massachusetts Institute of Technology

Signature of Author



Department of Ocean Engineering
May, 1987

Certified by



Professor J. K. Vandiver
Thesis Supervisor

Accepted by

A. D. Carmichael
Chairman, Departmental Committee on Graduate Students

A PERFORMANCE EVALUATION OF VORTEX-INDUCED VIBRATION
SUPPRESSION DEVICES FOR MARINE APPLICATIONS

by

Junghan Lee

Submitted to the Department of Ocean Engineering
on May , 1987 in partial fulfillment of the
requirements for the degree of Ocean Engineer.

Abstract

Experiments on vortex-induced vibration suppression devices were carried out at a canal of the Merrimack river in Lawrence, Massachusetts. Helical wire type and flag type suppression devices were attached to a cable 57.25 feet in length and 1.125 inches in diameter. The effectiveness of the suppression devices was measured in uniform and sheared flow, as well as under different tension. Vortex-induced vibration mechanisms of the related suppression devices were also studied.

Thesis Supervisor: J. K. Vandiver

Title: Professor of Ocean Engineering

Acknowledgements

I would like to express my special thanks to my advisor Prof. J. K. Vandiver for his kind encouragements, advise, and technical expertise. I am also thankful to Dr. T. Y. Chung for his patient explanations and advise in many ways. The experiment in Lawrence, with Prof. Vandiver and Dr. Chung was a very precious experience to me. Through the experiment, I, who lacked both in experience and theoretical background, learned the physical concepts of the vibration problem and the experiment itself. Also, I appreciate Daewoo Shipbuilding Co. Ltd. for the financial support during my study in M.I.T.. Lastly, I am thankful to my friends, Shyu, John, Bob, Takashi, and Wally. They all have made my life here less tiring and less difficult.

Table of Contents

Abstract	2
Acknowledgements	3
Table of Contents	4
List of Figures	6
List of Tables	8
1. Introduction	9
2. Mechanism of Suppression Devices	11
2.1 Vortex shedding mechanism	11
2.1.1 Basic model	11
2.1.2 Structural(system) properties	15
2.1.3 Exciting forces	17
2.1.4 Response	22
2.2 Vortex shedding suppression mechanisms	25
2.2.1 Structural means	26
2.2.2 Hydrodynamic means	26
2.2.3 Classification of suppression devices	26
2.2.4 Helical wire suppression devices	27
2.2.5 Flag suppression devices	28
2.2.6 Stability	33
3. Experiment on Suppression Devices	36
3.1 Purposes of experiment	36
3.2 Description of the experiment	37
3.2.1 Experiment site	37
3.2.2 Experimental setting	37
3.2.3 Experiment procedures	43
3.2.4 Suppression devices	43
3.3 Data processing	49
3.3.1 Flow profile, reference velocity, and tension	49
3.3.2 Selection of acceleration data	53
3.3.3 Time series signal	53
3.3.4 Spectra	55

3.3.5 Rms values	55
3.4 Performance comparison	56
3.4.1 Experiment conditions	56
3.4.2 Acceleration comparison	60
3.4.3 Displacement comparison	60
3.4.4 Velocity comparison	67
3.5 Findings and discussion	67
3.5.1 Helical wire type devices	67
3.5.2 Plain flag type devices	74
3.5.3 Split flag type devices	77
4. Summary and Conclusions	81
References	83
Appendix	86

List of Figures

Fig. 2.1	Model of a circular cylinder subjected to vortex-induced vibration	12
Fig. 2.2	Response model of harmonic exciting force in a flexible cylinder with pin-end joints	14
Fig. 2.3	Transfer function of a cable at $x=0.1L$ excited at $x=L/3$ ($T=1$, $m=1/400$, $c=2\pi/400$, and $L=1$) (after (8))	16
Fig. 2.4	Vortex formation and shedding cycle from a cylinder (after (12))	19
Fig. 2.5	Feedback mechanism of vortex-induced vibration	23
Fig. 2.6	Effectiveness of helical wires(after (28)) (a) Effect of number of starts (b) Effect of wire size (c) Effect of pitch	29
Fig. 2.7	Effectiveness of splitter plates(after (20)) (a) C_p comparison (b) C_d vs. Reynolds number (c) Strouhal number vs. splitter length	31
Fig. 2.8	(a) Vibration of pile during flag unfurling(after (5)) (b) Streamlined fairing(after (2))	32
Fig. 2.9	Stability condition of vortex-induced vibration	34
Fig. 3.1	Test site (Lawrence, Massachusetts)	38
Fig. 3.2	Test site arrangement	39
Fig. 3.3	Test cable	40
Fig. 3.4	Uniform and sheared flow profiles	41
Fig. 3.5	Test cable supporting system	42
Fig. 3.6	Tension adjusting system	44
Fig. 3.7	Experiment equipment hook-up diagram	45
Fig. 3.8	Sketches of suppression devices	47
Fig. 3.9	Turbulence level of flow velocity profile	50
Fig. 3.10	Typical flow direction and velocity data in sheared flow	51
Fig. 3.11	Spectrum of flow velocity signal shown in Fig. 3.10	52

Fig. 3.12	Time series cross-flow acceleration signals at L/4 (SL) : Sheared flow Low tension	54
Fig. 3.13	Cross-flow acceleration spectrum at L/4 (UL0) :Bare cable, ref. vel. 1.59 ft/sec, Uniform Low tension	61
Fig. 3.14	Cross-flow acceleration spectrum at L/4 (UL2) :Triple helical, ref. vel. 1.62 ft/sec, Uniform Low tension	62
Fig. 3.15	Cross-flow acceleration spectrum at L/4 (SL0) :Bare cable, ref. vel. 2.51 ft/sec, Sheared Low tension	63
Fig. 3.16	Cross-flow acceleration spectrum at L/4 (SL2) :Triple helical, ref. vel. 2.50 ft/sec, Sheared Low tension	64
Fig. 3.17	Cross-flow acceleration spectrum at L/4 (SH0) :Bare cable, ref. vel. 2.57 ft/sec, Sheared High tension	65
Fig. 3.18	Cross-flow acceleration spectrum at L/4 (SH2) :Triple helical, ref. vel. 2.82 ft/sec, Sheared High tension	66
Fig. 3.19	Displacement trajectories at L/4 (UL) (a) Bare cable, ref. vel. 1.59 ft/sec, Uniform Low tension (b) Triple helical, ref. vel. 1.62 ft/sec, Uniform Low tension	68
Fig. 3.20	Displacement trajectories at L/4 (SL) (a) Bare cable, ref. vel. 2.51 ft/sec, Sheared Low tension (b) Triple helical, ref. vel. 2.50 ft/sec, Sheared Low tension	69
Fig. 3.21	Cross-flow acceleration spectrum at 13L/16 (SL0) :Bare cable, ref. vel. 2.51 ft/sec, Sheared Low tension	72
Fig. 3.22	Cross-flow acceleration spectrum at 13L/16 (SL2) :Triple helical, ref. vel. 2.50 ft/sec, Sheared Low tension	73
Fig. 3.23	Cross-flow acceleration spectrum at L/4 (SL3) :Plain long flag, ref. vel. 3.22 ft/sec, Sheared Low tension	75
Fig. 3.24	Cross-flow acceleration spectrum at L/4 (SL4) :Split short flag, ref. vel. 3.16 ft/sec, Sheared Low tension	76
Fig. 3.25	Cross-flow acceleration spectrum at L/4 (SL6) :Split short flag, ref. vel. 3.34 ft/sec, Sheared Low tension	78
Fig. 3.26	Displacement trajectories at L/4 (UL5) :Split long flag, ref. vel 1.55 ft/sec, Uniform Low tension	80

List of Tables

Table 3.1	Description of suppression devices	46
Table 3.2	Cross-flow RMS value comparison	57
Table 3.3	Experiment conditions of Table 3.2	58

Chapter 1

Introduction

With the development of offshore technology, vortex-induced vibration has become an important consideration in the design and operation of mooring lines and ocean structures. Vortex-induced vibration can cause mechanical failure of ocean structures as well as create noise which deteriorates the signal transmission of instruments in underwater environments. Separate aspects of the mechanism, such as shedding frequency, drag and lift force, pressure distribution, hydrodynamic damping, resonance with the structure, and coherence of the vibration have been extensively studied. However, because of the complex interaction between structural properties and the fluid mechanisms, a satisfactory analytical model sufficient for engineering implementation is not currently available.

It is well known that vortex vibration can be suppressed by various structural and hydrodynamic means. Some of the suppression devices, which have been developed during wind-induced vibration studies, can be adopted to the vortex-induced vibration in marine field, with some reservations. Many of the scattered experimental results on suppression devices, which have been mainly obtained at the laboratory level, are useful for initial feasibility studies. However, for actual applications, it is prudent to implement the suppression device after an experimental confirmation to ensure successful performance.

Many of the governing variables for suppression devices are correlated; thus, the study of the vortex-induced vibration mechanism is essential for the understanding of the phenomenon, as well as for technical applications. Some of the

successful application examples on drill casings and mooring lines for instruments are found in (1 - 6).

This thesis evaluates the performance of helical wire and flag type suppression devices, and studies mechanisms of vortex-induced suppression devices in marine environments. In Chapter 2, the mechanisms of suppression devices, which were used for the experiments detailed in Chapter 3, are mainly covered. Other general types of suppression devices are also reviewed briefly. In Chapter 3, descriptions of the experiment and the performance evaluation of the suppression devices are made. Finally, summary and conclusions are drawn in Chapter 4.

Chapter 2

Mechanism of Suppression Devices

2.1 Vortex shedding mechanism

A detailed analysis of a vortex shedding mechanism is too complex to be treated as a whole; however, each of the governing factors may be modeled and explained separately. The study of the each variable is important for understanding the vibration response of the integrated system. In this section, a basic model of vortex-vibration mechanism is considered, and the effects of several variables are studied, based on the model.

2.1.1 Basic model

A cylindrical structure subjected to a vortex-induced vibration can be modeled as in Fig. 2.1. Assuming the angle (θ) with respect to the reference line is small, the vertical (y) direction and angular momentum equations are expressed as follows.

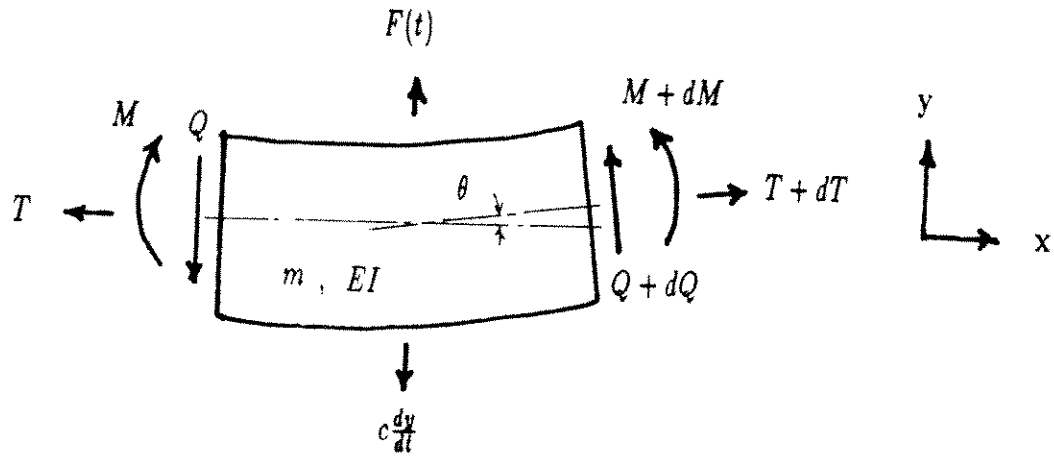
y direction momentum:

$$(m + m_a) \frac{\partial^2 y}{\partial t^2} = -c \frac{\partial y}{\partial t} + \frac{\partial Q}{\partial x} + \frac{\partial}{\partial x} \left(T \frac{\partial y}{\partial x} \right) + F_y(t) \quad (2.1)$$

angular momentum:

$$\frac{\partial}{\partial t} (I\omega) = \frac{\partial M}{\partial x} + Q \quad (2.2)$$

As the rotary inertia of the modeled cylinder is negligible, the right side



$$d\theta = \frac{\partial \theta}{\partial x} dx = \frac{\partial^2 y}{\partial x^2} dx$$

$$dT = \frac{\partial T}{\partial x} dx$$

$$dQ = \frac{\partial Q}{\partial x} dx$$

m : unit mass in air

m_a : added mass

c : damping coefficient

EI : bending stiffness

T : tension

Q : shear force

M : bending moment

Fig. 2.1 Model of a circular cylinder subjected to vortex-induced vibration

of eqn. 2.2 is reduced to zero. Therefore,

$$Q = -\frac{\partial M}{\partial x} \quad (2.3)$$

For a homogeneous material with constant tension, the general equation of a cylinder in a vortex-induced vibration is obtained by using a beam deflection formula(7) and eqn. 2.3, which is

$$-T \frac{\partial^2 y}{\partial x^2} + (m + m_a) \frac{\partial^2 y}{\partial t^2} + c \frac{\partial y}{\partial t} - EI \frac{\partial^4 y}{\partial x^4} = F_y(t) \quad (2.4)$$

When we think about the flexible cable, the bending rigidity term($EI \frac{\partial^4 y}{\partial x^4}$) reduces to zero, and the sum of unit mass(m) and added mass(m_a) is replaced with the equivalent unit mass(m_e). Then the equation is simplified as

$$-T \frac{\partial^2 y}{\partial x^2} + c \frac{\partial y}{\partial t} + m_e \frac{\partial^2 y}{\partial t^2} = F_y(t) \quad (2.5)$$

However, the response affects the external force, and the system is not linear. In order to understand the steady state system response, we first try a linearized model sketched in Fig. 2.2.

When the cable has simple pin-end connections, and a unit harmonic external force $f(t)$ is applied at location a , the response at x is assumed to be

$$y(x, a, \omega) = H(x, a, \omega) e^{i\omega t} \quad (2.6)$$

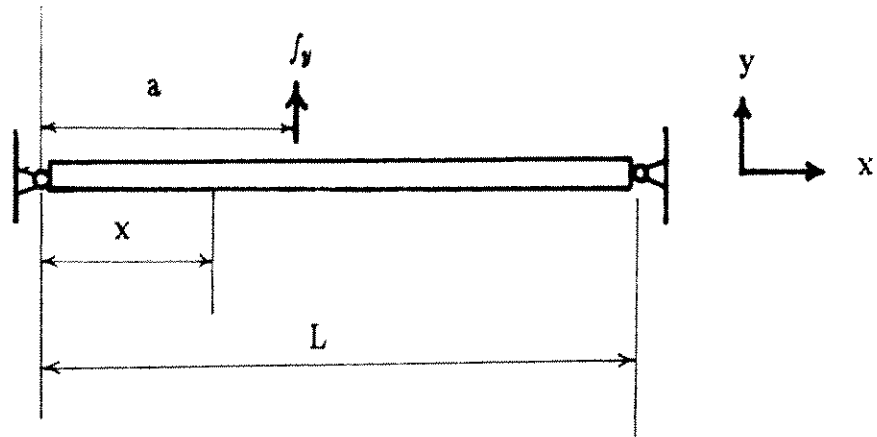
Applying eqn. 2.6 to eqn. 2.5, and from boundary conditions, we obtain(8)

$$H(x, a, \omega) = \frac{\sinh \lambda_1 (L - a)}{T \lambda_1 \sinh \lambda_1 L} \sinh \lambda_1 x \quad \text{for } 0 < x < a$$

$$H(x, a, \omega) = \frac{\sinh \lambda_1 a}{T \lambda_1 \sinh \lambda_1 L} \sinh \lambda_1 x (L - a) \quad \text{for } a < x < L \quad (2.7)$$

where

$$\lambda_1 = \left[\left(\frac{m_e \omega^2}{T} \right)^2 + \left(\frac{c\omega}{T} \right)^2 \right]^{\frac{1}{4}} \left(\sin \frac{\theta}{2} + i \cos \frac{\theta}{2} \right)$$



- L : length of a cylinder
- T : tension of a cylinder
- c : damping coefficient
- m_e : effective mass
- $f_y(a)$: exciting force at a
- $y(x)$: response at x

Fig. 2.2 Response model of harmonic exciting force in flexible cylinder with pin-end joints

and

$$\tan(\theta) = \frac{c}{m_e \omega}$$

The example of transfer function $H(0.1, \frac{1}{3}, \omega)$ in the case of $T = 1(\text{lb or } \frac{\text{slug} \times \text{ft}}{\text{sec}^2})$, $m_e = 1/400(\frac{\text{lb} \times \text{sec}^2}{\text{ft}} \text{ or } \text{slug}/\text{ft})$, $L = 1(\text{ft})$, and $c = \frac{2\pi}{40}(\frac{\text{lb} \times \text{sec}}{\text{ft}} \text{ or } \frac{\text{slug}}{\text{ft} \times \text{sec}})$ is shown in Fig. 2.3. From eqn. 2.7, the response spectrum at x ($S_y(x, \omega)$) subjected to exciting spectrum $S_f(a, \omega)$ is

$$S_y(x, \omega) = |H(x, a, \omega)|^2 S_f(a, \omega) \quad (2.8)$$

If the exciting force $F(t)$ is distributed along the cable, the response at x is

$$S_y(x, \omega) = \sum_{j=1}^n \sum_{k=1}^n H^*(x, a_j, \omega) H(x, a_k, \omega) S_f(a_j, a_k, \omega) \quad (2.9)$$

where

$H(x, a_j, \omega)$ = the response x to a unit harmonic exciting force at a_j

$S_f(a_j, a_k, \omega)$ = cross-spectral density between the exciting forces

$f(a_j, t)$ at a_j and $f(a_k, t)$ at a_k

n = number of exciting forces

In reality, the modeling and calculation of the exciting forces and cross-spectral density of eqn. 2.9 are very complicated; therefore, only qualitative behaviors of the variables related to the vortex-vibration mechanism are studied in the following sections.

2.1.2 Structural(system) properties

The system properties, such as tension, bending stiffness, mass, and damping constitute the vibration system, as simplified in eqn. 2.4. Each of the variables affects the system transfer function.

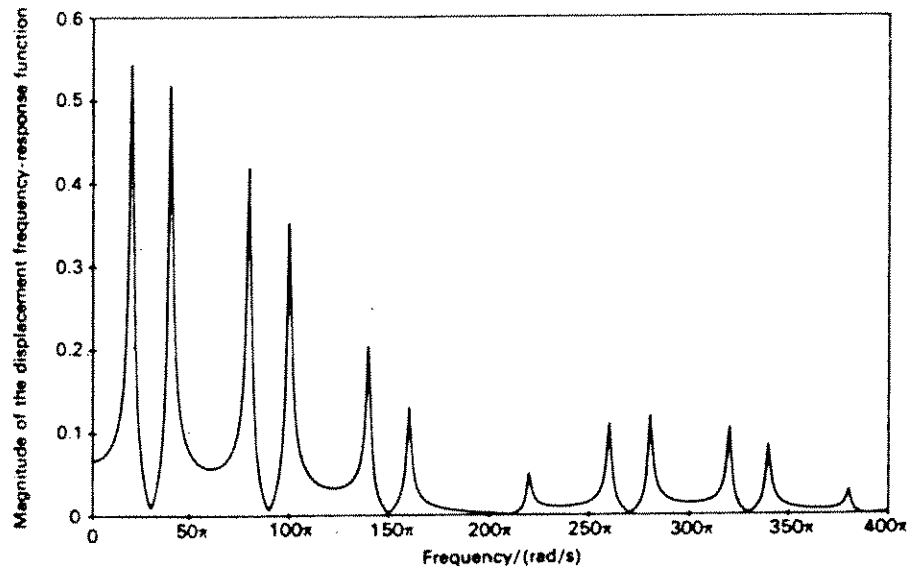


Fig. 2.3 Transfer function of a cable at $x=0.1L$ excited at $x=L/3$
 ($T=1$, $m=1/400$, $c=2\pi/400$, and $L=1$) (after (8))

- Tension(T), bending stiffness(EI), and effective mass(m_e)

The system frequency transfer function, which generally has peaks at its natural frequencies, greatly affects the magnitudes of response. When damping is neglected, the fundamental frequency(f_1) of a beam under tension in air with length l and hinged ends is

$$f_1 = \frac{1}{2L} \sqrt{\frac{\pi^2 EI}{L^2 m_e} + \frac{T}{m_e}} \quad (2.10)$$

Therefore, the tension and bending stiffness are important factors which increase the natural frequency of the structure, and effective(equivalent) mass per unit length(m_e) reduces it. The effective mass includes hydrodynamic added mass, which for simplicity is usually assumed to be constant. In reality, it may be a time dependent quantity. But it is assumed to be constant in this work. When a more complex model with variable geometry, nonhomogeneous material, and variable tension is considered, the response characteristics will be determined by the complicated wave dispersion relations.

- Damping(c)¹

At resonance, the inertia and stiffness terms cancel one another in the response function, and only the damping term becomes in dynamic equilibrium with the exciting forces. Therefore, small damping produces large responses. In flow-induced vibration prediction, the hydrodynamic contribution to the total damping is not only very important, but also difficult to estimate(9). The uncertainties related with the added mass and hydrodynamic damping make the response prediction difficult..

2.1.3 Exciting forces

¹ This viscous damping coefficient(c) is defined by force per velocity in unit length

- Vortex formation and shedding

An ideal flow around a cylinder does not separate, but with viscosity, the flow separates and results in pressure difference around the cylinder. Prantl(10) studied the vortex formation by taking a series of instantaneous streamline pictures, and postulated that "the vortex formation is accomplished by a spiral rolling up of free shear layers". Perry et al.(11) explained the vortex formation process by flow visualization methods: "During starting flow, the cavity behind the cylinder is closed. However, once the vortex shedding process begins, the 'closed' cavity becomes open, and an instantaneous 'alleyway' of fluid is formed which penetrates the cavity". Recently, Cantwell et al.(12) measured the flow velocity components in various phases by averaging many experimental results. Fig. 2.4 shows the vortex formation and shedding cycle suggested by Cantwell et al.(12). Some analytic studies provide us basic theoretical backgrounds for vortex formation. Reference (13) shows the wake instability behind a circular cylinder causes the vortex formation. Other studies on the vortex formation and shedding process are found in (14-16).

- Drag and lift forces

When a cylinder is placed in a flowing fluid, dynamic forces are created around the cylinder. The forces, which are caused by pressure differences, are composed of steady component drag force, and oscillating component drag and lift forces. In most cases, the cross-flow vibration due to the oscillating lift force is more significant than the in-line vibration.

The mean drag force(F_d) exposed to a constant flow velocity(V) is

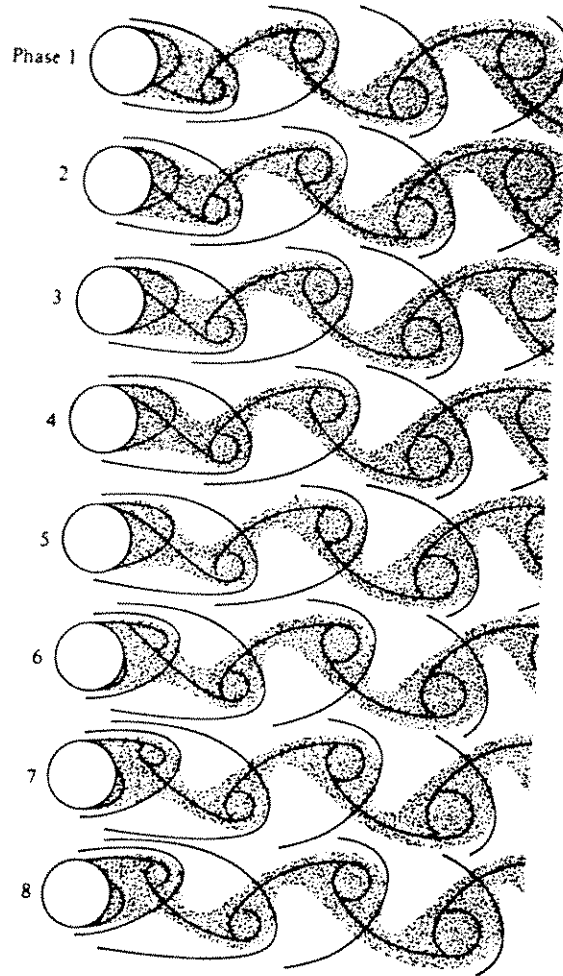


Fig. 2.4 Vortex formation and shedding cycle from a cylinder
(after (12))

calculated by the experimental formula

$$F_d = \frac{1}{2} C_d \rho S V^2 \quad (2.11)$$

where

C_d : drag coefficient

ρ : density of fluid

S : frontal area

The drag and lift coefficients are largely dependent upon geometry of structure, Reynolds number, turbulence level, and surface roughness. The study of the drag and lift forces for circular cylinders has been an important part of fluid mechanics. An bibliographical summary is found in (12).

When the cylinder is oscillating, the lift or drag coefficient may be expressed in a root mean square(RMS) form($(\overline{C_d^2})^{1/2}$). In that case, the coefficients (C_l, C_d) follow certain probability density functions(17)². Most measurements of drag and lift coefficients have been made on fixed cylinders. They may have different values when the cylinder is in motion. If a cylinder is oscillating, either in-line or cross-flow direction, the relative velocity of the cylinder is also alternating even in a constant flow condition. Therefore, it is obvious that the response output velocity affects the exciting force by changing the relative velocity and direction. In most studies, the in-line and cross-flow vibration are treated independently, but there could be interactions between the two modes. The cross-flow vibration affects the steady

² Experimental results reveal the probability density function generally follows the Gaussian distribution. Therefore, the lift and drag force are not simple harmonic functions with fixed amplitudes and frequencies.

component in-line drag force(18). The steady component of the in-line drag generally increases with the cross-flow vibration amplitude. It is generally known that the in-line vibration frequency is approximately twice that of cross-flow vibration. Nath's study(19) shows the roughness of cylinder due to marine accretion greatly affects the drag and lift coefficients.

The study of pressure distribution measurements around cylinders are useful not only for the determination of the drag or lift force, but also for the understanding of the vortex formation and shedding process. The related studies are found in (12, 20-22).

- Shedding frequency

The dominant vortex shedding frequency(f_s) is proportion to Strouhal number(S_t) and the flow velocity(V) divided by cylinder diameter(D).

$$f_s = S_t \frac{V}{D} \quad (2.12)$$

The shedding frequency is dependent on Reynolds number, geometry, and surface roughness but independent of material density. At Reynolds number up to approximately 3×10^5 , the shedding occurs in a narrow band range, but above this range(transition range), the vortex shedding becomes irregular. Strouhal numbers of noncircular sections are referenced to (23). The shedding frequency of an oscillating cylinder may have a different value from that of a stationary cylinder. When a cylinder is oscillating, the vortex shedding frequency tends to change from stationary cylinder shedding frequency to the cylinder vibration frequency, which sometimes results in lock-in.

From eqn. 2.11 and 2.12, the cross-flow exciting force at location x can be expressed as

$$f(x, t) = F_l(x) e^{i2\pi f_s t} \quad (2.13)$$

where f_s is shedding frequency, and $F_l(z)$ is magnitude of the lift force in eqn. 2.11.

The exciting forces expressed in eqn. 2.9 are correlated within a certain length, and the correlation of exciting forces is very important in the determination of the response.

2.1.4 Response

Once system properties and input forces are defined, the response is uniquely determined. However, the structural and hydrodynamic properties interact each other, and thus result in an integrated nonlinear feedback mechanism (Fig. 2.5).

The dimensionless amplitude of vortex-induced vibration can be expressed as a function of non-dimensionalized parameters,

$$\frac{y}{D} = F\left(\frac{L}{D}, \frac{VD}{\nu}, \frac{V}{f_n D}, \frac{m}{\rho D^2}, \zeta\right) \quad (2.14)$$

The above variables represent geometry, Reynolds number, reduced velocity, mass ratio, and damping coefficient respectively. In what follows, some of the important features of the vortex-induced vibration response are briefly reviewed.

- Lock-in

When a vortex shedding frequency coincides with one of the natural frequencies of a structure and the damping is not high, the response amplitude increases appreciably. In the neighborhood of the frequency, the shedding frequency does not follow the Strouhal relationship (eqn. 2.12), but follows the structural natural frequency. The typical relationship with shedding frequency and the flow velocity in lock-in mode is found in (24). It is known that the shedding frequency, caused by the flow velocity ranging 0.7 to 1.3

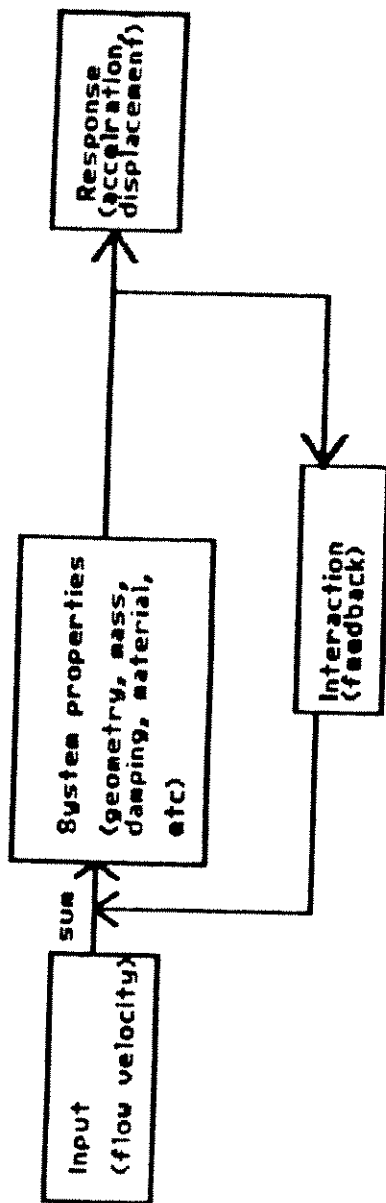


Fig. 2.5 Feedback mechanism of vortex-induced vibration

times that of the resonant velocity, is maintained at the resonant frequency, and the amplitude becomes fairly even with some low frequency modulation(24,25). In lock-in mode, the vortex formation region is shortened, and the correlation length is increased(26), which magnifies the response amplitude. The persistence of the frequency, which also increases the amplitude, could be explained by hysteresis effects. Zdravkovich(26) explained the hysteresis effects by using the existence of two modes of vortex shedding in the synchronization range. An extensive study of the lock-in mechanism is found in references (25,26).

- Coherence

Spanwise coherence of vortex shedding is important in the prediction of response. The coherence(or correlation) length varies with Reynolds number, length/diameter ratio, and surface roughness. Experimental results reveal that for Reynolds numbers between 1.1×10^4 and 4.5×10^4 , the coherence length is approximately 3 to 6 times of the cylinder diameter for stationary cylinders(18). For oscillating cylinders, the correlation length increases appreciably especially in the lock-in mode.

- Reduced velocity

The reduced velocity(V_r) in eq. 2.15 is the parameter to judge the possibility of lock-in,

$$V_r = \frac{V}{f_n D} \quad (2.15)$$

where

V : flow velocity

f_n : natural frequency

D : cylinder diameter

For a Strouhal number of 0.2, the reduced velocity in the lock-in mode becomes 5.

- Stability parameter

The stability parameter (K_s) defined by eq. 2.16 is one of the parameters that governs response amplitude,

$$K_s = \frac{2m_e\zeta}{\rho D^2} \quad (2.16)$$

where

m_e : equivalent unit mass

ζ : damping coefficient³

ρ : fluid density

D : cylinder diameter

The lower the stability parameter, the larger the response amplitude. With the same principle, by increasing the parameter, the vibration level may be reduced significantly. Studies on response amplitude versus the stability parameter are found in (18,24).

2.2 Vortex shedding suppression mechanisms

³ The damping coefficient is calculated from the logarithm decreament of the displacement amplitude in a vacuum.

As mentioned in section 2.1.1, the response amplitude of vortex-induced vibration is the result of the system properties and the input forces. Therefore, the response amplitude can be reduced by changing the system properties and/or by reducing the input forces. Extensive review papers in (27,28,24) are referenced for vortex vibration suppression mechanisms and applications.

2.2.1 Structural means

The variables studied in section 2.1.2 can be altered to reduce vibration. For example, by changing the frequency transfer function, the resonant vibration range may be avoided, and by increasing the damping or the stability parameter, the vibration level may be reduced. Some types of suppression devices use damping effects(24), but none are suitable for marine applications.

2.2.2 Hydrodynamic means

The reduction of lift forces naturally reduces the vortex-induced vibration response. The exciting forces may be reduced by adopting a hydrodynamic means of suppression. The suppression devices affect the separation point, the vortex formation, the width of wake, and the correlation of the vorticity along a cylinder. At the same time, they affect the geometry, unit mass, and damping of the structure subjected to a vortex-induced vibration.

2.2.3 Classification of suppression devices

The hydrodynamic means of suppression devices are grouped as follows:

(1) Surface protrusion(Boundary layer device)

These types of devices influence the generation of turbulence in the boundary layer which reduces the pressure difference. However, most surface

protrusion devices increase the in-line drag force. Typical examples of surface protrusion devices are helical wires, strakes, and vertical fins.

(2) Shroud

The increase of surface roughness generally reduces the vortex formation; however, the shroud type suppression devices are not so effective in marine environments. Examples of shroud are referenced to (24,27).

(3) Wake stabilizer

By stabilizing rear wakes, the exciting force is reduced significantly. Splitter plates, guiding plates, guiding vane, fringes, hair fairing, and ribbon are examples.

The first two types of the suppression device (surface protrusion, shroud) are classified as omni-directional, and the last (wake stabilizer), as uni-directional devices. But by adopting a weathervaning device, the wake stabilizer type can also be used for an omni-directional purpose.

The suppression devices tested and described in Chapter 3 are regarded as helical wire and flag types. Therefore, the mechanisms of these two suppression devices are studied here.

2.2.4 Helical wire suppression devices

The helical strake and helical wire are the most frequently used suppression devices in wind-induced vibration field. Sharp edged strakes are known to be more effective than round wires in vibration suppression. Edge vortices generated behind the helical wires suppress the separation of the boundary layer and narrow the wake. The helix also discourages the correla-

tion of the vortex shedding along the cylinder by forcing the wake to become three dimensional.

The diameter of the helical wire(h) to cylinder diameter(D), pitch ratio, and number of starts are important parameters in helical wire type devices. Commonly used types of the helical wires are $\frac{h}{D}$, 0.1, pitch, 8-16 D , and three starts(27). Substantial deviation from these suggested values may cause large vibration amplitude, sometimes exceeding that found for the plain cylinder(27). Weaver(28) carried out extensive experiments to find the optimum number of starts, size, and pitch of helical wires. The results show that the diameter of the helical wire has equal effects as the size of helical strake. Fig. 2.6 shows the effects of helical wire size, pitch, and the number of starts in vibration suppression. The helical wire reduces the vibration amplitude; however it increases the in-line drag force. With the increase of turbulence, the suppression effect is reduced. Therefore, the turbulence level should also be considered in the estimation of vibration level. For marine applications, the helical wire has disadvantages in handling and marine accretion problems.

Application examples of helical strakes in offshore drill casing are found in (2,3). The results showed that a three start helical wire with a pitch of 5D and radial protrusion 0.1D($h/D=0.1$) for a 36 inch drill casing reduced the vibration to an almost negligible level(3).

2.2.5 Flag suppression devices

Flags prevent the interaction of alternating pressure on each side of the flag. The flags stabilize the rear wake and the re-attachment of the flow, and dissipate vibration energy. The experimental results of splitter plates

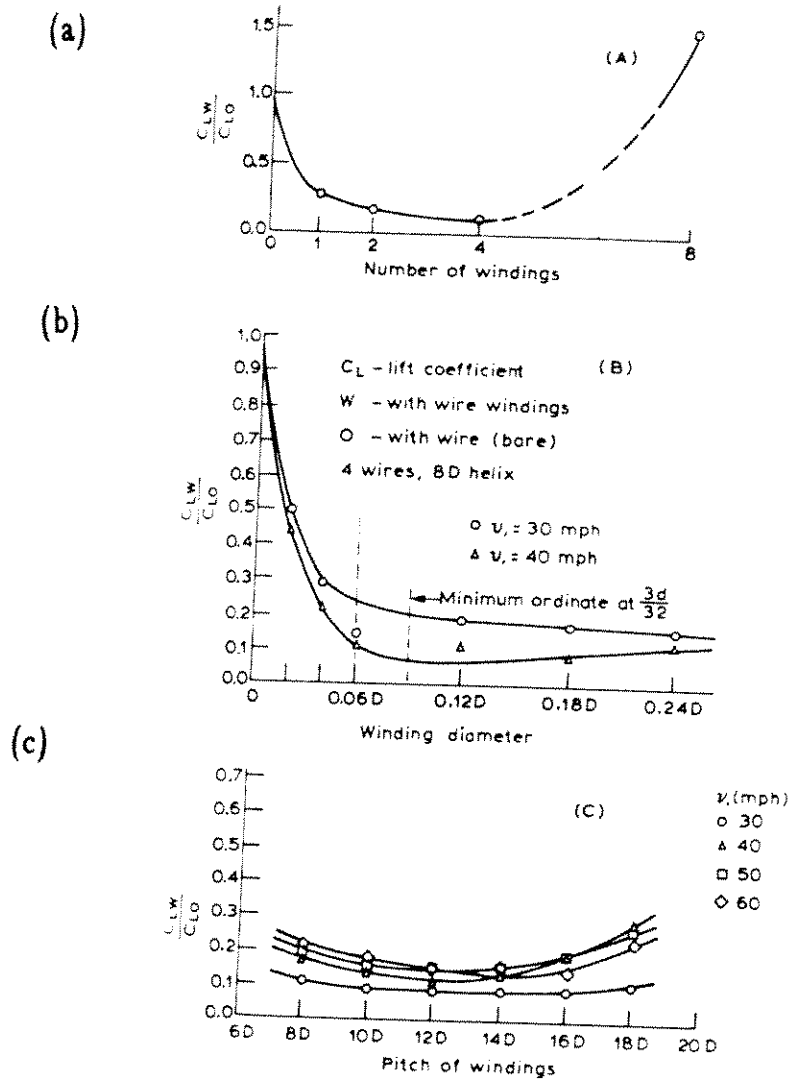


Fig. 2.6 Effectiveness of helical wires(after (28))
 (a) Effect of number of starts
 (b) Effect of wire size
 (c) Effect of pitch

are rather abundant, and most of the characteristics may be ascribed to the flag as it can be regarded as a flexible splitter plate. It is known that the appropriate length of the flag is 5-7 times that of the cylinder diameter. But the optimum trailing length of the flag for flexible cylinders is longer than for the rigid cylinder case. The stiffer flags are more effective in vibration suppression, but flexible flags have advantages in reducing lift force at some angles of attack. In mooring cable applications, the stiffness of flag is limited by handling problems. Gerald(30) and Apelt(20) show that a suitable length of splitter plate reduces the pressure difference as much as 50 percent. Fig. 2.7 (a) compares the pressure and wake distribution of cylinders with and without splitter plates. Reynolds number also influences the effectiveness of the splitter plate(Fig. 2.7 (b)). Fig. 2.7 (c) shows the effects on shedding frequencies of different splitter plate lengths. If the flow direction changes, the flag may wrap the cable and make the flag inoperative. Therefore, the flag type devices should only be used in uni-directional cases.

Generally, the flag type suppression devices increase the in-line drag force by the increasing wetted surface area. In order to reduce the drag force, hair type fairings are often used, but the effectiveness of vibration suppression is questionable. Ribbon type fairing may be used for mooring line applications. Commonly used ribbon type fairing are 4-6D trailing length, 1-2D width, and 1-2D apart. The ribbon type fairing device also increases the drag like flag type devices. Vandiver et al.(31) showed the drag coefficients of most of vibration suppression devices are higher than those of rigid cylinders. Some commercially available vibration suppression devices are found in (29). Fisher et al.(5) reported that the vibration of offshore piles during installation was reduced by using flag type suppression device. The results are illustrated in Fig. 2.8 (a).

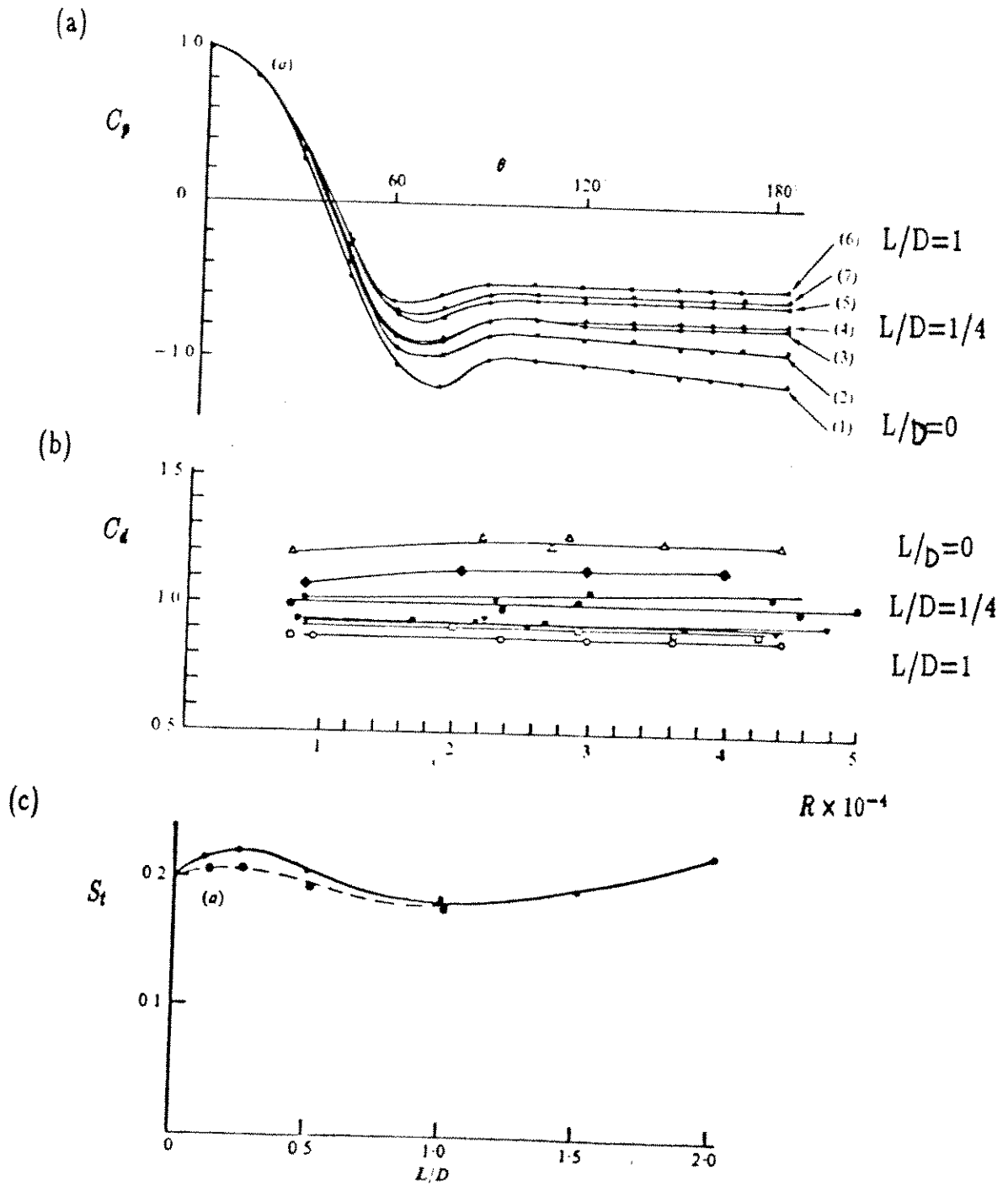


Fig. 2.7 Effectiveness of splitter plates(after (20))
 (a) C_p comparison
 (b) C_d vs. Reynolds number
 (c) Strouhal number vs. splitter length

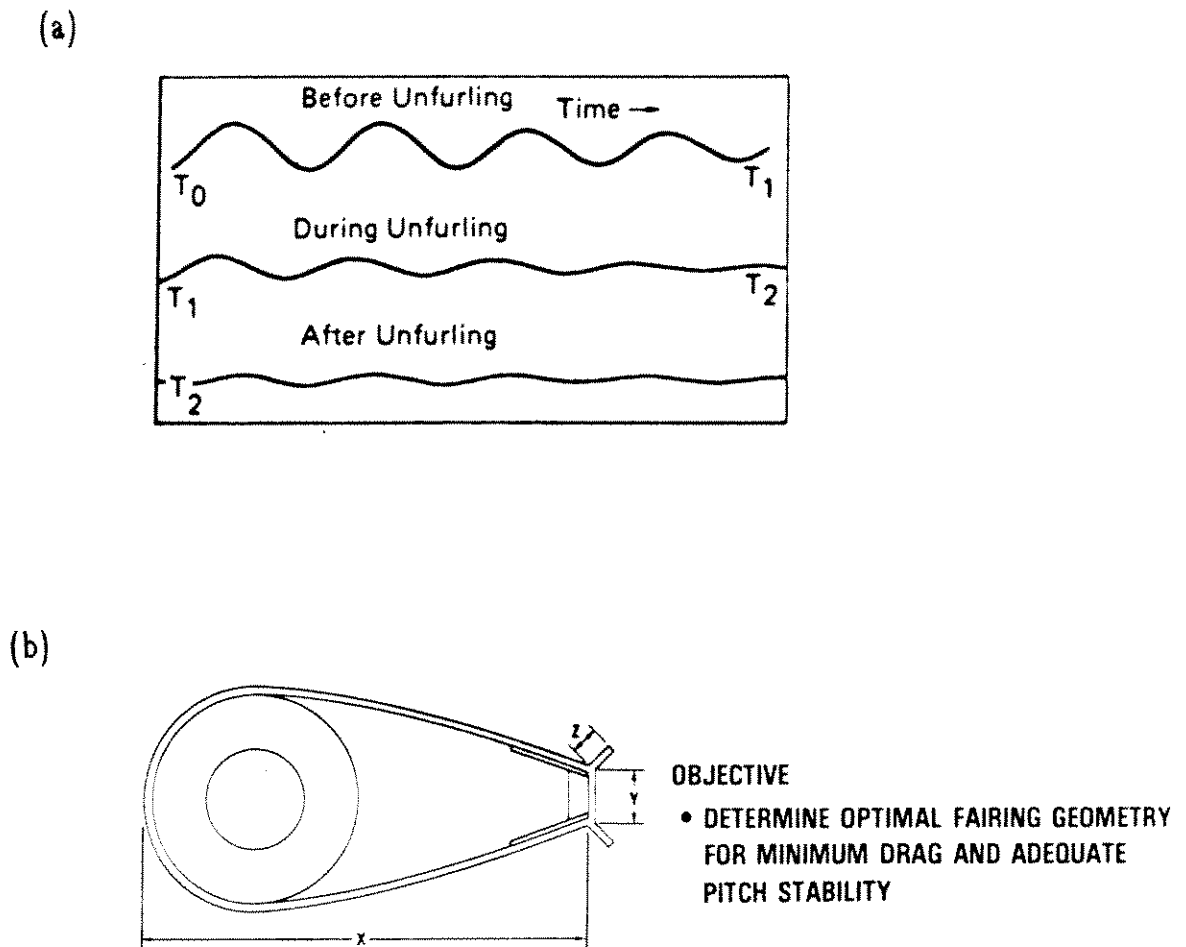


Fig. 2.8 (a) Vibration of pile during flag unfurling(after (5))
 (b) Streamlined fairing(after (2))

2.2.6 Stability

One of the other important considerations in vortex-induced vibration is the possibility of galloping due to the geometric instability. Most of the non-circular, wake stabilizer type, suppression devices are susceptible to this stability problem.

A simple model of stability condition is shown in Fig. 2.9. In Fig. 2.9, if flow comes with an angle of attack α^4 , the vertical direction force (F_y) is,

$$F_y(\alpha) = F_l(\alpha)\cos\alpha + F_d(\alpha)\sin\alpha \quad (2.17)$$

In order to be stable, the derivative of vertical force ($\frac{\partial F_y(\alpha)}{\partial \alpha}$) should be positive. For small angle α , the stability condition is,

$$\frac{\partial F_y(\alpha)}{\partial \alpha} = \frac{\partial F_l(\alpha)}{\partial \alpha} + F_d(\alpha) > 0 \quad (2.18)$$

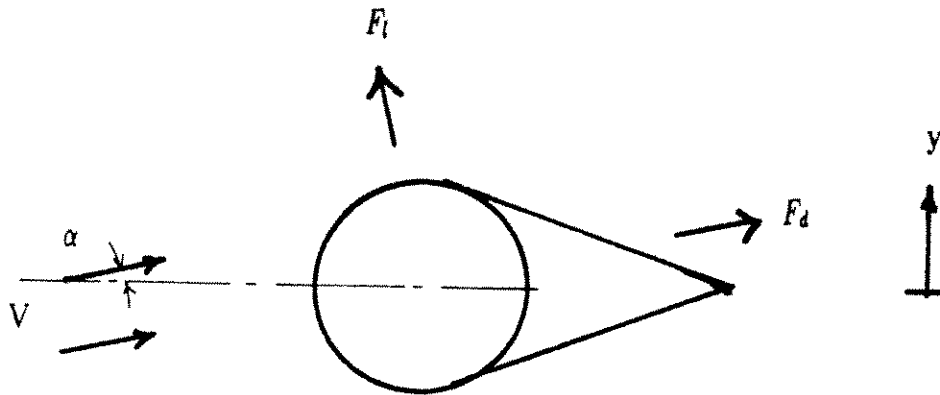
By using vertical force, lift and drag coefficients (C_y, C_l, C_d) in eqn. 2.11, the stability condition is rewritten as,

$$\frac{\partial C_y(\alpha)}{\partial \alpha} = \frac{\partial C_l(\alpha)}{\partial \alpha} + C_d(\alpha) > 0 \quad (2.19)$$

In eqn. 2.19, the lift coefficient ($C_l(\alpha)$) is function of geometry and Reynolds number of the structure as well as angle of attack α . The galloping phenomenon in flag type suppression devices is explained by the stability condition.

Reference (2) shows a typical stability problem in the design of a streamlined fairing device. Fig. 2.8 (b) shows the actual design parameters for the streamlined fairing. In that case, stable fin design was directly

⁴ If the structure is moving with a velocity y' , in zero angle of attack, the relative velocity becomes $((y')^2 + V^2)^{1/2}$ and the angle of attack becomes $\tan^{-1}(-\frac{y'}{V})$.



V : flow velocity

α : angle of attack

$F_l(\alpha)$: lift force at angle α

$F_d(\alpha)$: drag force at angle α

$F_y(\alpha)$: vertical force at angle α

$$(F_y(\alpha) = F_l(\alpha)\cos\alpha + F_d(\alpha)\sin\alpha)$$

stability condition : $\frac{\partial F_y(\alpha)}{\partial \alpha} > 0$

Fig. 2.9 Stability condition of vortex-induced vibration

related to the stability criteria. In most cases, the stability condition in eqn. 2.19 is found experimentally by varying the angle of attack. Another application example of a stability problem in a streamlined fairing is found in (4).

Chapter 3

Experiment on Suppression Devices

A series of experiments were carried out in the canal of the Merrimack river during the summer of 1986. The experiments on vibration suppression devices were the second part of the experiments, following experiments on vibration of flexible cylinders in sheared flows(32). Therefore, the bulk of the experimental settings used for this thesis are identical to those detailed in (32).

3.1 Purposes of experiment

Experiments on vibration suppression devices usually have been done in laboratories by changing only a few parameters. But in actual operations, there are many other unexpected uncertainties which are difficult to find in laboratory level experiments. Therefore, this experiment was prepared to study the vibration phenomenon and performance of various suppression devices in real field conditions. The purposes of this experiment were:

- To compare the vibration level of a bare cable and cables with suppression devices.
- To evaluate the performance of helical wire type and flag type suppression devices.
- To find performance characteristics of each suppression device in uniform and sheared flow cases, as well as under high and low tension cases.

3.2 Description of the experiment

3.2.1 Experiment site

The experiment site was located at the south canal of the Merrimack river in Lawrence, Massachusetts(Fig. 3.1¹). The width of the canal was 58 feet, and approximately 250 feet upstream of the test cable location, a gate house was located. The gate house had 4 gates, which controlled the flow of the canal(Fig. 3.2).

3.2.2 Experimental setting

- A 1.125 inch diameter, 57.25-foot long rubber cable was installed 1 foot below the canal surface. The test cable was connected to supporting frames, which carried the cable tension. (See Fig. 3.3.)
- By controlling the gates, uniform and sheared flow profiles could be made. Typical uniform and sheared flow profiles are found in Fig. 3.4.
- 6 pairs(vertical and horizontal components) of accelerometers² were imbedded inside the test cable. The locations of the accelerometers are specified with respect to the cable length from the north side of the canal(Fig. 3.5).
- A flow profile measuring device³ was located at 5 feet upstream of the test cable to record the flow velocities across the canal.
- A tension adjusting winch was connected to the end of 3 Kevlar cables, which were inserted inside the test cable to apply and carry the desired tension.(Fig.

¹ Fig. 3.1-3.3, 3.5, 3.6, and 3.9-3.11 were adopted from (32).

² Sundstrand Mini-pal model 2180 (1/2 inch diameter, and 1.5 inch long)

³ Neil Brown DRCM2 Acoustic Current Meter

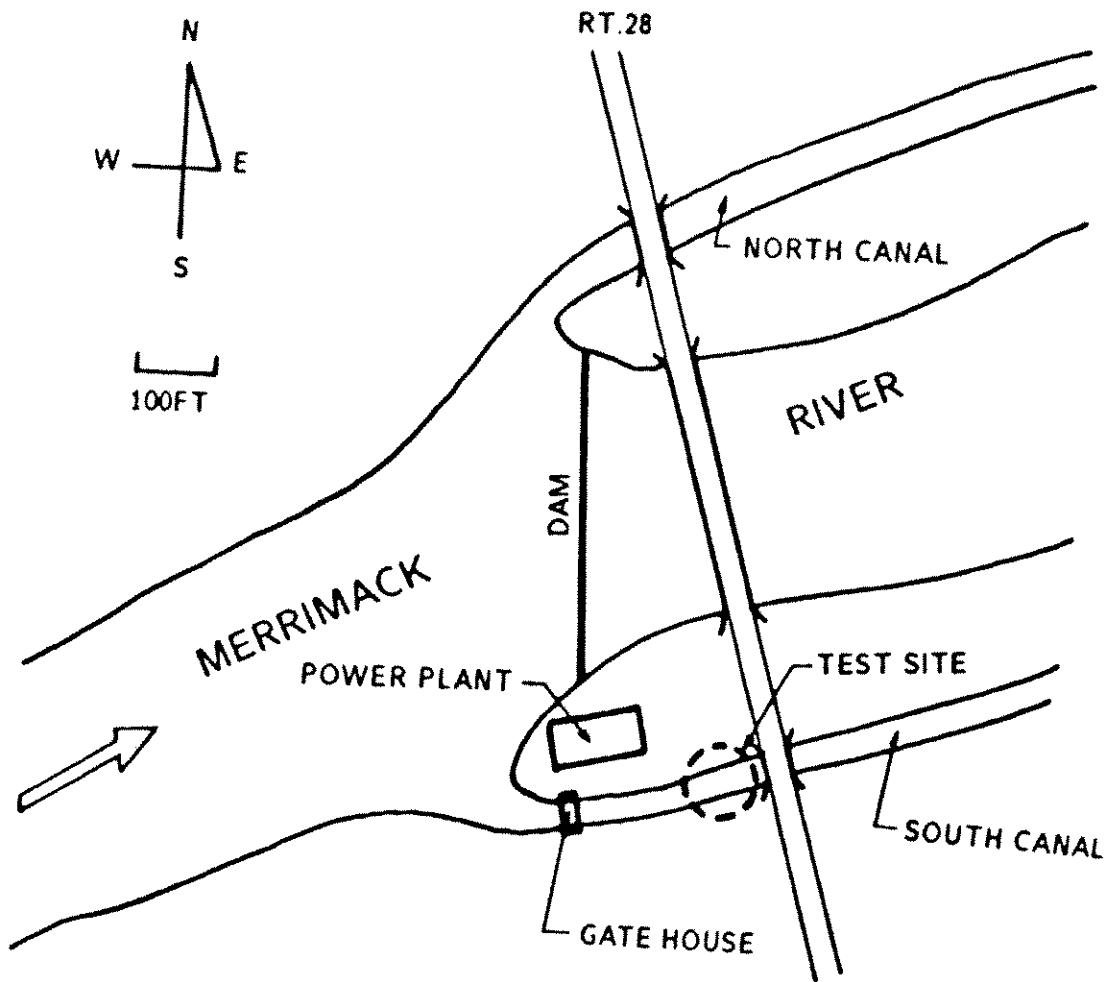


Fig. 3.1 Test site (Lawrence, Massachusetts)

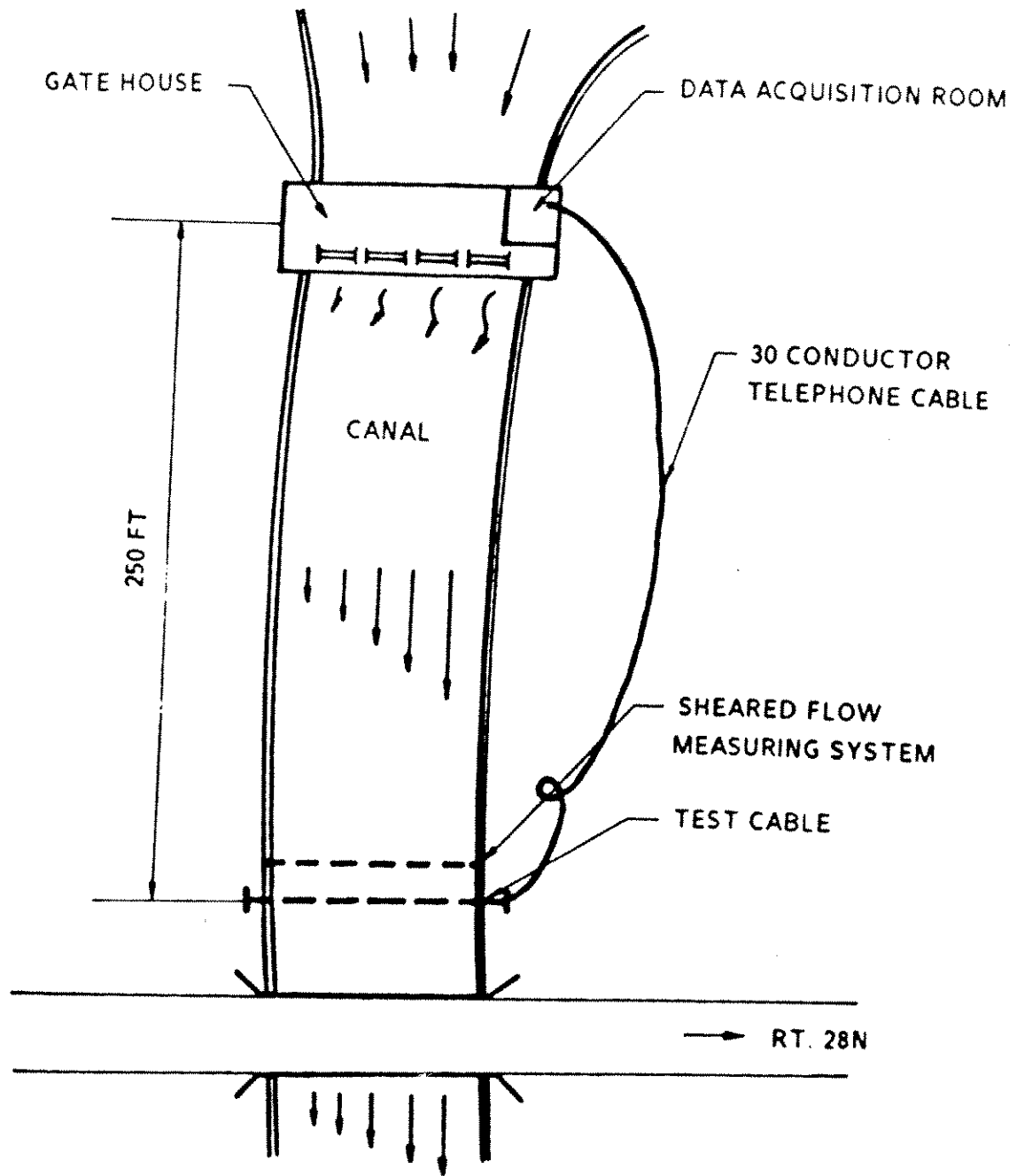
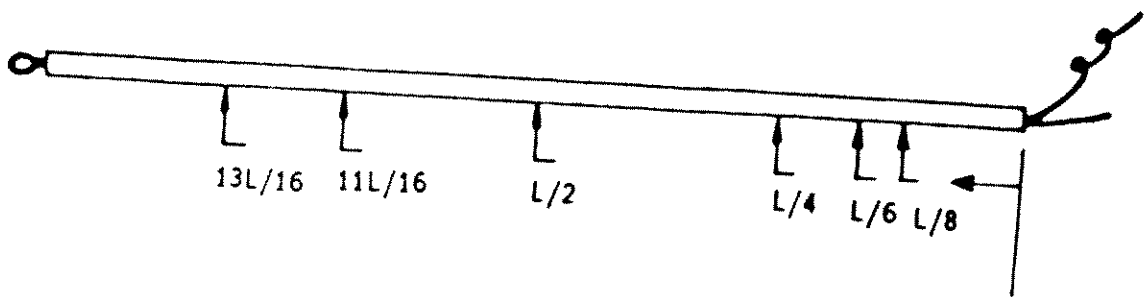


Fig. 3.2 Test site arrangement

(A) LOCATION OF ACCELEROMETERS



(B) CROSS SECTION OF TEST CABLE

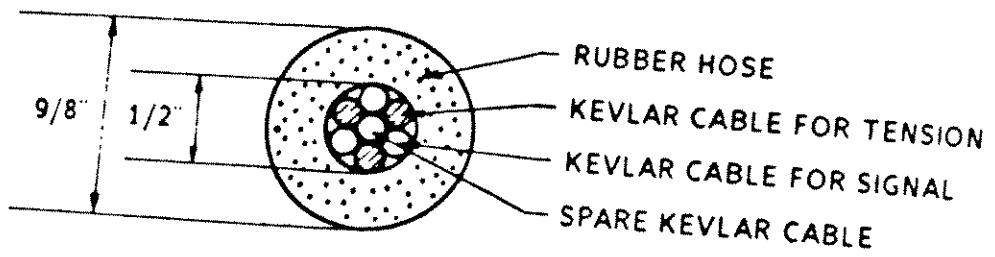


Fig. 3.3 Test cable

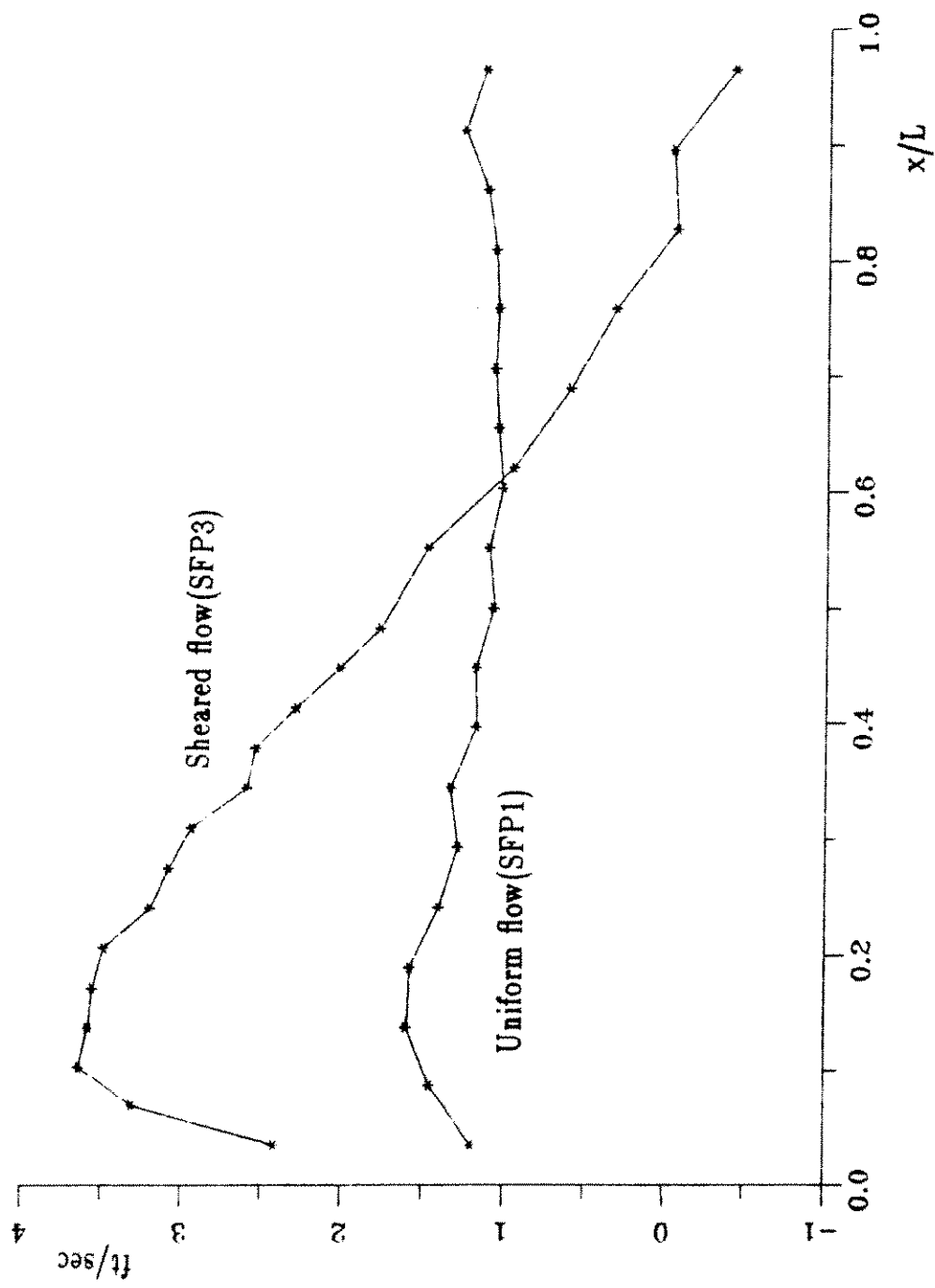


Fig. 3.4 Uniform and sheared flow profiles

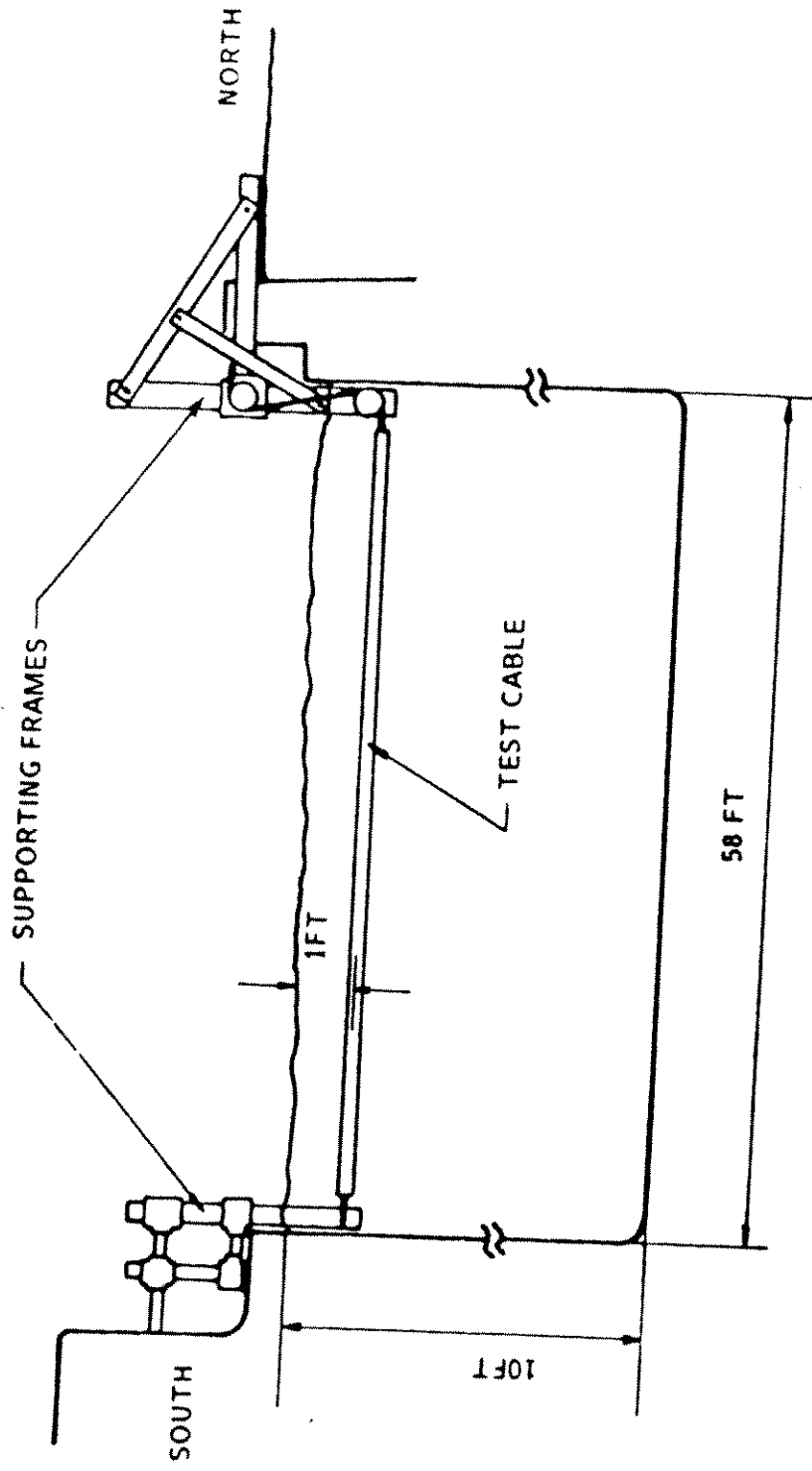


Fig. 3.5 Test cable supporting system

3.6). The tension could be adjusted from 50 to 500 pounds, and the applied tension was measured by a loadcell⁴(Fig. 3.6).

- Data acquisition equipment were located in the gate house. The hook-up diagram of the equipment is shown in Fig. 3.7.

3.2.3 Experiment procedures

- Each test configuration(1 bare cable and 6 cables with suppression devices) was installed in the canal.
- By adjusting the gates, the desired flow profile was set.
- Flow velocities along the test cable were measured to find the flow profile of each test run.
- The required tension was pre-adjusted by a hand operated winch.
- 6 pairs of acceleration, tension, and reference flow velocity⁵ signals were recorded in a DEC Minc-23 computer.

3.2.4 Suppression devices

Six types of suppression devices were used for this experiment. Each device is summarized in Table 3.1.(Also refer to Fig. 3.8.) The experiment on the bare cable was also carried out to compare with the cables with suppression devices.

⁴ Sensotec Model RM 2099

⁵ The velocity was measured in a fixed position(approx. L/10 position) during vibration data acquisition, whereas the flow profile is measured before the vibration test.

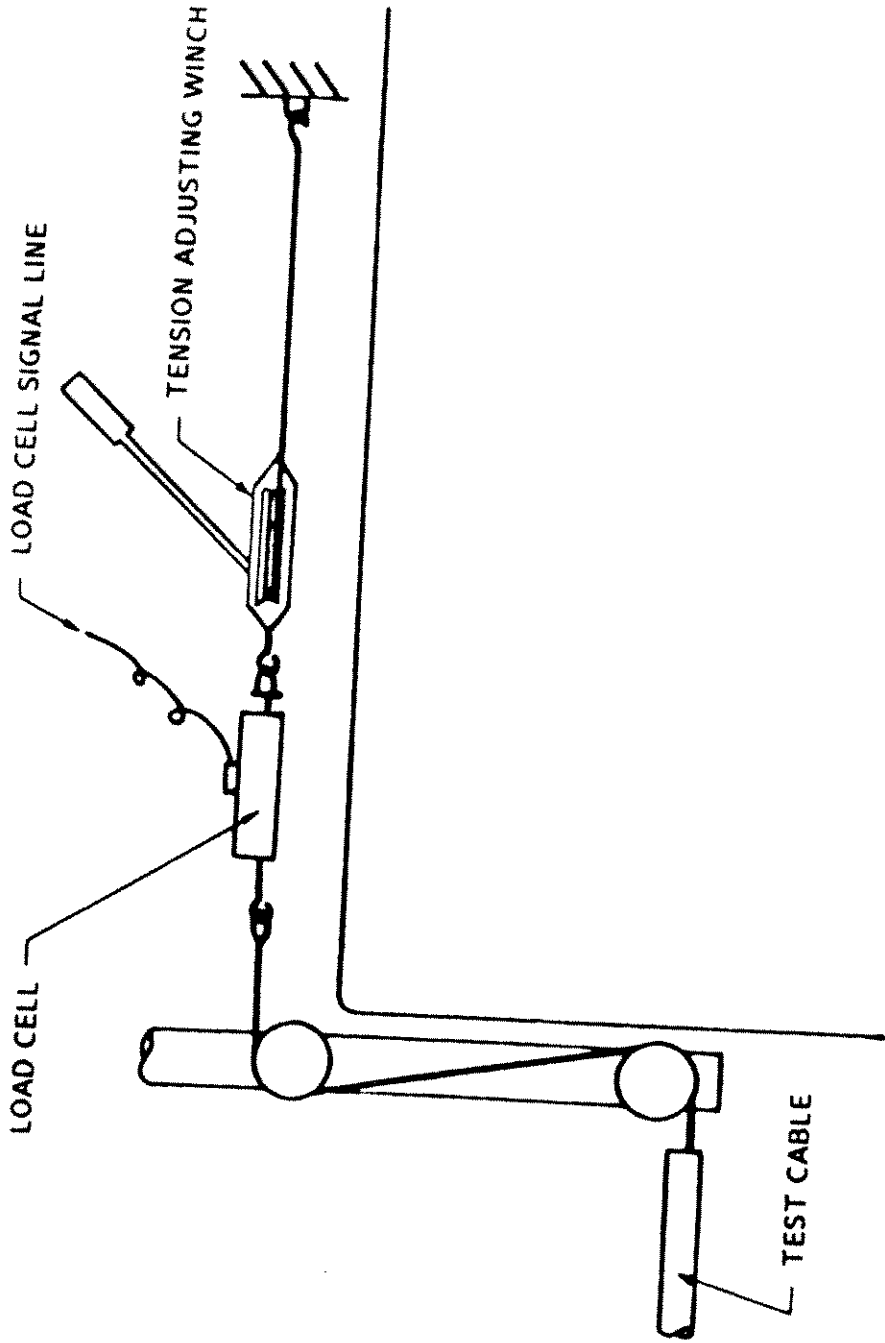


Fig. 3.6 Tension adjusting system

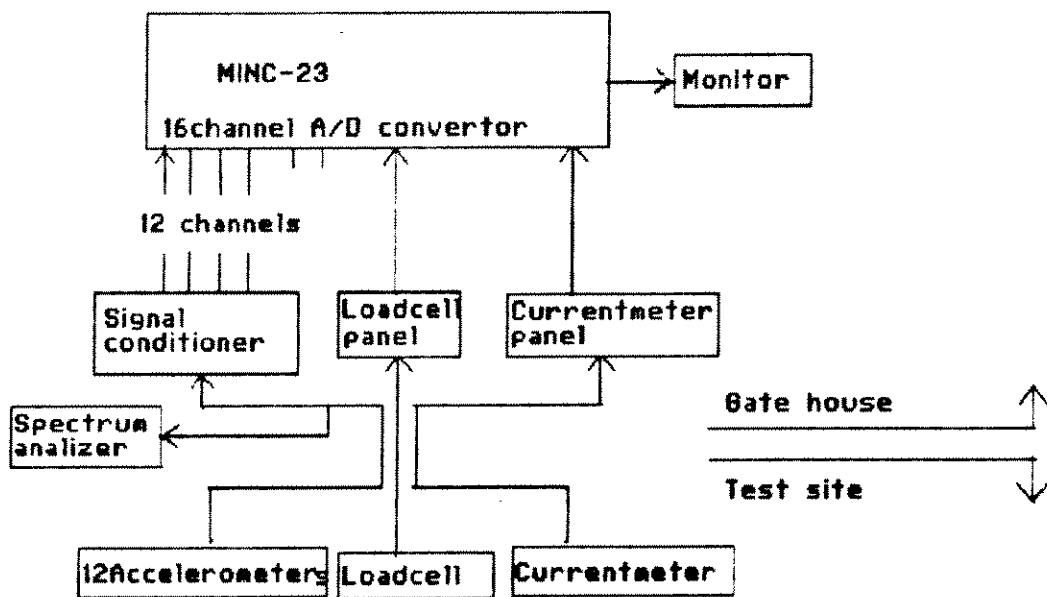

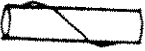
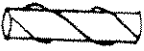

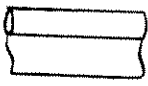
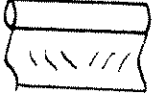
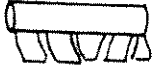


Fig. 3.7 Experiment equipment hook-up diagram

Sketch	Description	Remarks
	Bare Cable (type 0) unit weight ¹ : 0.58 lb/ft diameter : 1.125 in.	Fig. 3.3
	Single Helical (type 1) unit weight : 0.58 lb/ft pitch : 12 in, # of starts : 1 diameter of helical : 0.125 in.	Fig. 3.8 (1)
	Triple Helical (type 2) unit weight : 0.59 lb/ft pitch : 12 in, # of starts : 3 diameter of helical : 0.125 in.	Fig. 3.8 (2)
	Plain Long Flag (type 3) unit weight : 0.94 lb/ft length of flag : 9 in. no slits inside flag	Fig. 3.8 (3)
	Plain Short Flag (type 4) unit weight : 0.83 lb/ft length of flag : 5 in. no slits inside flag	Fig. 3.8 (4)
	Split Long Flag (type 5) unit weight : 0.94 lb/ft length of flag : 9 in. slits inside flag	Fig. 3.8 (5)
	Split Short Flag (type 6) unit weight : 0.83 lb/ft length of flag : 5 in. ribbon type flag	Fig. 3.8 (6)

¹ : Weight in air per foot including suppression device and cable

Table 3.1 Description of suppression devices

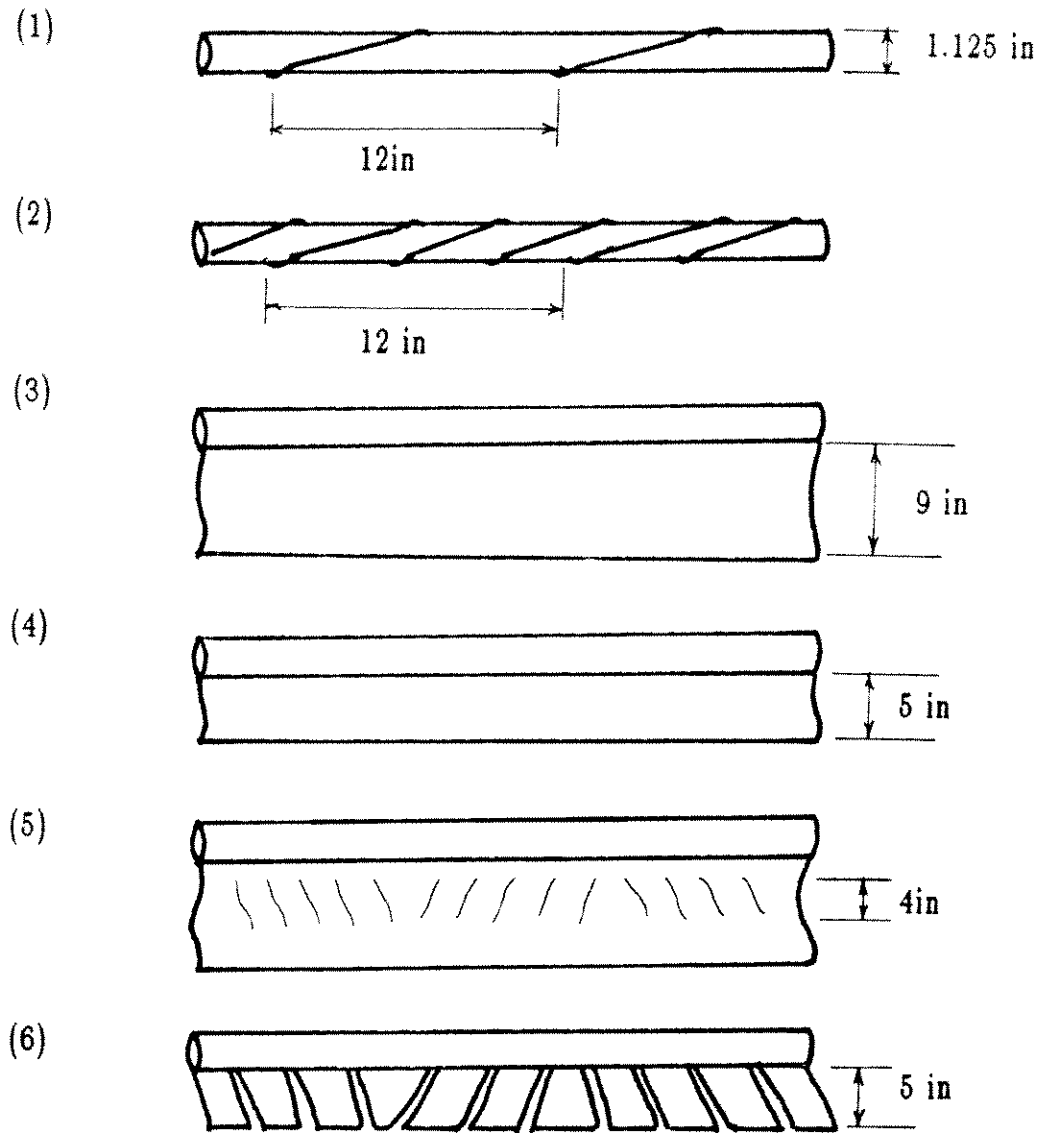


Fig. 3.8 Sketches of suppression devices

(0) Bare cable(type 0)

The bare cable was made of 1.125 inch diameter rubber hose, and its unit weight was 0.58 lb/ft.

(1) Single helical wire type(type 1)

A string with a diameter of 0.125 inches was wound around the bare cable to make a helical wire type suppression device. Its pitch was 12 inches and the number of starts was 1.

(2) Triple helical wire type(type 2)

In the above single helical wire type, 2 additional strings with the same pitch were wound around the cable.

(3) Plain long flag type(type 3)

A plastic sheet of 1/20 inch thickness was wrapped around the test cable leaving a 9-inch tail behind the cable. Unlike a splitter plate type device, the flag was flexible, which tended to adjust the flag direction according to external forces. The increased diameter of the cable due to the thickness of the flag was about 9 percent.

(4) Plain short flag type(type 4)

The plain short flags were made by cutting 4 inches of the flag tail from the plain long flag.

(5) Split long flag type(type 5)

The split long flag had the same dimensions and material properties as

those of the plain long flag, except that it had diagonal direction cuts inside the flag.

(6) Split short flag type(type 6)

By cutting 4 inches of the flag tail from the split long flag, ribbon type flags were made. This device was similar to an ordinary ribbon type device.

3.3 Data processing

3.3.1 Flow profile, reference velocity, and tension

- Flow profile

Flow profile data, which were measured by a current meter, consisted of absolute flow velocity and flow direction signals. The flow velocities normal to the test cable were calculated from the data and the orientation of the test site. The flow profile was made by plotting the averaged velocities along the test cable. Fig. 3.9 shows the sheared flow profile and its turbulence level.

- Reference flow velocity

The reference flow velocities, which were measured during vibration data acquisition, were averaged. The reference flow velocity for each test is shown in Table 3.3. Fig. 3.10 represents typical raw signals of flow velocity and direction with respect to magnetic north. Fig. 3.11 is the spectrum of the flow velocity.

- Tension

Tension data for each test case were also averaged and tabulated in

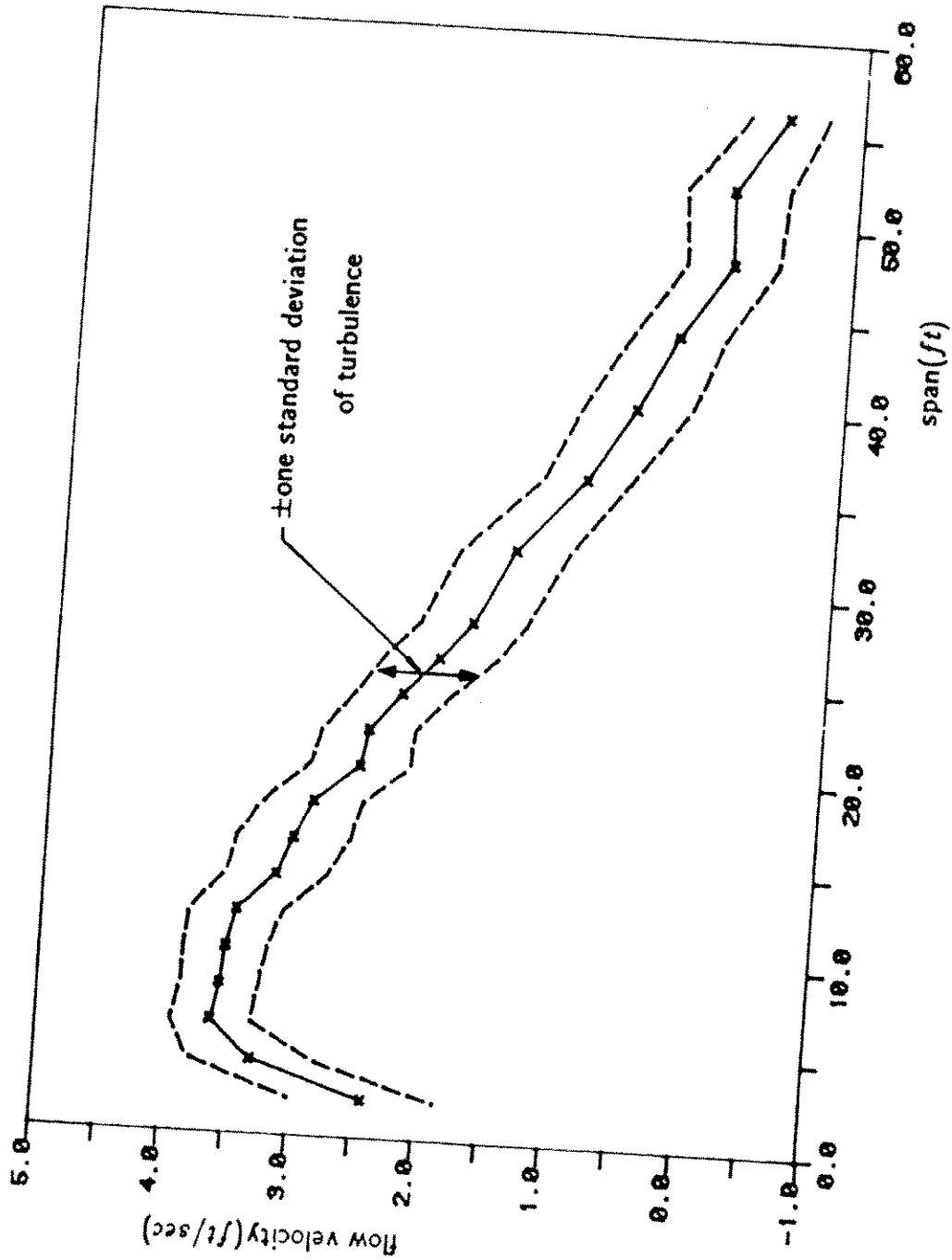


Fig. 3.9 Turbulence level of flow velocity profile

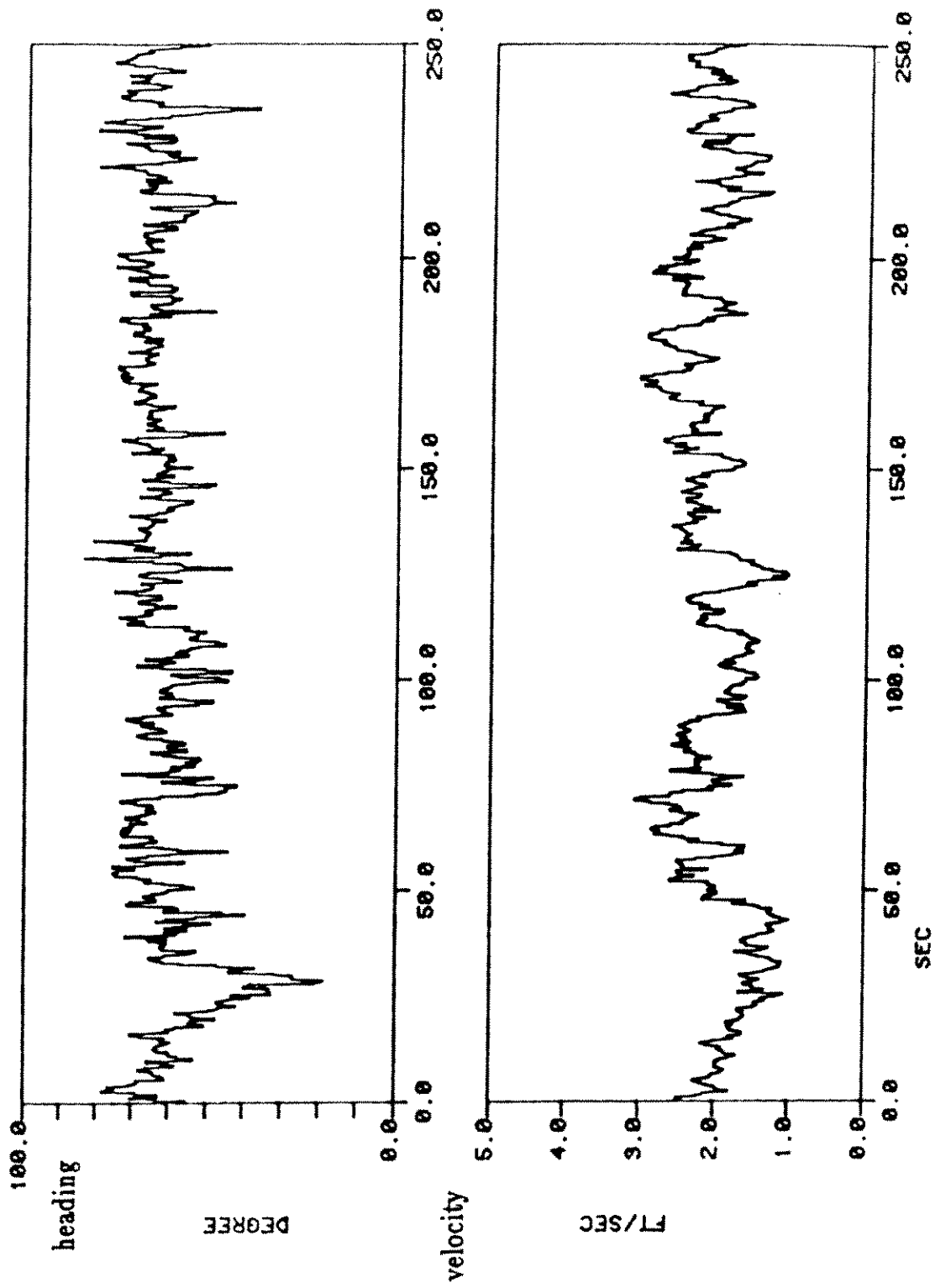


Fig. 3.10 Typical flow direction and velocity data in sheared flow

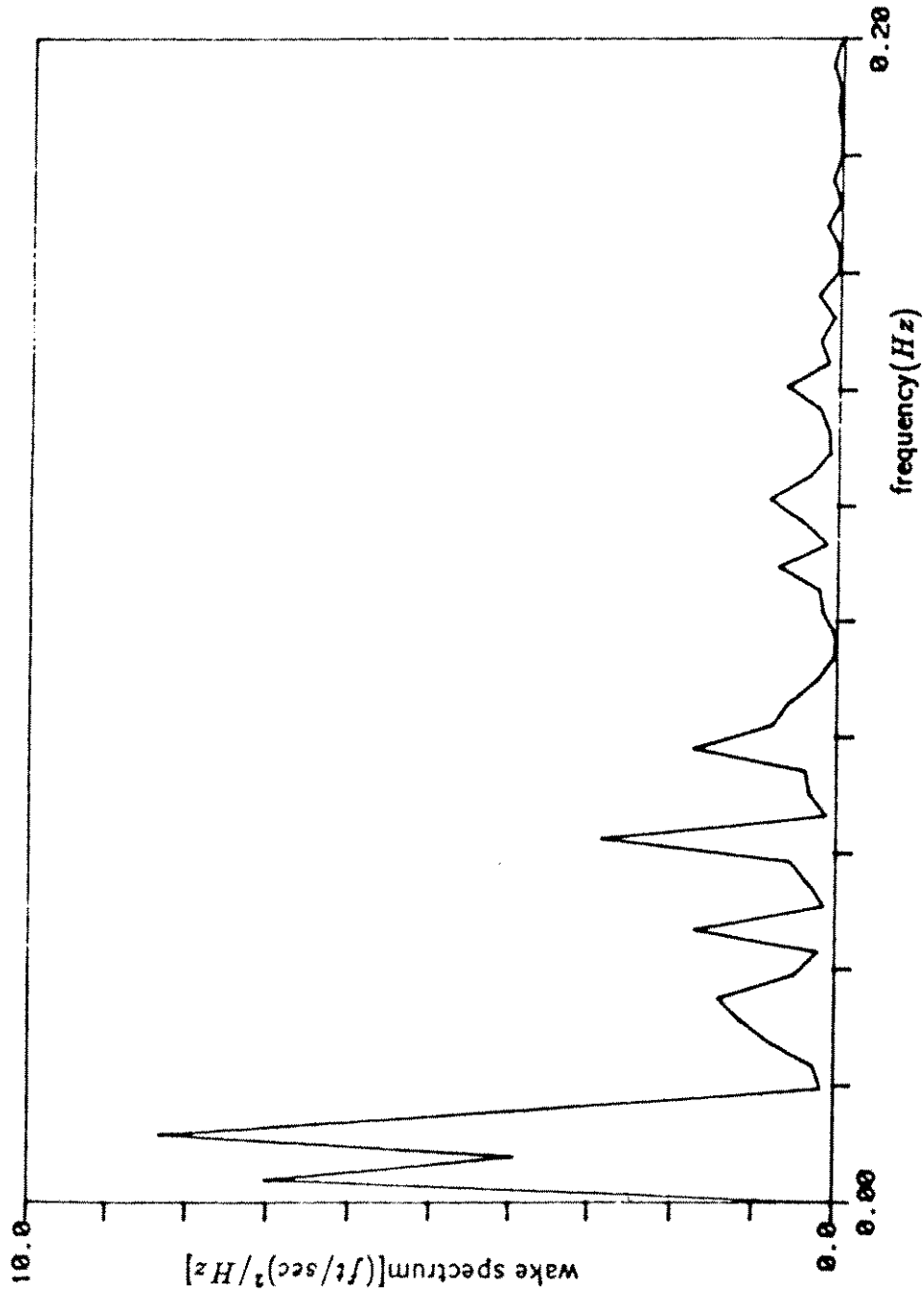


Fig. 3.11 Spectrum of flow velocity signal shown in Fig. 3.10

Table 3.3.

3.3.2 Selection of acceleration data

The acceleration data for each suppression device were composed of 14 or 7 sets⁶ of 1024 data points. The averaged spectra or rms(root mean square) values did not show in a complete way the characteristics of each suppression device, because of the large flow velocity fluctuations during the tests. For this reason, 1 set of 1024 data points for each case was selected for further data processing. The sampling frequency for the bare cable and single helical wire type cases was 50 Hz, and that for the triple helical and the flag type cases was 30 Hz.

3.3.3 Time series signal

- Acceleration

Each pair of accelerometers had a 90 degree phase difference in their sensing directions. The mean value of the vertical component was 1 gravity, whereas that of the horizontal direction was zero. As the orientations of the accelerometers changed during experiments, the actual vertical and horizontal components had to be calculated by using the vector rotation method detailed in (33). The decomposed vertical and horizontal components corresponded to cross-flow and in-line accelerations respectively. Cross-flow data were mainly dealt with in this thesis. The typical cross-flow acceleration signals are found in Fig. 3.12.

- Displacement

⁶ The bare cable and helical wire type devices(type 0-2) had 14 sets, and flag type devices(type 3-6) had 7 sets, respectively.

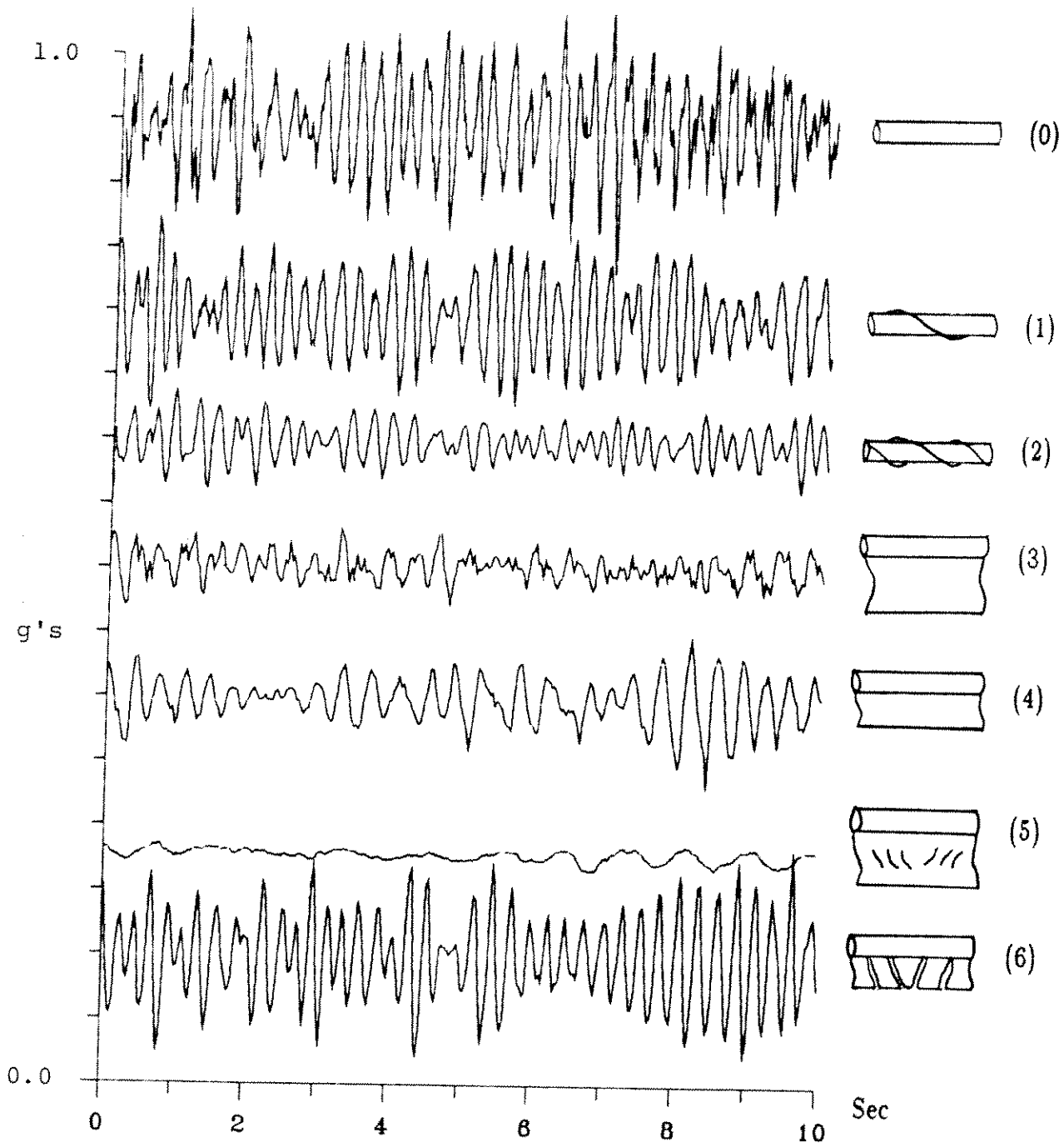


Fig. 3.12 Time series cross-flow acceleration signals at L/4 (SL)
: Sheared flow Low tension

The displacement(d) is obtained by integrating twice from the acceleration (a) (eqn. 3.1).

$$d(t) = \int_0^t \int_0^{t_1} a(t_0) dt_0 dt_1 \quad (3.1)$$

Because a raw acceleration signal contains low-frequency noise components, necessary filtering processes should be made in order to get a proper displacement signal. For this purpose, the "iir" filter program(23) was used. The filtering program is composed of least square-fittings, high-pass filter coefficient calculations, and integration procedures.

3.3.4 Spectra

- Acceleration spectra

Acceleration spectra were calculated by using the Fast Fourier Transform(FFT) program. From the FFT result, every 4 values were averaged⁷ to get smooth spectra.

- Displacement spectra

The displacement spectrum(S_d)(eqn. 3.2) is derived from the acceleration spectrum(S_a), which was calculated by the FFT program:

$$S_d(f) = \begin{cases} \left(\frac{1}{2\pi f}\right)^4 S_a(f) & \text{when } f > f_{cut-off} \\ 0 & \text{when } f < f_{cut-off} \end{cases} \quad (3.2)$$

where $f_{cut-off}$ is a cut-off frequency.

3.3.5 Rms values

Rms acceleration(R_a) and rms displacement(R_d) are obtained by taking

⁷ The resolutions of the spectra were reduced to 0.20 Hz for sampling frequency of 50 Hz, and 0.12 Hz for sampling frequency of 30 Hz.

the square-root of the integrated spectra in frequency domain (eqn. 3.3).

$$R_{a,d} = \left(\int_{f_a}^{f_b} S_{a,d}(f) df \right)^{1/2} \quad (3.3)$$

where f_a is the cut-off frequency, and f_b is the Nyquist frequency (half of the sampling frequency).

The rms values varied greatly according to the choice of the cut-off frequency; thus, in this thesis, both 0.5 Hz and 2 Hz cases were calculated.

3.4 Performance comparison

Experimental results of vortex-induced vibration suppression devices in uniform and sheared flow profiles and under low and high tension cases are summarized in Table 3.2. As shown in the table, the reference velocities for the tests were not same, therefore, RMS accelerations and displacements of the suppression devices could not be compared under exactly the same conditions. Nevertheless, the flow velocity differences rarely exceeded 10 percent; therefore, it did not usually affect the performance comparison too much.

3.4.1 Experiment conditions

- Uniform and sheared flow profiles

In uniform flow profile cases, the average reference flow velocity was approximately 1.6 ft/sec and the corresponding Reynolds number ($Re = VD/\nu$) was 1.2×10^4 . In sheared flow profile cases, the average reference velocity⁸ was approximately 3.1 ft/sec, and the Reynolds number at this case was 2.4×10^4 .

⁸ velocity measured at L/10 location.

RMS Type	Acceleration(g)		Displacement(in)	
	2.0 Hz ¹	0.5 Hz	2.0 Hz ¹	0.5 Hz
Bare Cable(UL0) ²	0.356	0.357	0.422	0.503
Single Helical(UL1)	0.283	0.285	0.377	0.419
Triple Helical(UL2)	0.267	0.268	0.290	0.321
Plain Long Flag(UL3)	0.025	0.088	0.023	0.888
Plain Short Flag(UL4)	n.a.	n.a.	n.a.	n.a.
Split Long Flag(UL5)	0.022	0.066	0.033	0.515
Split Short Flag(UL6)	0.133	0.295	0.163	0.995
Bare Cable(UH0) ³	0.517	0.518	0.450	0.496
Single Helical(UH1)	0.478	0.479	0.544	0.564
Triple Helical(UH2)	0.205	0.206	0.204	0.222
Plain Long Flag(UH3)	0.122	0.148	0.083	0.929
Plain Short Flag(UH4)	n.a.	n.a.	n.a.	n.a.
Split Long Flag(UH5)	n.a.	n.a.	n.a.	n.a.
Split Short Flag(UH6)	n.a.	n.a.	n.a.	n.a.
Bare Cable(SL0) ⁴	0.825	0.826	0.432	0.580
Single Helical(SL1)	0.675	0.676	0.369	0.417
Triple Helical(SL2)	0.327	0.328	0.204	0.279
Plain Long Flag(SL3)	0.181	0.189	0.225	0.466
Plain Short Flag(SL4)	0.268	0.275	0.342	0.652
Split Long Flag(SL5)	0.042	0.075	0.067	0.527
Split Short Flag(SL6)	0.342	0.344	0.194	0.507
Bare Cable(SH0) ⁵	1.030	1.030	0.476	0.617
Single Helical(SH1)	0.821	0.822	0.497	0.534
Triple Helical(SH2)	0.310	0.310	0.137	0.164
Plain Long Flag(SH3)	0.246	0.254	0.221	0.515
Plain Short Flag(SH4)	0.777	0.779	0.621	0.747
Split Long Flag(SH5)	n.a.	n.a.	n.a.	n.a.
Split Short Flag(SH6)	0.465	0.466	0.416	0.506

Hz¹ : cut - off frequency

UL² : uniform flow low tension case

UH³ : uniform flow high tension case

SL⁴ : sheared flow low tension case

SH⁵ : sheared flow high tension case

Table 3.2 Cross-flow RMS value comparison

Type	Profile ¹	Ref. Vel ²	Tension ³	Source ⁴
Bare Cable(UL0)	SFP1	1.592	69	L73115 L/4 #1
Single Helical(UL1)	SFP1	1.538	72	L73113 L/4 #2
Triple Helical(UL2)	SFP1	1.619	55	L73101 L/4 #7
Plain Long Flag(UL3)	SFP1	1.535	110	L81403 13L/16 #3
Plain Short Flag(UL4)	n.a.	n.a.	n.a.	n.a.
Split Long Flag(UL5)	SFP1	1.552	LT ⁵	L81502 L/4 #6
Split Short Flag(UL6)	SFP1	1.579	LT ⁵	L1506 L/4 #3
Bare Cable(UH0)	SFP1	1.582	447	L73117 L/4 #12
Single Helical(UH1)	SFP1	1.675	410	L73114 L/4 #14
Triple Helical(UH2)	SFP1	1.904	499	L73103 L/4 #1
Plain Long Flag(UH3)	SFP1	1.595	458	L81401 L/4 #1
Plain Short Flag(UH4)	n.a.	n.a.	n.a.	n.a.
Split Long Flag(UH5)	n.a.	n.a.	n.a.	n.a.
Split Short Flag(UH6)	n.a.	n.a.	n.a.	n.a.
Bare Cable(SL0)	SFP3	2.508	87	L73121 L/4 #5
Single Helical(SL1)	SFP3	2.907	67	L73109 L/4 #2
Triple Helical(SL2)	SFP3	2.499	82	L73108 L/4 #12
Plain Long Flag(SL3)	SFP3	3.220	54	L81406 L/4 #1
Plain Short Flag(SL4)	SFP3	3.161	160	L81407 L/4 #6
Split Long Flag(SL5)	SFP3	3.335	LT ⁵	L1503 11L/16 #2
Split Short Flag(SL6)	SFP3	3.338	LT ⁵	L81509 L/4 #2
Bare Cable(SH0)	SFP3	2.569	392	L73122 #14
Single Helical(SH1)	SFP3	3.152	353	L3110 L/4 #13
Triple Helical(SH2)	SFP3	2.815	434	L73107 L/4 #6
Plain Long Flag(SH3)	SFP3	3.188	427	L81405 L/4 #3
Plain Short Flag(SH4)	SFP3	3.234	560	L81408 L/4 #3
Split Long Flag(SH5)	n.a.	n.a.	n.a.	n.a.
Split Short Flag(SH6)	SFP3	3.471	HT ⁶	L81510 L/4 #2

Profile¹ : Flow profile pattern shown in figure 3.4

Ref. Vel² : Reference flow velocity(ft/sec) measured at L/10 position

Tension³ : Average tension(lb) during measurement

Source⁴ : Source of data(ex. L73105 L/4 #8: 8th 1024 data at L/4 of run code L73105)

LT⁵ : Approx. 80 lb(exact value is not available)

HT⁶ : Approx. 400 lb(exact value is not available)

Table 3.3 Experiment conditions of Table 3.2

The overall flow profiles are shown in Fig. 3.3. The average reference velocity of each experiment is shown in Table 3.3.

- Low and high tension cases

The average tension was approximately 80 lb in low tension cases, and 400 lb in high tension cases. From the relationship for natural frequencies in Section 2.1.2, the fundamental frequencies of the low and high tension cases in the air were 0.6 Hz and 1.3 Hz, respectively. (The bending stiffness was small compared to the tension term.)

- Location of accelerometers

For each experiment, 6 locations ($L/8$, $L/6$, $L/4$, $L/2$, $11L/16$, and $13L/16$) of acceleration signals were measured. In this thesis, mainly $L/4$ location signals, which proved most usable (stable) throughout the experiments, were compared wherever possible.

- Organization of data

Twenty-eight different experimental setups were carried out. A typical experimental setup is shown in Table 3.2. The first (U or S), the second (L or H), and the third (0-6) experiment codes stand for the flow condition, the tension condition, and the type of suppression device respectively. For example, the "SL4" means sheared flow, low tension, and plain short flag type suppression device.

- Limitations

Especially during the test of flag type (type 3-6) suppression devices, many of the accelerometers malfunctioned. As a result, some sets of data

could not be recovered. In certain cases (shown in Table 3.3), other location signals were substituted for the L/4 location signals. That made the performance evaluation a little difficult.

It was assumed that a flow profile did not change in a certain flow pattern condition, and that the flow profile was proportion to the averaged reference flow velocity, which was measured at a fixed location during vibration data acquisition. But the turbulence level shown in Fig. 3.10 and 3.11 affected the instantaneous reference velocity and the flow profile. Therefore, the uncertainties caused by the turbulence should be considered in the interpretation of the experiment results.

In this experiment, the cross-flow and in-line vibration signals were measured, but other important parameters, such as drag forces, were not measured. Therefore, the drag force comparison could not be made quantitatively.

3.4.2 Acceleration comparison

The typical 10-second acceleration signals of suppression devices in a sheared flow low tension case are shown in Fig. 3.12. The rms values at the L/4 location are tabulated in Table 3.2. The time domain acceleration signals and rms values reveal that all of the suppression devices were effective to a certain degree. In comparing the performance of the devices, the experimental conditions detailed in Table 3.3 should be considered. Fig. 3.13-3.18 represent the acceleration spectra comparison between a bare cable and a cable with a triple helical suppression device (type 2) in uniform and sheared flow profiles.

3.4.3 Displacement comparison

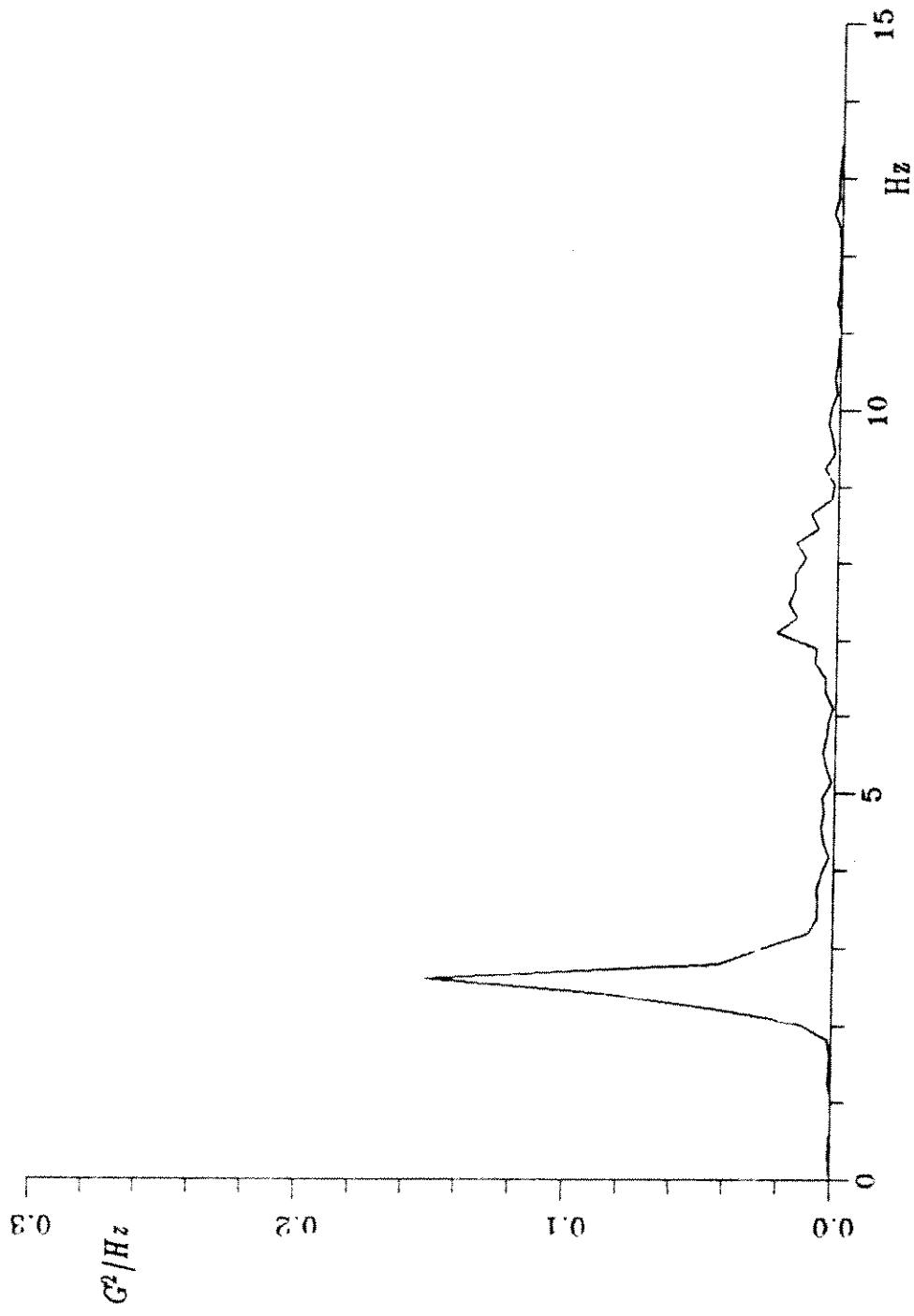


Fig. 3.13 Cross-flow acceleration spectrum at L/4 (ULO)
:Bare cable, ref. vel. 1.59 ft/sec, Uniform Low tension

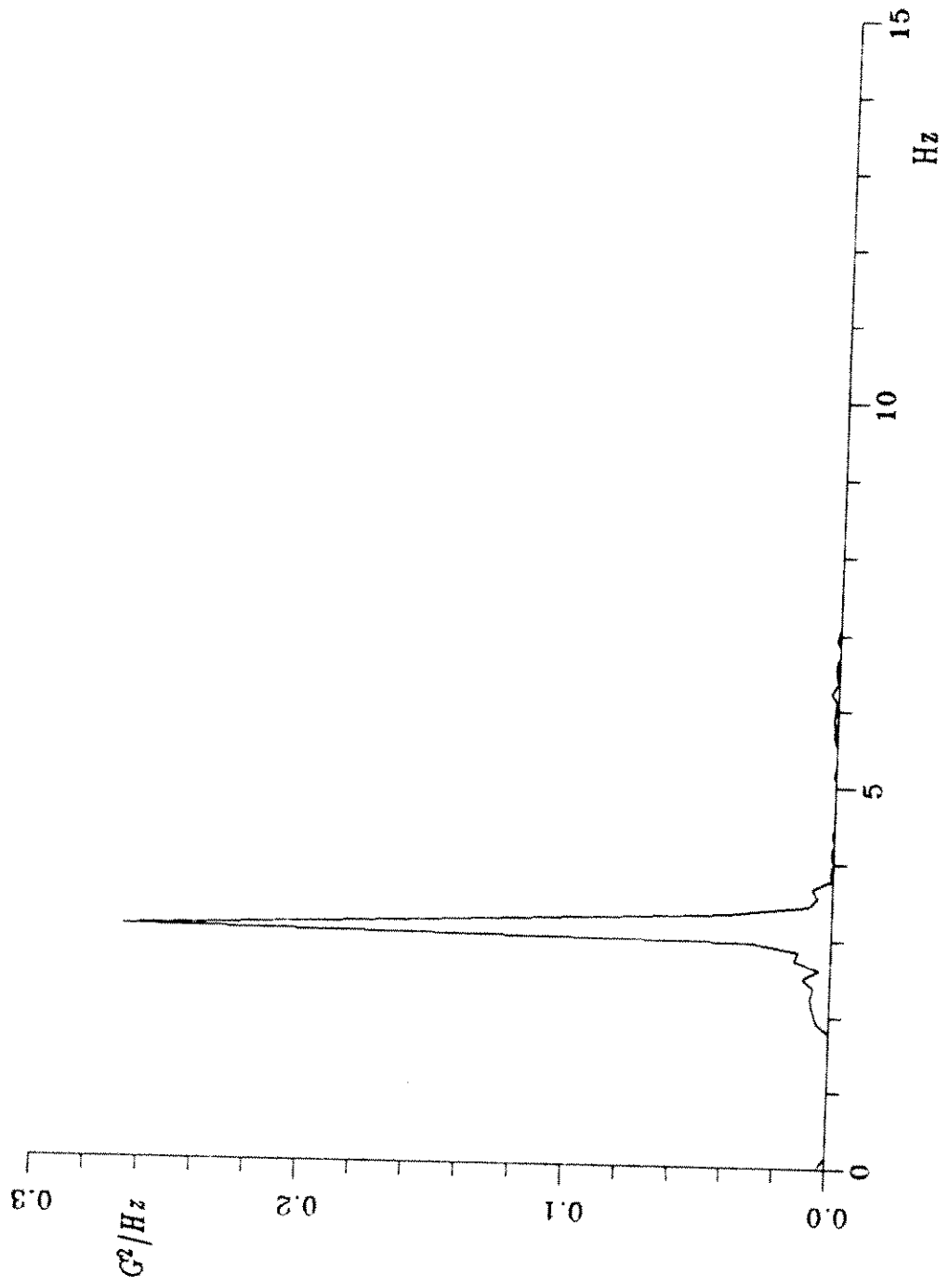


Fig. 3.14 Cross-flow acceleration spectrum at L/4 (UL2)
:Triple helical, ref. vel. 1.62 ft/sec, Uniform Low tension

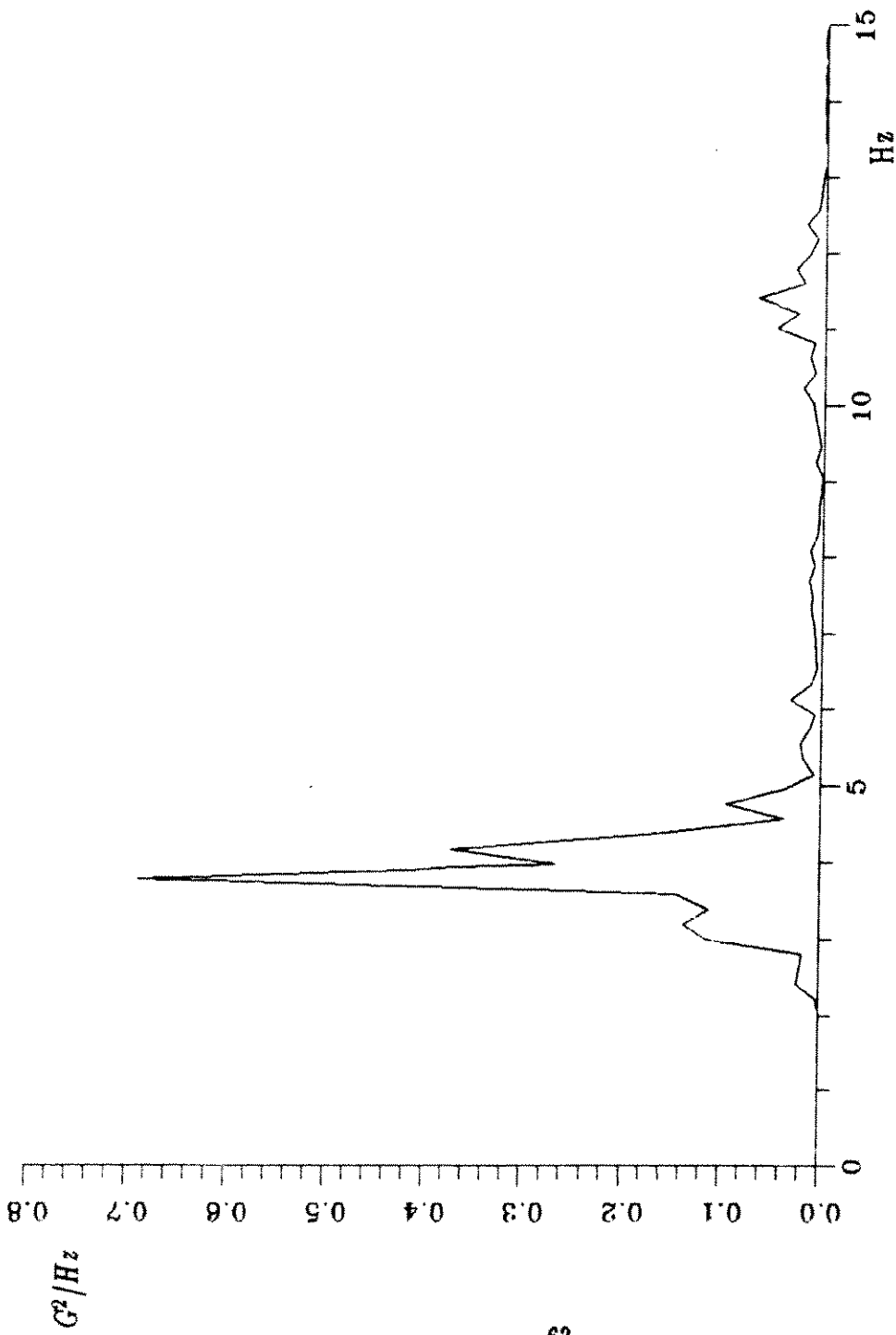


Fig. 3.15 Cross-flow acceleration spectrum at L/4 (SL0)
:Bare cable, ref. vel. 2.51 ft/sec, Sheared Low tension

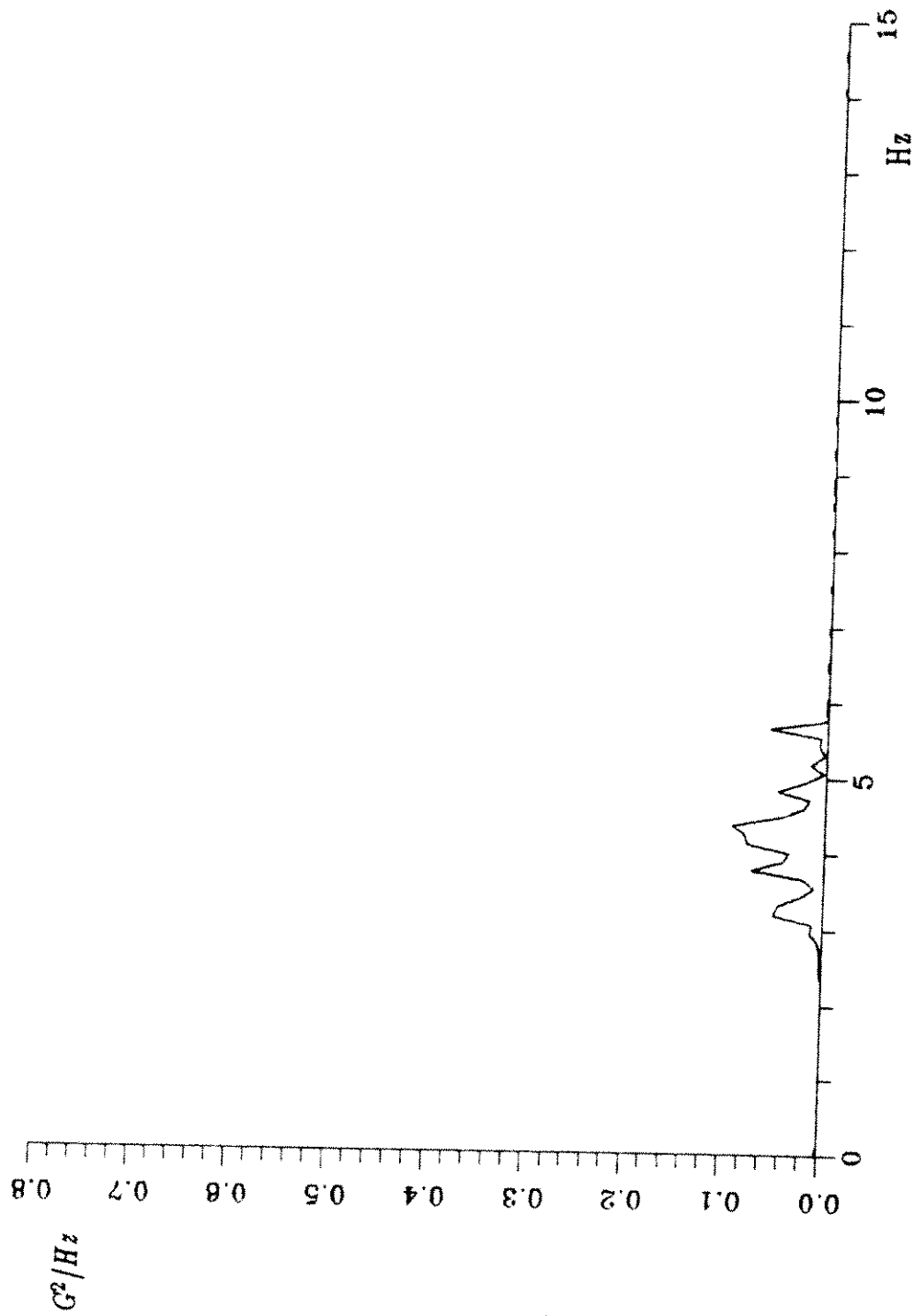


Fig. 3.16 Cross-flow acceleration spectrum at L/4 (SL2)
:Triple helical, ref. vel. 2.50 ft/sec, Sheared Low tension

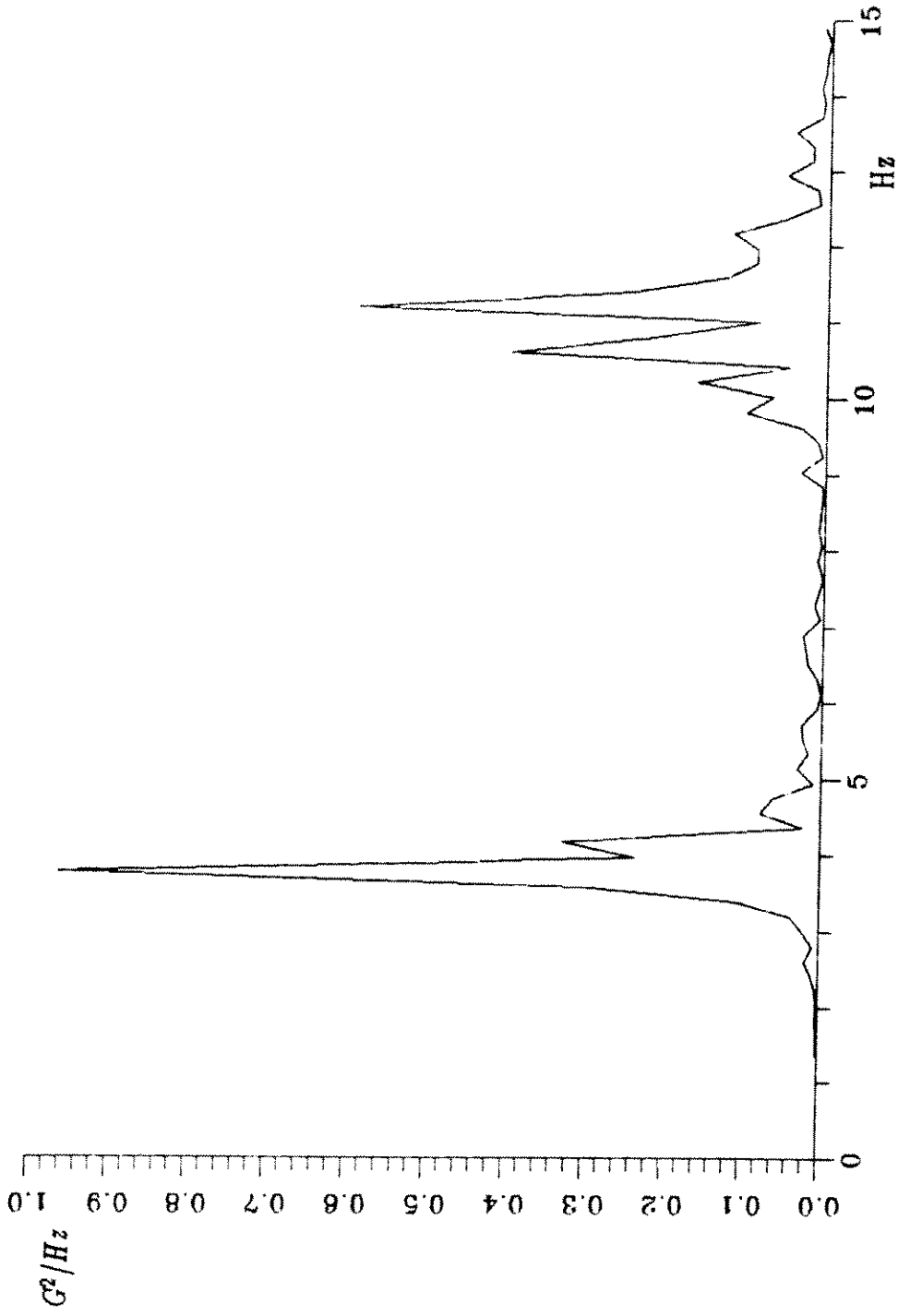


Fig. 3.17 Cross-flow acceleration spectrum at L/4 (SH0)
:Bare cable, ref. vel. 2.57 ft/sec, Sheared High tension

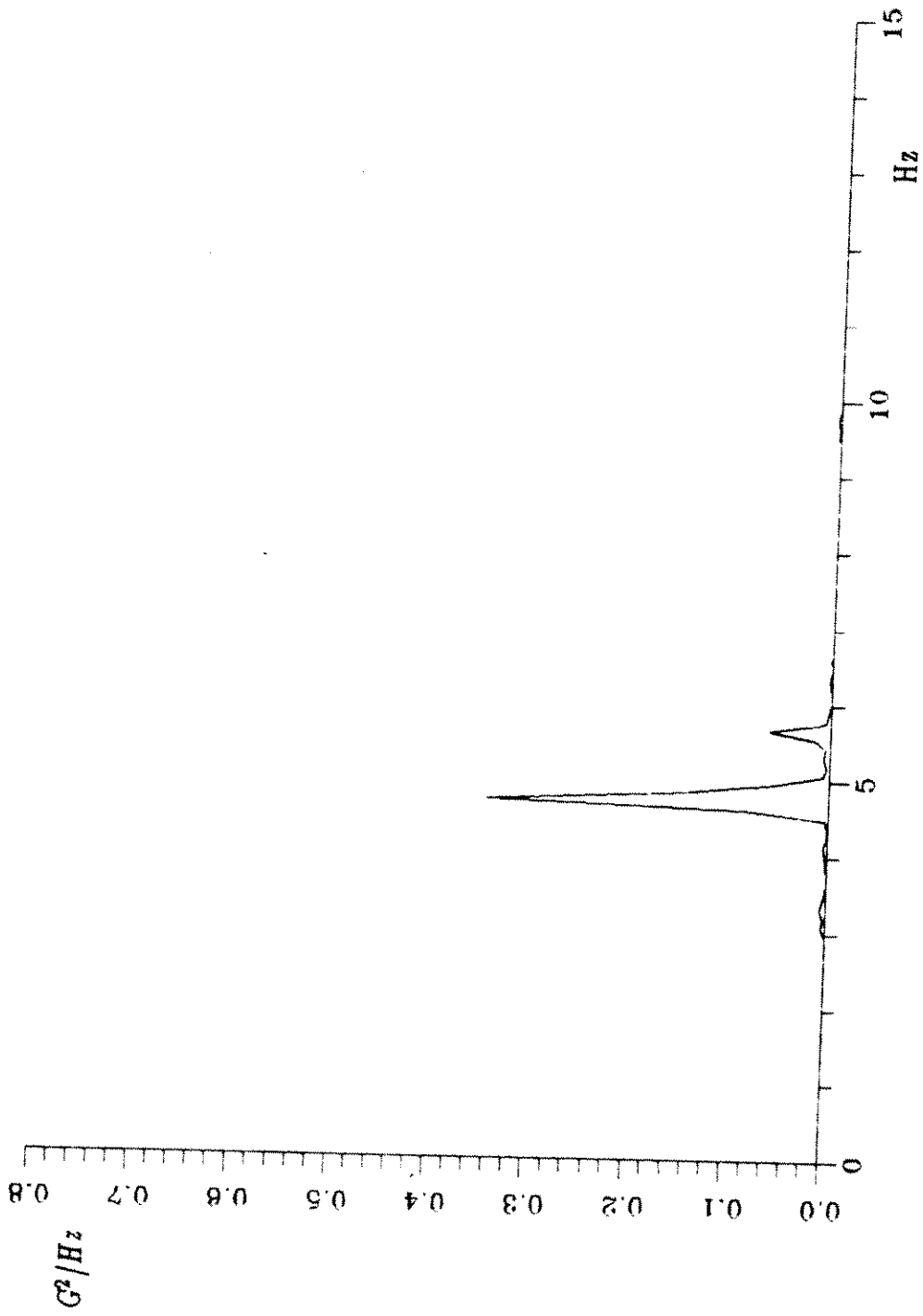


Fig. 3.18 Cross-flow acceleration spectrum at L/4 (SH2)
:Triple helical, ref. vel. 2.82 ft/sec, Sheared High tension

Rms displacement values of cables with suppression devices are tabulated in Table 3.2. Since the values were very sensitive to the cut-off frequency, rms values for both 0.5 and 2.0 Hz cut-off frequencies were made. Time domain vertical and horizontal displacements were derived from acceleration signals by using the filtering program (cut-off frequency: 2.0 Hz). Fig. 3.19 and Fig. 3.20 show the displacement comparisons between cables with and without suppression devices in uniform and sheared flow profile cases.

3.4.4 Velocity comparison

Rms velocity comparisons among suppression devices were not elaborated here. When they are needed for an exciting energy (or power) comparison, they can be derived from acceleration spectra.

3.5 Findings and discussion

Based on the results in Table 3.2 and other data sets, the following observations were carefully drawn. The limitations in Section 3.4.1 were considered in the derivation of the observations.

3.5.1 Helical wire type devices (type 1-2)

- *The acceleration spectra had peaks at corresponding shedding frequencies.*

In uniform flow profiles, the shedding frequencies showed quite narrow bands and the shedding frequencies closely followed the Strouhal relation (eqn. 2.12). From Fig. 3.13, and 3.14, the Strouhal number was approximately 0.17, which is slightly lower than that of stationary cylinder.

- *In addition to the first shedding frequency, relatively low repetitive peaks occurred at*

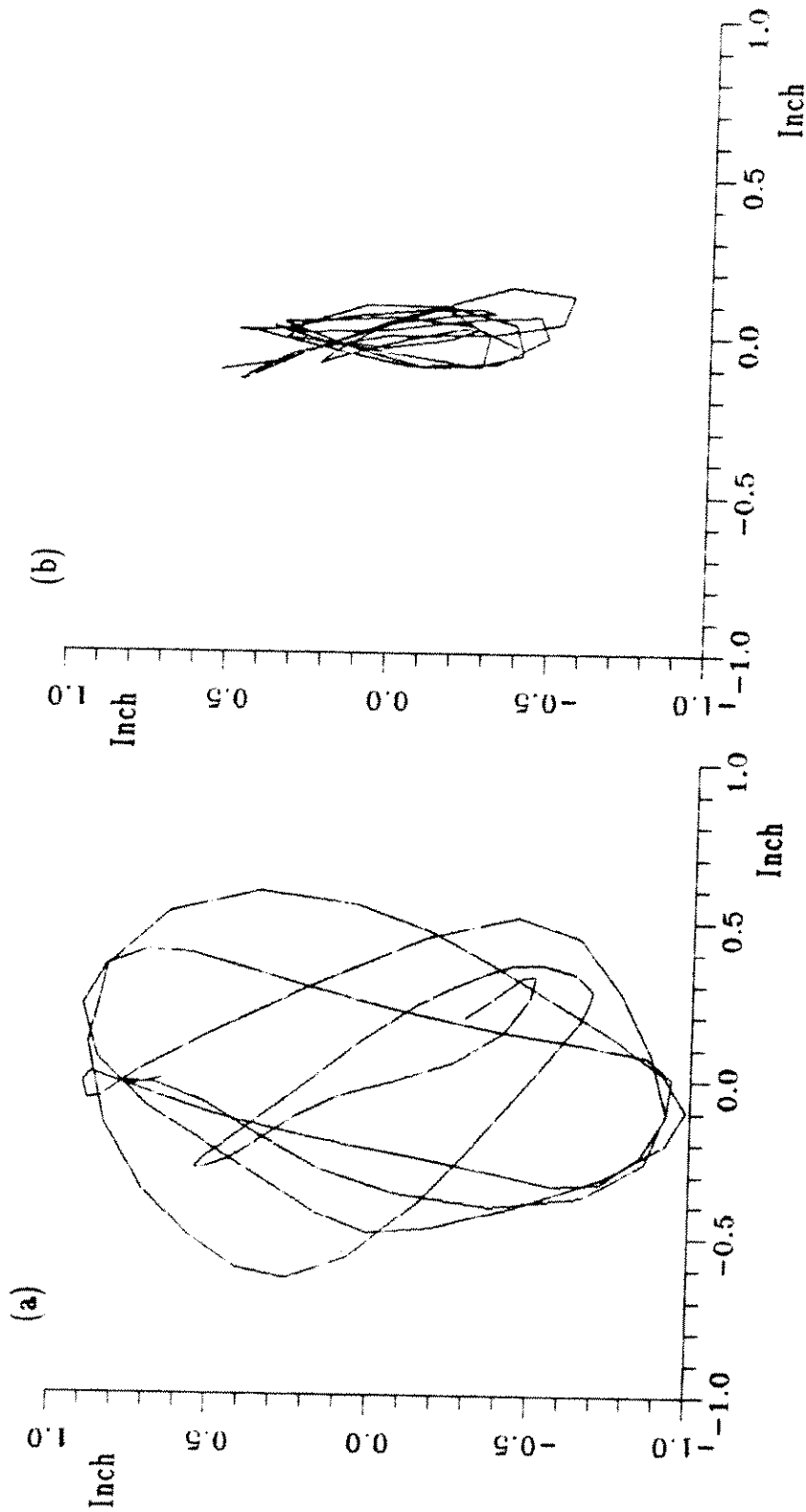


Fig. 3.19 Displacement trajectories at $L/4$ (UL)
 (a) Bare cable, ref. vel. 1.59 ft/sec, Uniform Low tension
 (b) Triple helical, ref. vel. 1.62 ft/sec, Uniform Low tension

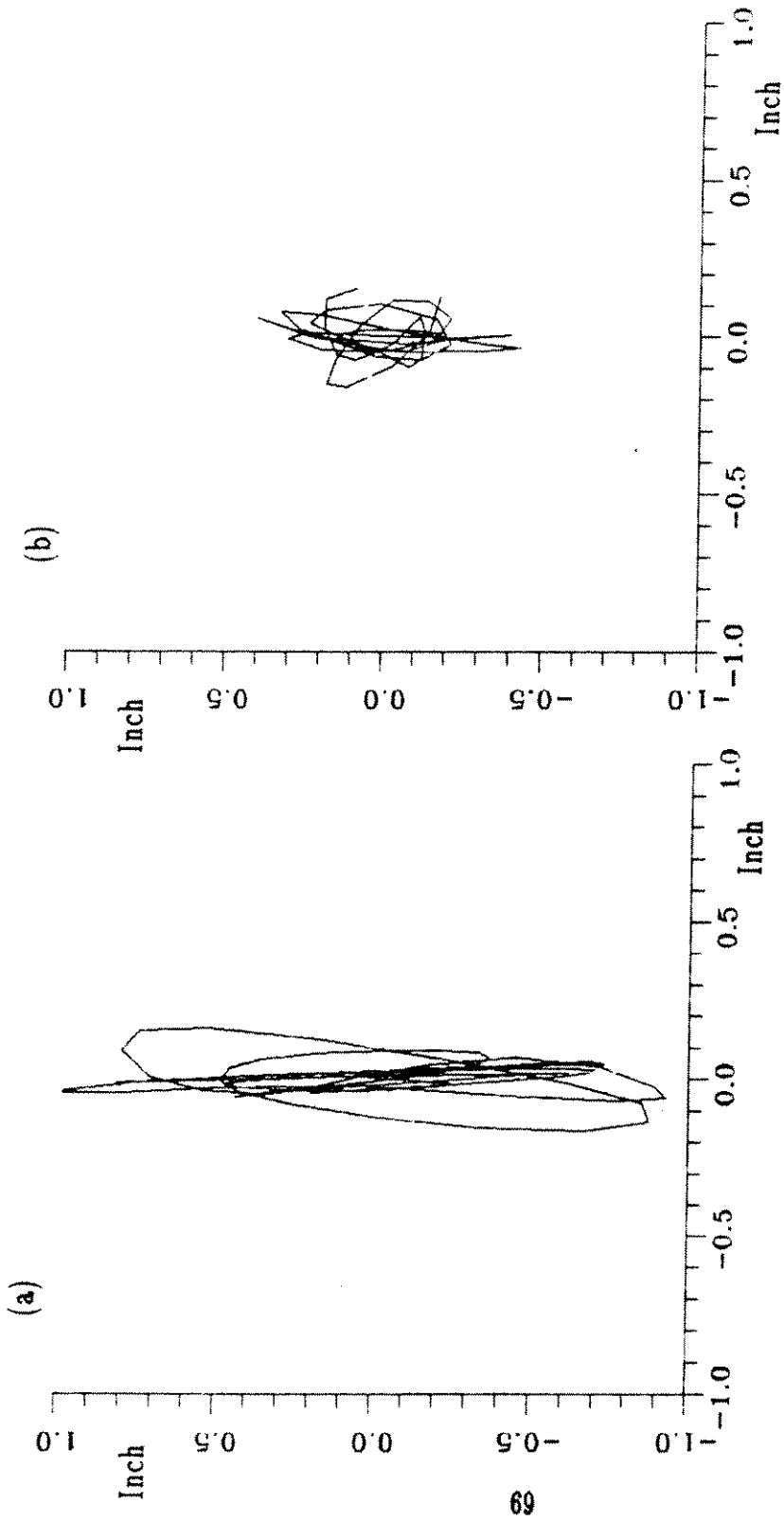


Fig. 3.20 Displacement trajectories at L/4 (SL)
 (a) Bare cable, ref. vel. 2.51 ft/sec, Sheared Low tension
 (b) Triple helical, ref. vel. 2.50 ft/sec, Sheared Low tension

integer times of the shedding frequency. (See Fig. 9.13, 9.15, and 9.17.)

It is generally known that the in-line vibration frequency is approximately twice that of the cross-flow vibration frequency, and that there are certain relations between two vibration modes(33). Consequently, the cross-flow vibration is slightly⁹ affected by the in-line vibration. The in-line and cross-flow correlation explains the frequency doubling or multiplication.

- In bare cable(type 0) and single helical wire(type 1) cases, the 1 and 3 times of the shedding frequency components were much higher than those of 2 and 4 times. But in the triple helical wire(type 2) case, the high frequency components, especially 3 times of the shedding frequency were reduced greatly. (Refer to Fig. 9.14, 9.16, and 9.18.)

The experiment results in Fig. 3.14, and 3.16 reveal that the triple helical wire tends to reduce the high frequency components. The 3 times of the shedding frequency components are believed to be caused by the in-line vibration effects; thus, the reduction of the components explains that the triple helical wire reduces the in-line vibration amplitude and/or the correlation between the cross-flow and in-line vibration. But, the high frequency component is less important when a velocity or displacement is considered¹⁰ because of integration effects.

- In the sheared flow profile, the spectra showed broader band peaks; nevertheless, all aforementioned observations were commonly found(Fig.9.15-18).

From the Strouhal relation(eq. 2.12), the shedding frequency is proportion to flow velocity; thus in a sheared flow pattern, many shedding fre-

⁹ The in-line vibration amplitude is usually much smaller than that of cross-flow.

¹⁰ The velocity or displacement spectrum is obtained by multiplying $(\frac{1}{2\pi f})^2$, or $(\frac{1}{2\pi f})^4$ from acceleration spectra.

quencies are involved. As the exciting force increases with flow velocity, the high velocity region still dominates the vibration of the whole cylinder. This is the reason that the response in sheared flow is broader band than in uniform flow, but many of the characteristics found in uniform flow case are common. These observations were found both in bare cable and cables with suppression devices.

- *In the sheared flow case, the vibration amplitude at $13L/16$ location was smaller than that of $L/4$ location, but the spectra showed almost the same trend (Fig. 3.21, 3.22).*

Low frequency components caused by a local shedding frequency at $13L/16$ was almost negligible; thus, the high velocity region shedding frequency dominated the whole vibration due to the large exciting forces compared with the low velocity region. The hydrodynamic damping also reduced the energy propagation from the high velocity region to the low velocity region.

- *High and low tension cases did not show any striking differences in spectra. However, the high tension case tended to result in slightly narrower band peaks, especially in sheared flow cases. (Refer to Fig. 3.17, and 3.18.)*

In the low tension case, the interval between the natural frequencies for a flexible pin-end cable becomes narrow. As the tension increases, the interval also increases in proportion to the square-root of the tension (\sqrt{T}). For this reason, in the low tension case, many natural frequency modes are easily involved, which tend to scatter the spectra in wide frequency ranges.

- *The rms acceleration and displacement of helical wire type cases (type 1-2) were less than those of a bare cable case. But the performance of the triple helical wire type (type*

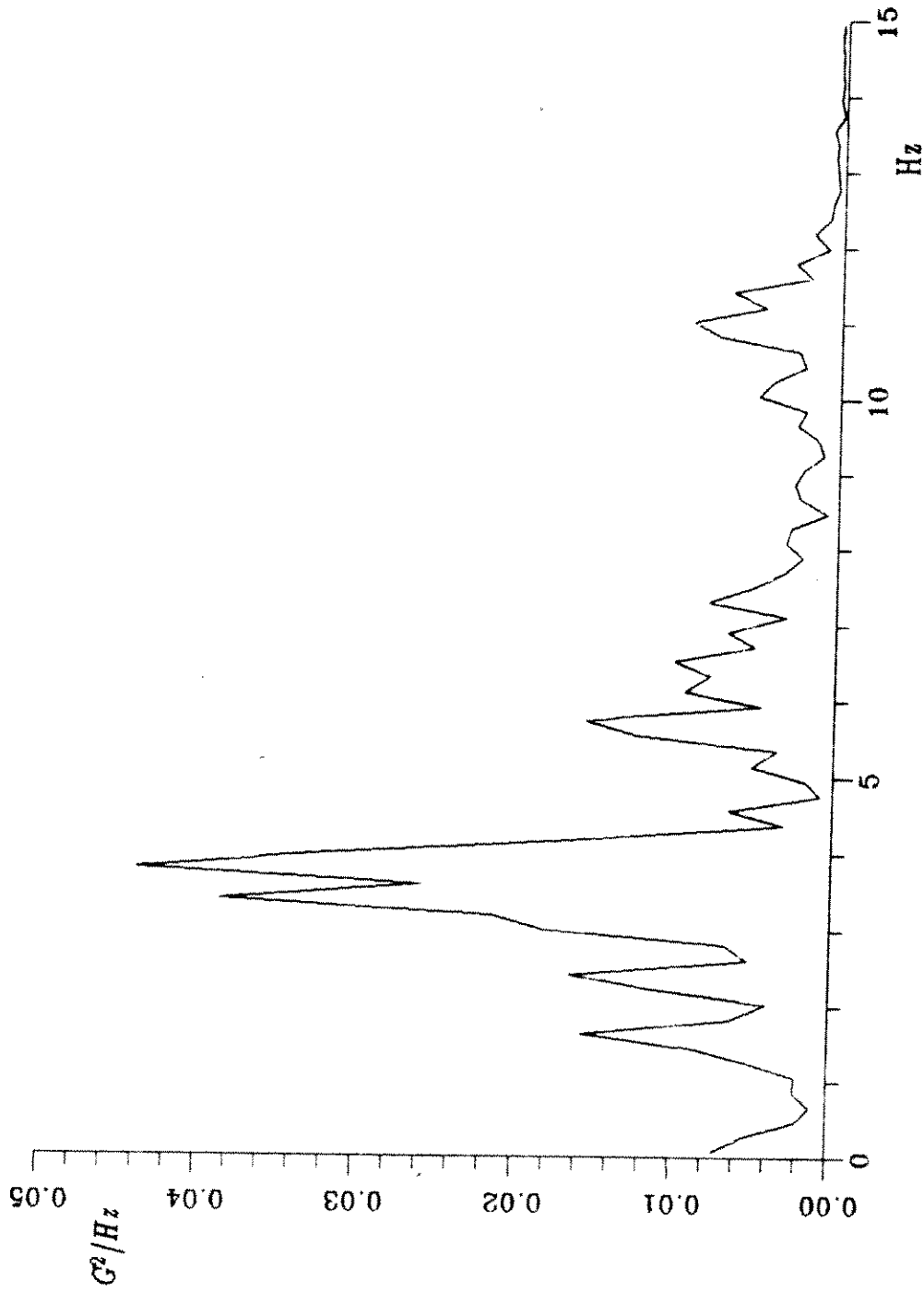


Fig. 3.21 Cross-flow acceleration spectrum at 13L/16 (SL0)
:Bare cable, ref. vel. 2.51 ft/sec, Sheared Low tension

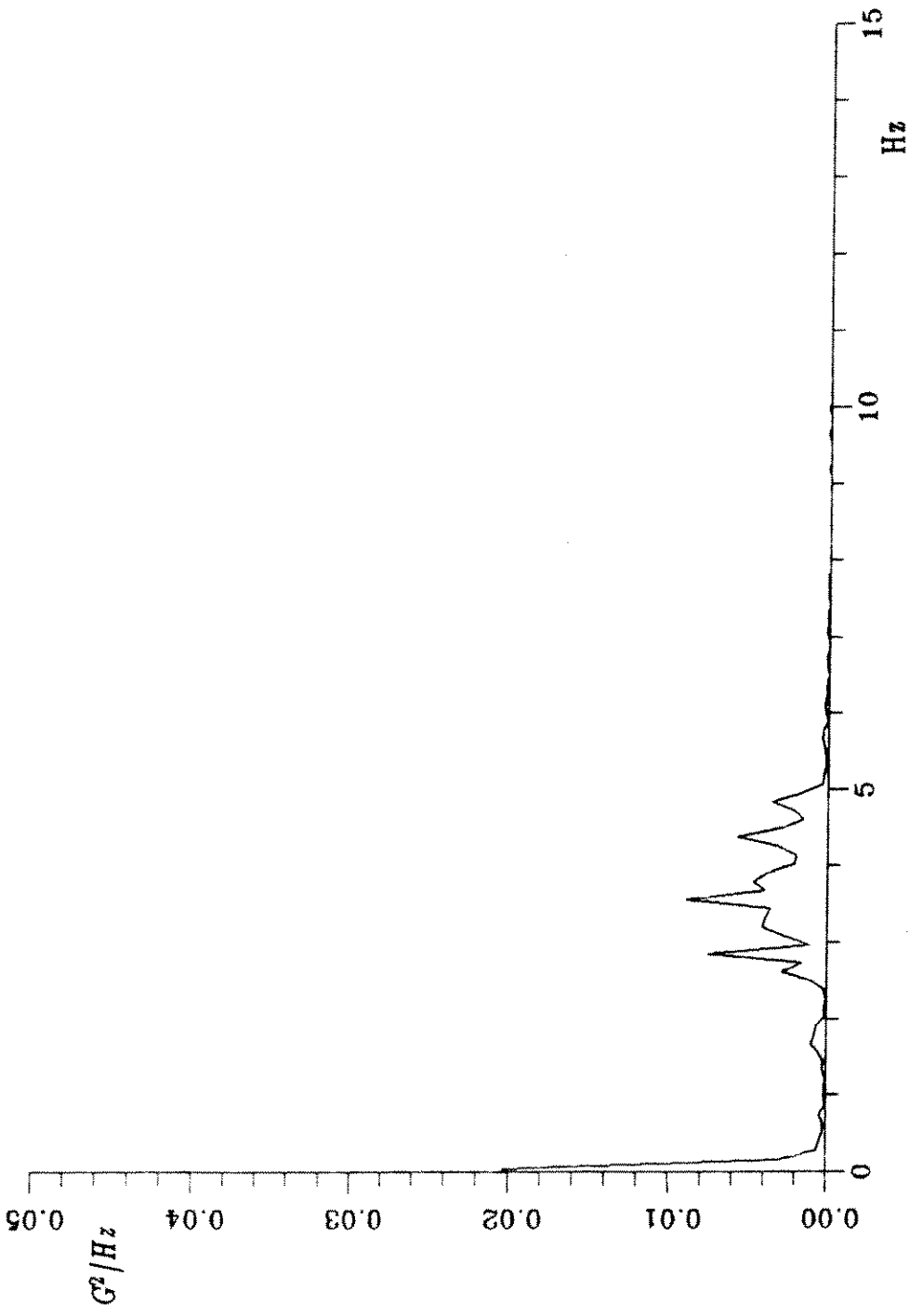


Fig. 3.22 Cross-flow acceleration spectrum at 13L/16 (SL2)
:Triple helical, ref. vel. 2.50 ft/sec, Sheared Low tension

2) was far better than the single wire type (type 1) case. (From Table 3.2, average acceleration of triple helical wire was 0.28, whereas, that of single helical wire was 0.56.)

In helical wire type suppression devices, the performance is strongly dependent upon parameters such as diameter ratio of helical wire to cable, pitch, and number of starts as shown in Fig.2.6.

- Shedding frequencies of the helical wire type case (type 1-2) remained almost as the same as those of bare cable case (Fig.3.14, 3.16).

The geometry changes of helical wires were almost negligible; hence, the shedding frequency remained as a similar range. The suppression devices reduced the amplitude of the exciting force without changing the whole vortex shedding mechanism pattern very much.

3.5.2 Plain flag type devices (type 3-4)

- Shedding frequencies moved to the low frequency region, and frequencies higher than twice of the first shedding frequency almost completely disappeared. Especially in the long flag case (type 3), very low frequency (approx. 1 Hz) components were observed (Fig. 3.23, 3.24).

A cable with a flag type device does not have the same Strouhal number as a circular cable. The flags tend to reduce the Strouhal number, and change the system transfer function due to the increased added mass and damping. As a result, the high frequency components are weakened by the exciting force and the system transfer function, which acts like a low-pass filter.

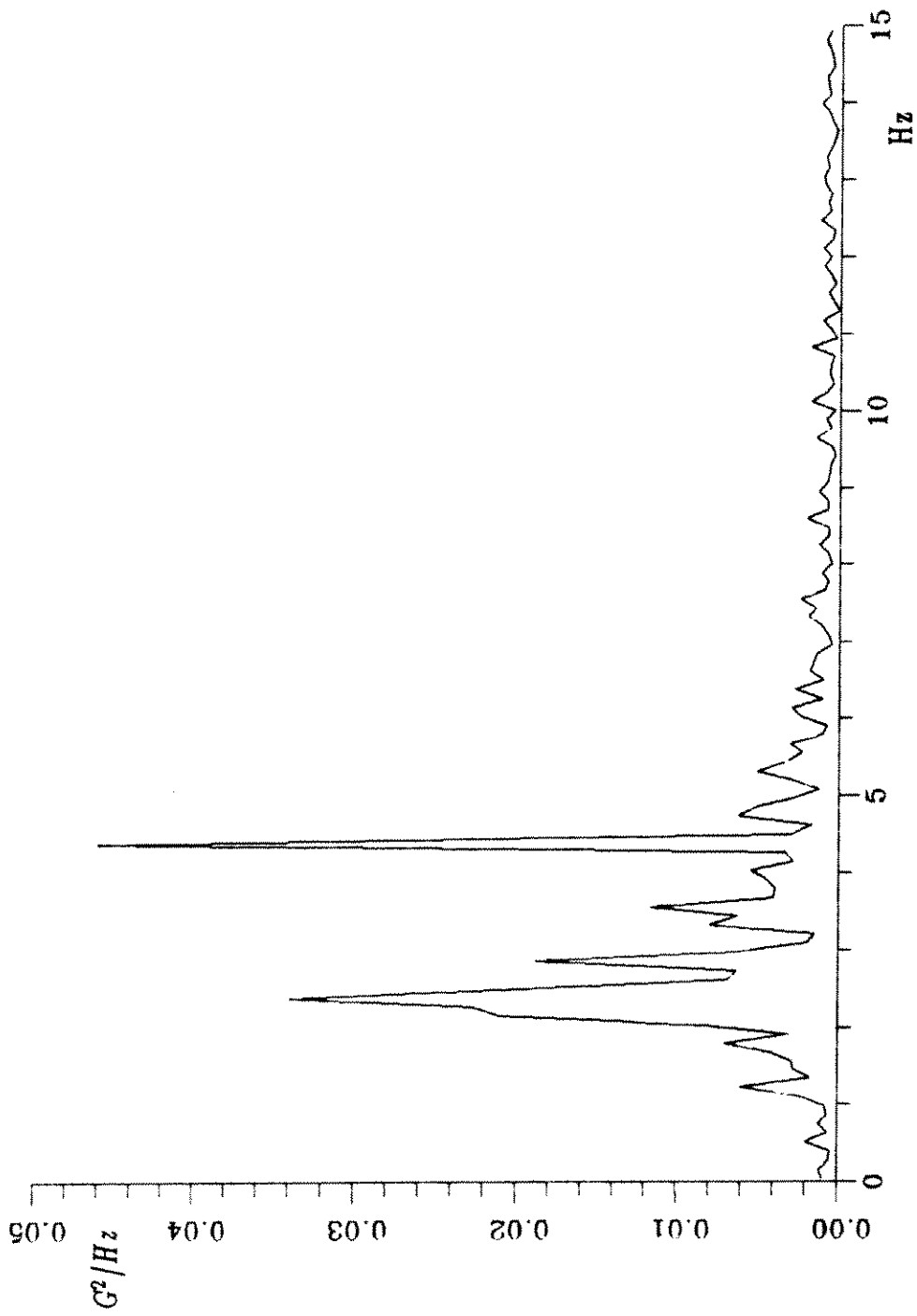


Fig. 3.23 Cross-flow acceleration spectrum at L/4 (SL3)
:Plain long flag, ref. vel. 3.22 ft/sec, Sheared Low tension

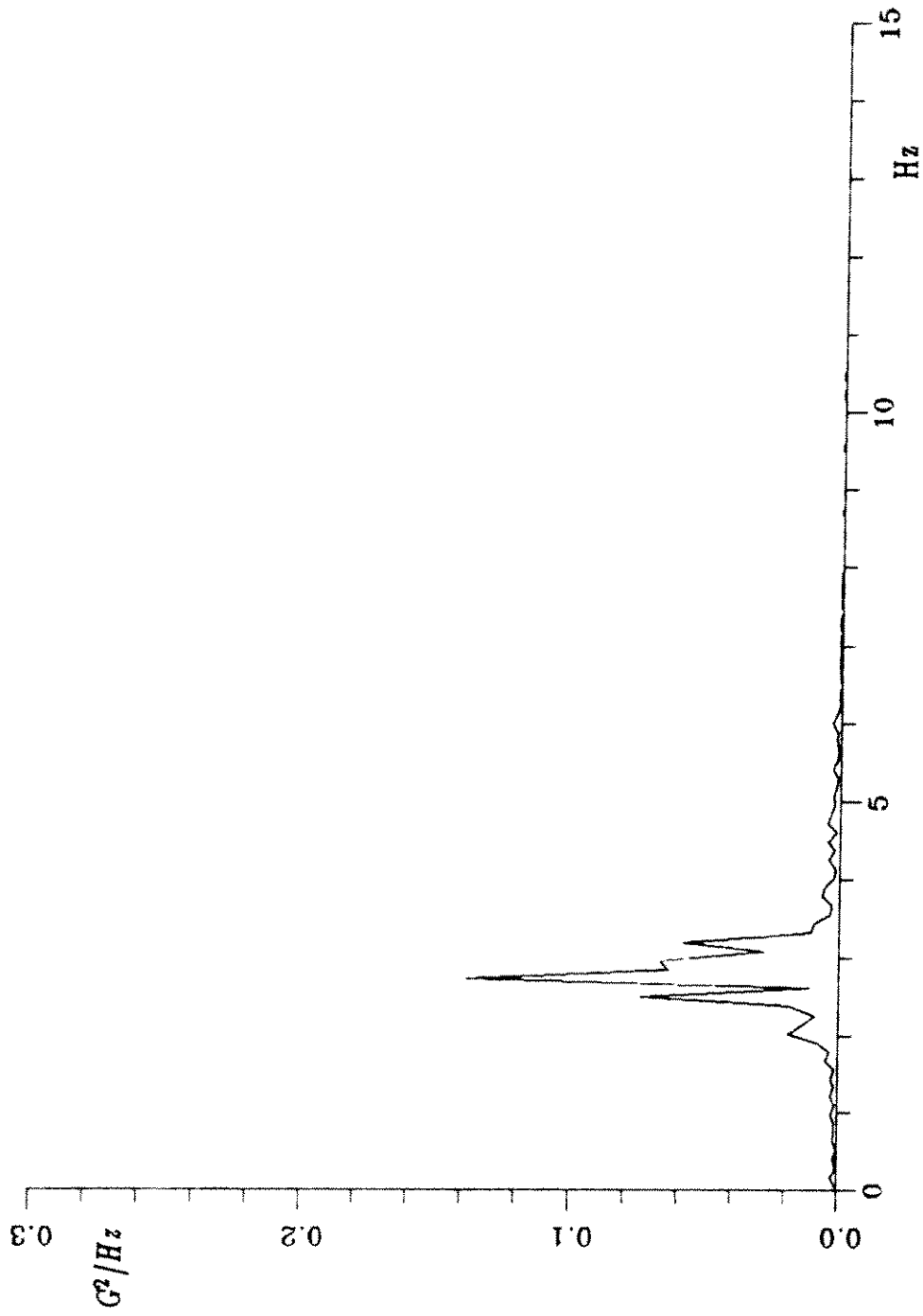


Fig. 3.24 Cross-flow acceleration spectrum at L/4 (SL4)
:Split short flag, ref. vel. 3.16 ft/sec, Sheared Low tension

- *In the short flag(type 4) case, the response showed ordinary vortex vibration pattern, but in the long flag type, the response represented totally different patterns.*

In the short flag case, the flag effects are not great; therefore, the vibration characteristics are not widely different from those of the bare cable case. But, the flag made the vortex-shedding mechanism more complicated by adding the lift problem on the flag. The flag type suppression devices also involve the stability problem like galloping. The galloping is explained by the stability condition shown in Section 2.2.6. The responses of the flag type suppression devices are the combination of the vortex vibration and the galloping problem.

- *The rms accelerations for flag type devices reduced remarkably, but the displacements were difficult to calculate exactly because of the low frequency noise and galloping components.*

As shown in eqns. (3.2) and (3.3), the displacement spectrum is very much affected by the cut-off frequency. In flag type devices, the acceleration signal also contains quite a low frequency signal; thus, it is not easy to eliminate the noise components from the signal. Since the time domain displacement is sensitive to low frequency components, suitable filtering processes had to be used.

3.5.3 Split flag type devices(type 5-6)

- *Split flags showed similar results as plain flag type devices. Most of the observations in section 3.5.2 were commonly found. (Refer to Fig. 3.25.)*

Basically, the split flag had the same features as the plain flags, except

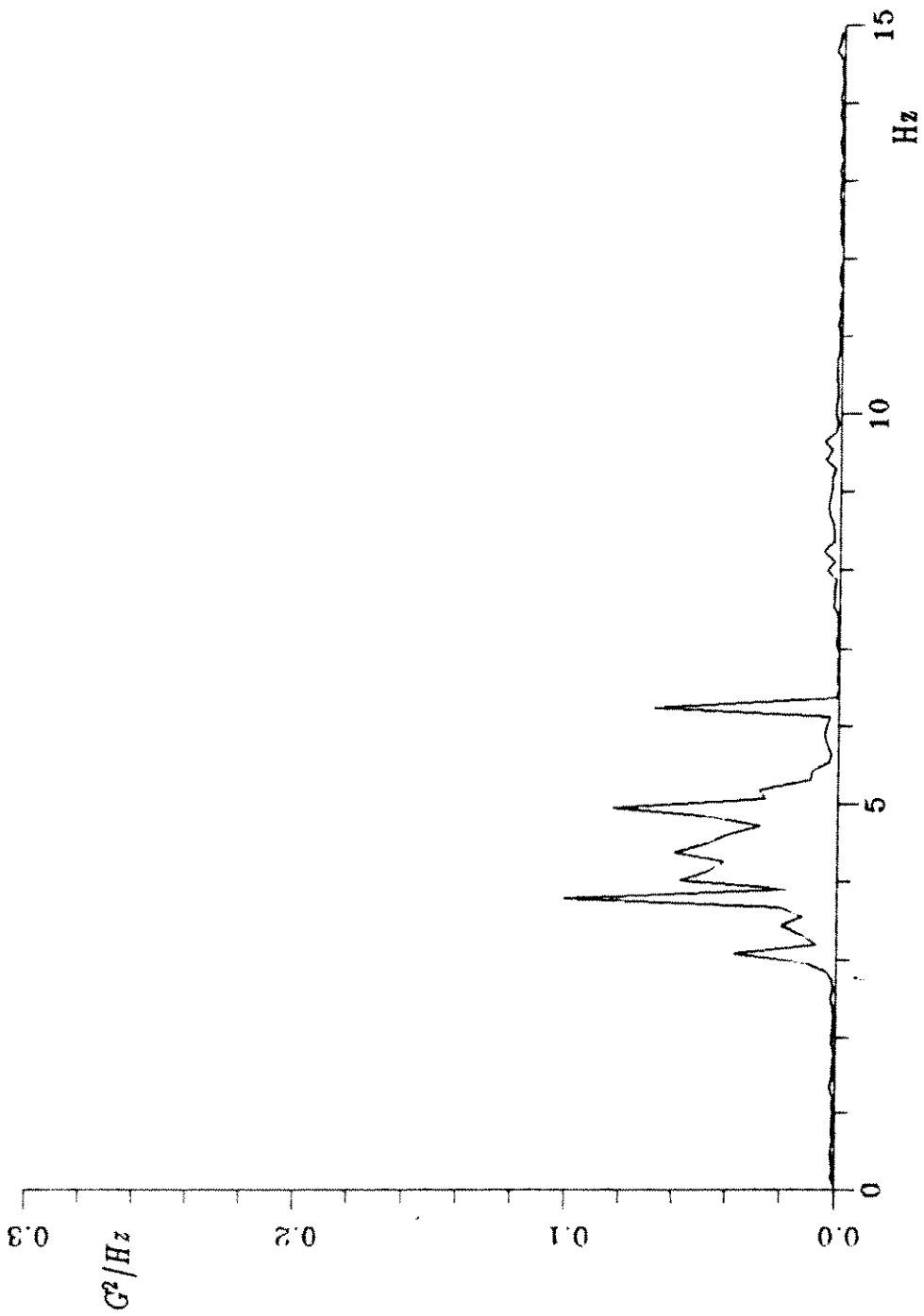


Fig. 3.25 Cross-flow acceleration spectrum at L/4 (SL6)
:Split short flag, ref. vel. 3.34 ft/sec, Sheared Low tension

that the former had slits inside the flag; therefore, most of the characteristics are expected to be the same.

- *In split long flag(type 5), the vibration amplitudes were reduced to almost negligible level. However, the drag forces were increased significantly¹¹.*

In addition to the flags, the slits increased the frontal area normal to the flow direction, which resulted in the large drag. Flag type devices are known to increase the drag, and the slits in the split flag increased the drag additionally, which resulted in larger drag than plain flags case. It was found that the split long flag(type 5) suppression device is not suitable for most of the applications due to the large drag.

- *In the split long flag suppression device, the in-line(horizontal) direction displacement of the cable was larger than the cross-flow(vertical) direction displacement.*

Normally, the cross-flow vibration is greater than the in-line vibration in vortex-induced vibration, however, unexpected large in-line vibration was occurred. It is believed that the large drag force and its fluctuation influenced the in-line motion greatly. (Refer to Fig. 3.26¹².)

It is also expected that the unsteadiness of the flow condition could affect the low frequency drag and in-line(horizontal) displacement.

¹¹ The drag force was not measured quantitatively, but large drag was observed during the experiment.

¹² The figures were made by double integrating the time series acceleration(cut-off frequency of 0.5 Hz), hence the displacements may be affected by the filtering and related data processes.

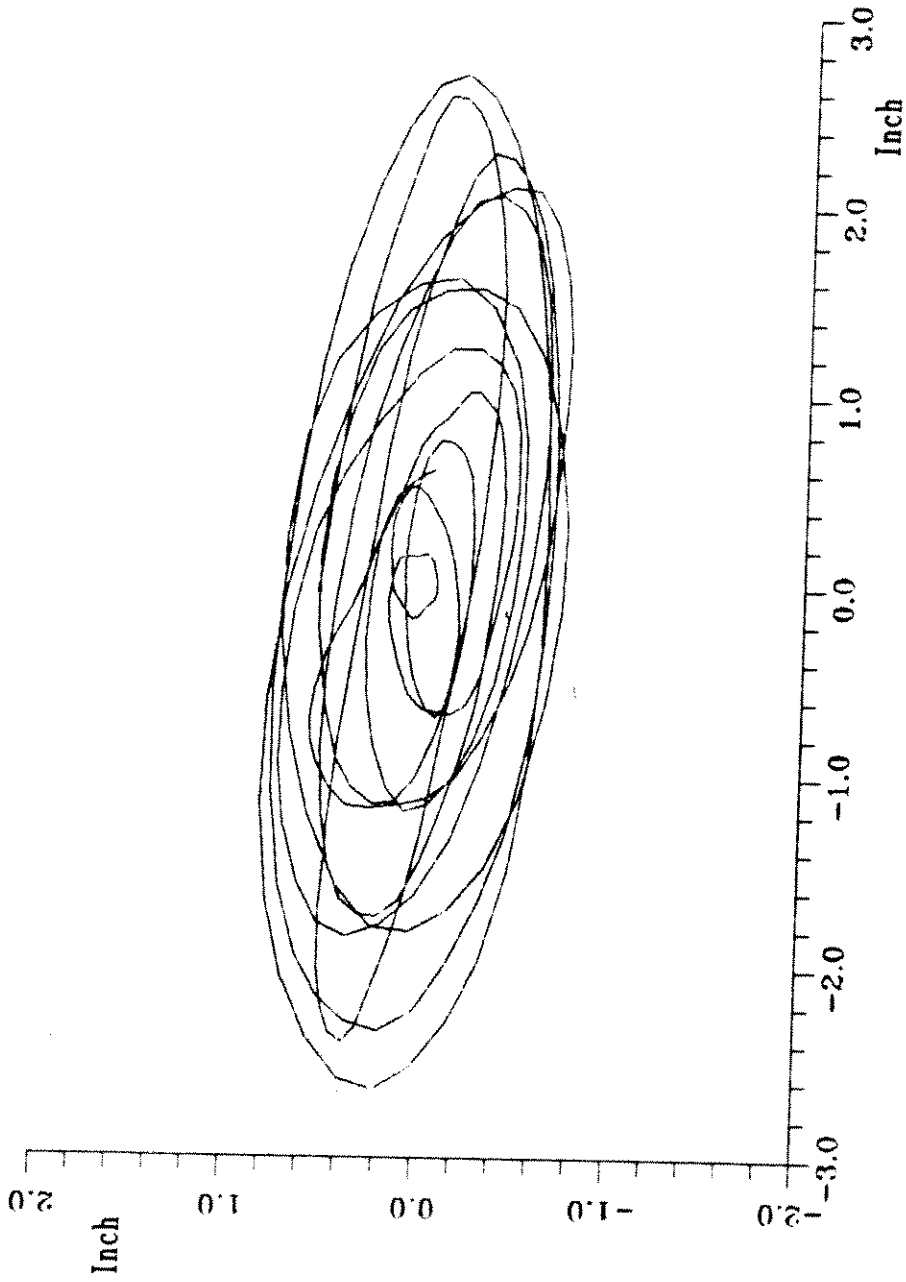


Fig. 3.26 Displacement trajectories at L/4 (UL5)
:Split long flag, ref. vel 1.55 ft/sec, Uniform Low tension

Chapter 4

Summary and Conclusions

- Experiments on helical wire and flag type vortex-vibration suppression devices were carried out.
- As expected, the helical wire and flag types of suppression devices were proved to be partially effective both in the uniform and the sheared flow. However, some of the uncertainties during the experiments on flag type suppression devices made the further analysis difficult.
- In helical type suppression devices, the performance were very much affected by parameters such as wire to cable diameter, pitch, and number of starts.
- The flag type devices reduced the vibration level, but greatly increased the in-line drag force. Therefore, the flag type device is not suitable for applications where large drag is not allowed.
- The flag type devices also caused stability problems, such as galloping. The stability condition in Section 2.2.6 should be considered in the design of wake stabilizer type suppression devices.
- Mechanisms of vortex vibration and the suppression devices were reviewed for theoretical background of the experimental result analysis and their engineering applications.
- The mechanisms studied in Chapter 2 and the experimental results in Chapter

3 may be used as the basis of design guidance of the vortex-induced vibration.

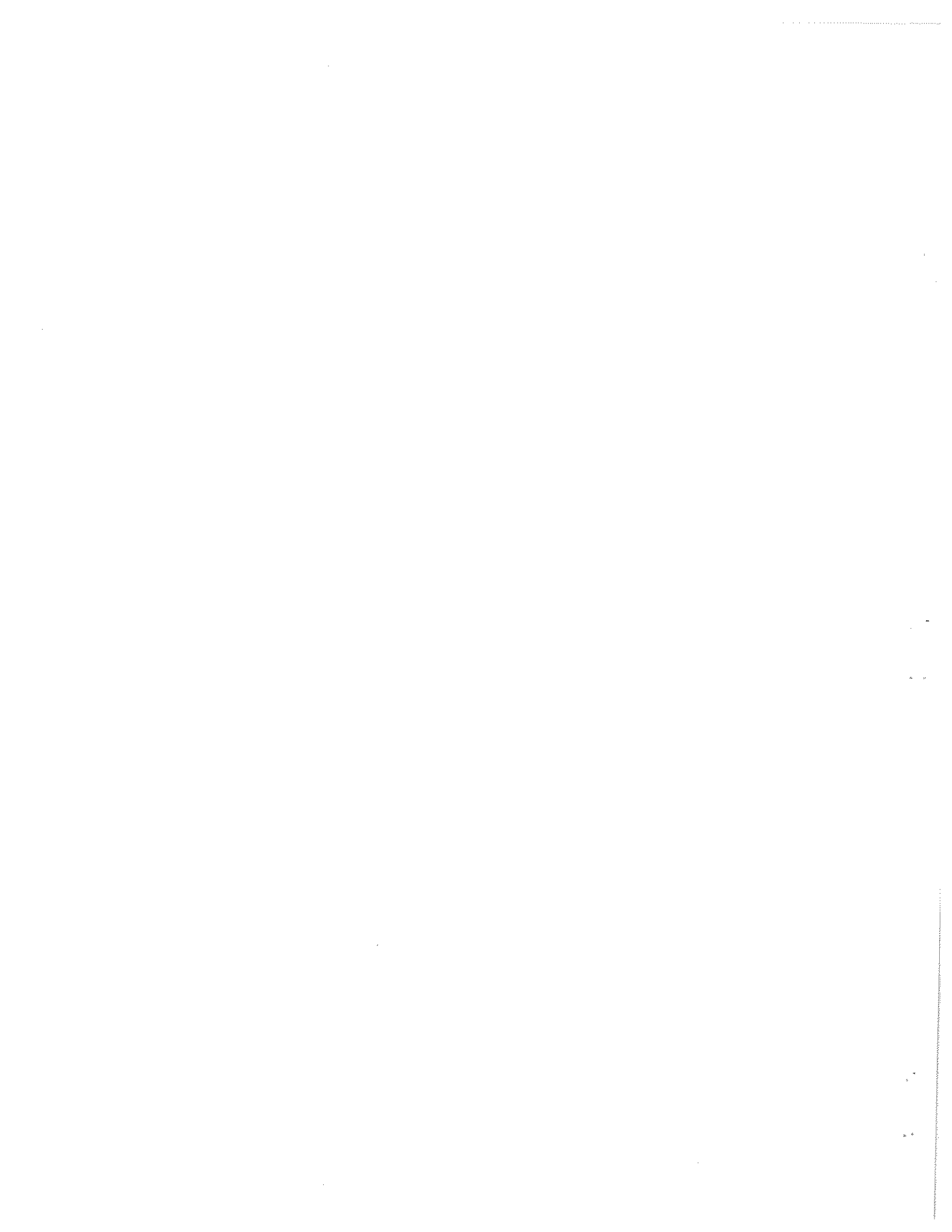
- In a vortex-induced vibration field, experiments are important for engineering applications, and the experiments should be done carefully, fully considering their conditions and variables.
- Data obtained in Lawrence experiment, whether used in this thesis or not, will be useful for future studies on vibration suppression devices. Especially, more extensive studies on helical wire type suppression devices may be made from the experimental data.

References

1. Shanks, F. E., "High-Current, Deepwater Drilling Experiences", SPE/IADC 13491, *SPE/IADC Drilling Conference*, 1985.
2. Gardner, Terry N., and Cole, M. Wayne, "Deepwater Drilling in High Current Environment", *Offshore Technology Conference*, OTC 4316, 1982.
3. Brown, Derek, and Bartle, Mike, "The Cause and Cure of Vibration-Induced Failure of Drill Casing in High Tidal Currents", EUR 338, *European Petroleum Conference*, 1982.
4. Grant, Robert, "Riser Fairing for Drag and Vortex Suppression", OTC 2921, *Offshore Technology Conference*, 1977.
5. Fisher, F. Joseph, Jones, Warren T., and King, Roger, "Current-Induced Oscillations of Cognac Piles During Installation - Prediction and Measurement".
6. Hays, E. E., Nowak, Richard T., and Boutin, Paul. R., "Strumming Tests on Two Faired Cables", unpublished, Woods Hole Oceanographic Institution Report WHOI-75-47, 1975.
7. Meirovitch, L., *Elements of Vibration Analysis*, McGraw-Hill, Inc., 1975.
8. Newland, D. E., *An Introduction to Random Vibration and Spectral Analysis*, Longman Inc., 1984.
9. Vandiver, J. K., and T. Y. Chung, "Hydrodynamic Damping on Flexible Cylinders in Sheared Flow", OTC 5524, *Offshore Technology Conference*, 1987.
10. Prandtl, L., "The Generation of Vortices in Fluids of Small Viscosity", *J. Royal Aero/ Soc.*, 1929.
11. Perry, A. E., Chong, M. S., and Lim, T. T., "The Vortex-shedding Process Behind Two-dimensional Bluff Bodies", *Journal of Fluid Mechanics*, Vol. 116, pp 77-90, 1982.
12. Cantwell, B. and Coles, D., "An Experimental Study of Entrainment and Transport in the Turbulent Near Wake of a Circular Cylinder", *Journal of Fluid Mechanics*, Vol. 136, pp 321-374, 1983.
13. Triantafyllou, G. S., Triantafyllou, M. S., and Chryssostomidis, C., "On the Formation of Vortex Streets Behind Stationary Cylinders", *Journal of Fluid Mechanics*, Vol. 170, pp 461-477, 1986.
14. Perry, A. E. and Steiner, T.R., "Large-scale Vortex Structures in Turbulent

- Wakes Behind Bluff Bodies. Part 1. Vortex Formation", *Journal of Fluid Mechanics*, Vol. 174, pp 233-270, 1987.
15. Steiner, T. R. and Perry, A. E., "Large-scale Vortex Structures in Turbulent Wakes Behind Bluff Bodies. Part 2. Far-wake Structures", *Journal of Fluid Mechanics*, Vol. 174, pp 271-298, 1987.
 16. Nakamura, Y. and Ohya, Y., "Vortex Shedding from Square Prisms in Smooth and Turbulent Flows", *Journal of Fluid Mechanics*, Vol. 164, pp 77-89, 1986.
 17. Shewe, G., "On the Force Fluctuations Acting on a Circular in Crossflow from Subcritical up to Transcritical Reynolds Numbers" *Journal of Fluid Mechanics*, Vol. 133, pp 265-285, 1983.
 18. King, Roger, "A Review of Vortex Shedding Research and its Application", *Ocean Engineering*, Vol. 4, pp141-171, 1977.
 19. Nath, J. H., "Hydrodynamic Coefficients for Macro-roughnesses", OTC 3989, *Offshore Technology Conference*, 1981.
 20. Apelt, C. J., West, G. S., and Szewczyk, Albin A., "The Effects of Wake Splitter Plates on the Flow Past Circular Cylinder in the $10000 < R < 50000$ ", *Journal of Fluid Mechanics*, Vol 61, pp187-198, 1973.
 21. Bearman, P. W. and Obasaju, E. D., "An Experiment Study of Pressure Fluctuation on Fixed and Oscillating Square-section Cylinders", *Journal of Fluid Mechanics*, Vol. 119, pp 297-321, 1982.
 22. Dalton, C. and Chantranuvatana, B., "Pressure Distributions Around Circular Cylinders in Oscillating Flow", *Journal of Fluids Engineering*, Vol. 102, 191-195, 1980.
 23. Blevins, R. D., *Flow-induced Vibration*, Litton Educational Publishing, Inc., 1977.
 24. Every, M. J., King R., and Weaver, D. S., "A Brief Survey of Vortex Excited Vibrations of Cylinders and Cables in the Marine Environment and Their Suppression".
 25. Walshe, D. E. and Wootton, L. R., "Preventing Wind-induced Oscillation of Structures of Circular Section", *Proceedings, Institution of Civil Engineers*, Vol 47, 1970.
 26. Zdravkovich, M. M., "Modification of Vortex Shedding in the Synchronization Ranges", *Journal of Fluids Engineering*, Vol. 104, 1982.
 27. Zdravkovich, M. M., "Review and Classification of Various Aerodynamic and Aerodynamic Means for Suppressing Vortex Shedding", *Journal of Wind Engineering and Industrial Aerodynamics*, Vol 7, 1981.

28. Weaver, W., "Wind-Induced Vibrations in Antenna Members, *Journal of Engineering Mechanics Div.*, 87, 1961.
29. Hafen, B. F., Meggit, D. J., and Lin, F. C., "Strumming Suppression - An Annotated Bibliography", Civil Engineering Laboratory Technical Memorandum M-44-76-5, Naval Construction Battalion Center.
30. Gerrald, J. H., "The Mechanics of the Formation Region of Vortices Behind Bluff Bodies", *Journal of Fluid Mechanics*, Vol 25, pp401-413, 1966.
31. Vandiver, J. K. and Pham, T. Q., "Performance Evaluation of Various Strumming Suppression Devices", Report Number 77-2, Massachusetts Institute of Technology, 1977.
32. Chung, T. Y., "Vortex-Induced Vibration of Flexible Cylinders in Sheared Flows", Ph. D. thesis, Massachusetts Institute of Technology, 1987.
33. Jong, J. Y., "The Quadratic Correlation Between In-line and Cross-flow Vortex-Induced Vibration of Long Flexible Cylinders", Ph. D. thesis, Massachusetts Institute of Technology, 1984.



Appendix

Rms values of acceleration and displacement for helical wire suppression devices in "additional low sheared flow" (flow profile 'SFPA' in Fig. A.1) were summarized in Table A.1. Fig. A.2-3, and Fig. A.12-13 are time series cross-flow acceleration signals at $L/4$ and $13L/16$ locations, and Fig. A.4-9, and Fig. A.14-19 are the spectra. The displacement trajectories of $L/4$ location are shown in Fig. A.10-11.

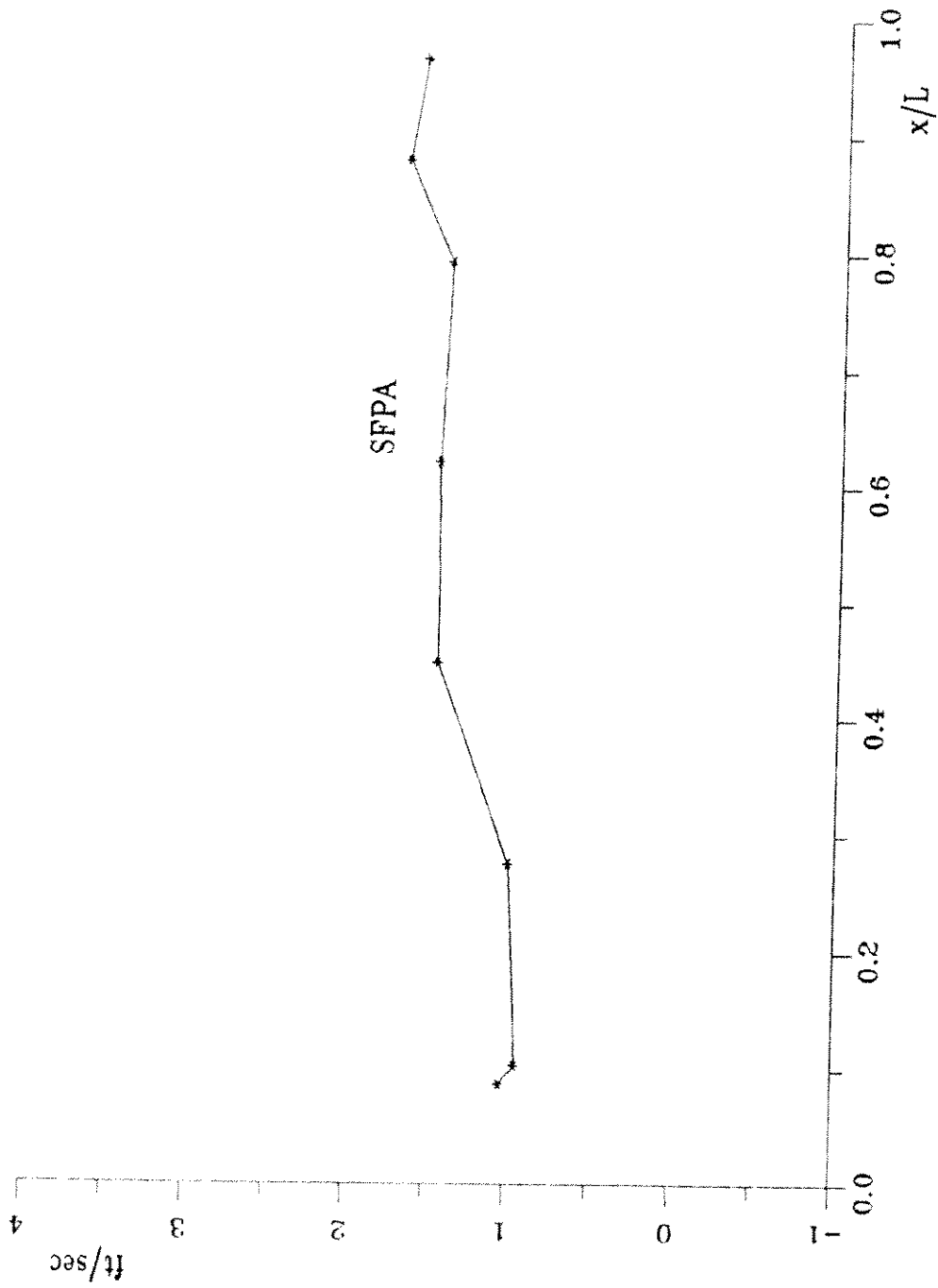


Fig. A.1 Additional low sheared flow profile

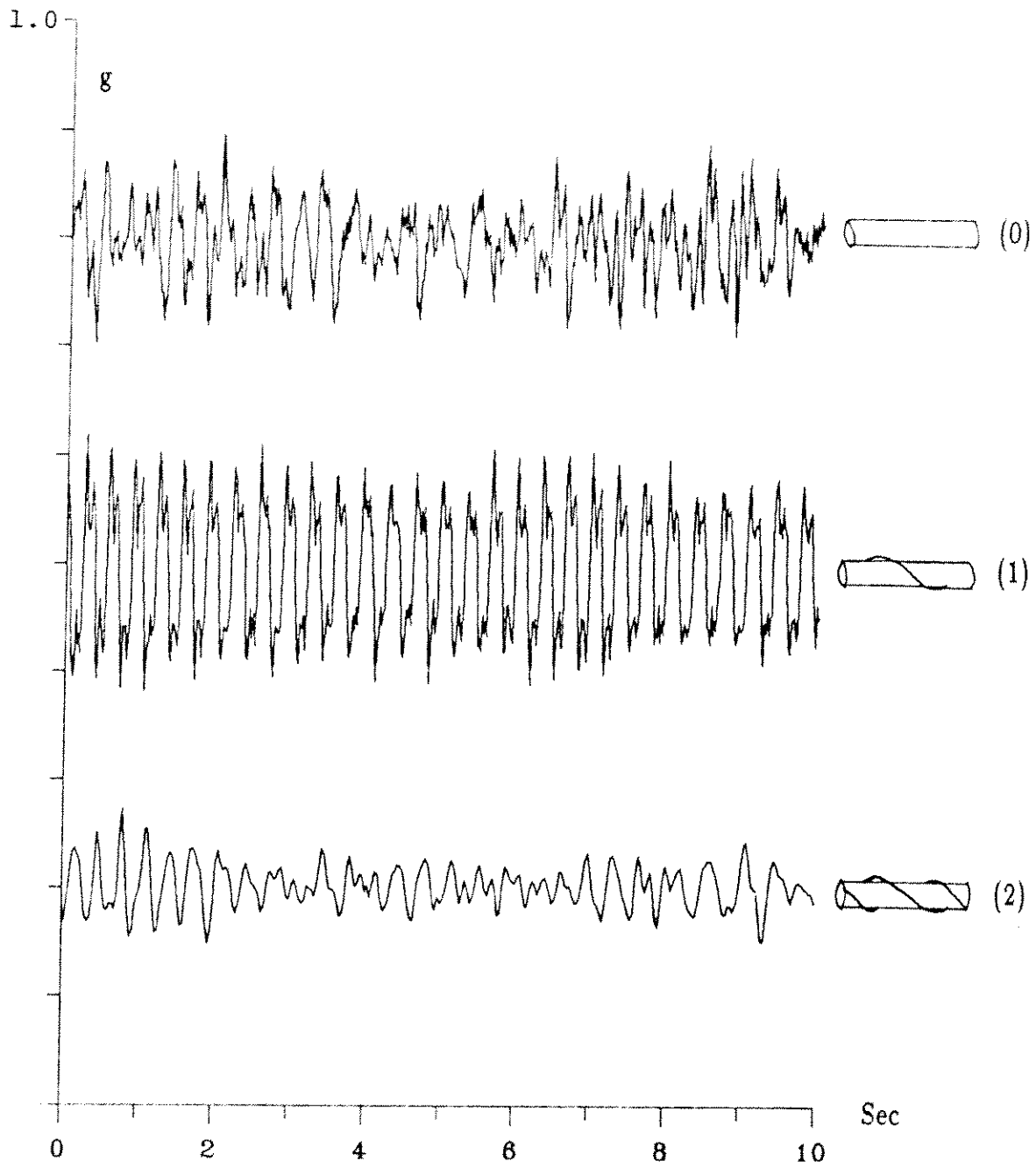


Fig. A.2 Time series cross-flow accel. signals at $L/4$
: Additional low sheared low tension

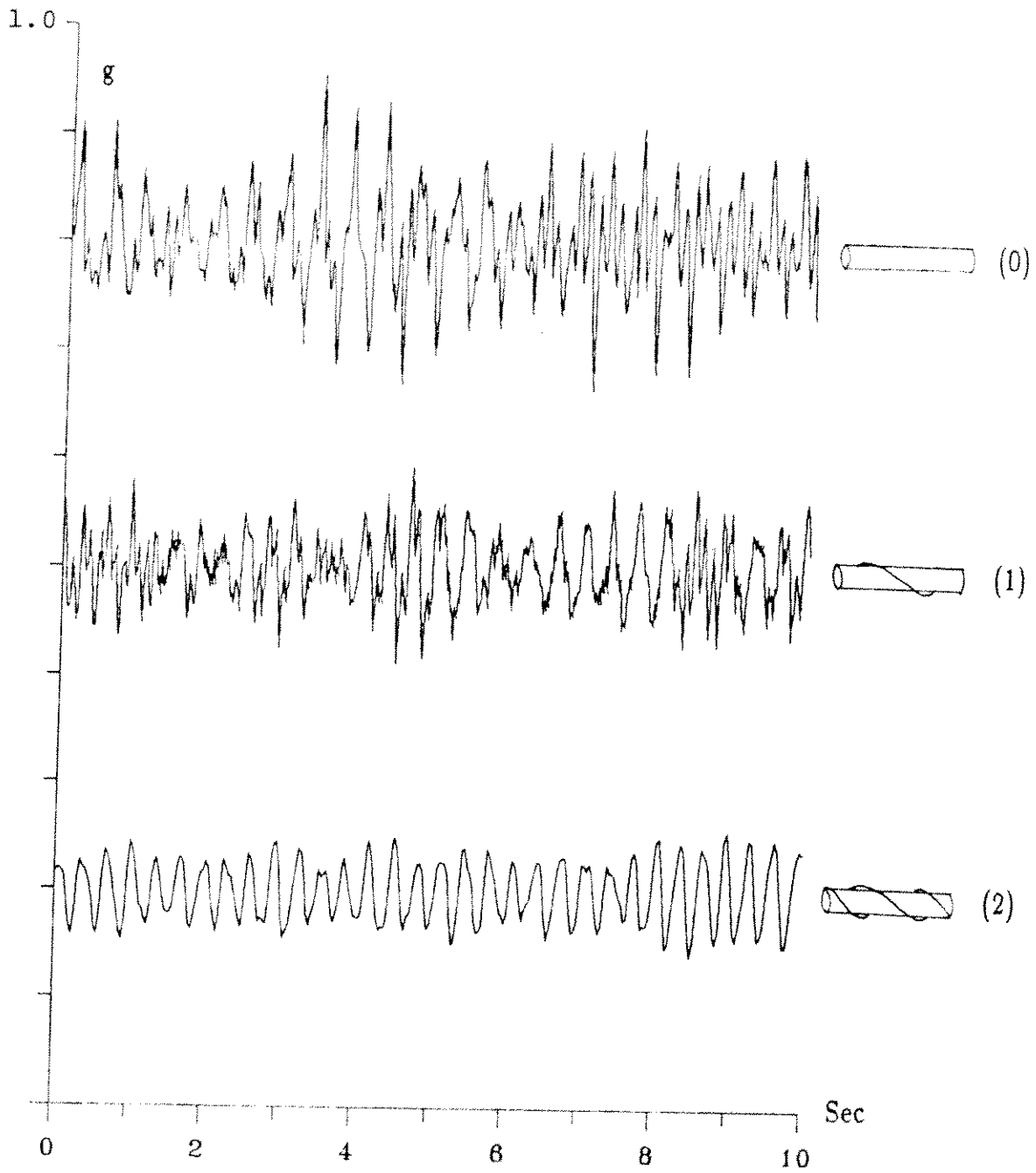


Fig. A.3 Time series cross-flow accel. signals at $L/4$
: Additional low sheared high tension

RMS Type	Acceleration (g)		Displacement (in)	
	2.0 Hz ¹	0.5 Hz	2.0 Hz ¹	0.5 Hz
at L/4				
Bare Cable(AL0) ²	0.371	0.382	0.379	0.566
Single Helical(AL1)	0.545	0.546	0.581	0.597
Triple Helical(AL2)	0.182	0.190	0.218	0.287
Bare Cable(AH0) ³	0.461	0.464	0.567	0.615
Single Helical(AH1)	0.273	0.278	0.302	0.358
Triple Helical(AH2)	0.261	0.262	0.277	0.296
at 13L/16				
Bare Cable(AL0) ²	0.305	0.305	0.252	0.269
Single Helical(AL1)	0.184	0.185	0.186	0.204
Triple Helical(AL2)	0.149	0.150	0.156	0.175
Bare Cable(AH0) ³	0.275	0.275	0.347	0.355
Single Helical(AH1)	0.373	0.374	0.418	0.441
Triple Helical(AH2)	0.244	0.247	0.264	0.292

Hz¹ : cut - off frequency

AL² : Additional low sheared flow low tension case

AH³ : Additional low sheared flow high tension case

Table A.1 Cross-flow RMS value comparison

Type	Profile ¹	Ref. Vel ²	Tension ³	Source ⁴
Bare Cable(AL0)	SFPA	1.051	70	L73120 L/4,13L/16 #11
Single Helical(AL1)	SFPA	1.043	115	L73112 L/4,13L/16 #1
Triple Helical(AL2)	SFPA	1.061	59	L73105 L/4,13L/16 #4
Bare Cable(AH0)	SFPA	1.541	424	L73118 L/4,13L/16 #2
Single Helical(AH1)	SFPA	1.145	329	L73111 L/4,13L/16 #3
Triple Helical(AH2)	SFPA	1.556	547	L73106 L/4,13L/16 #12

Profile¹ : Flow profile pattern shown in figure A.1

Ref. Vel² : Reference flow velocity(ft/sec) measured at L/10 position

Tension³ : Average tension(lb) during measurement

Source⁴ : Source of data(ex. L73105 L/4 #8 : 8th 1024 data at L/4 of run code L73105)

Table A.2 Experiment conditions of Table A.1

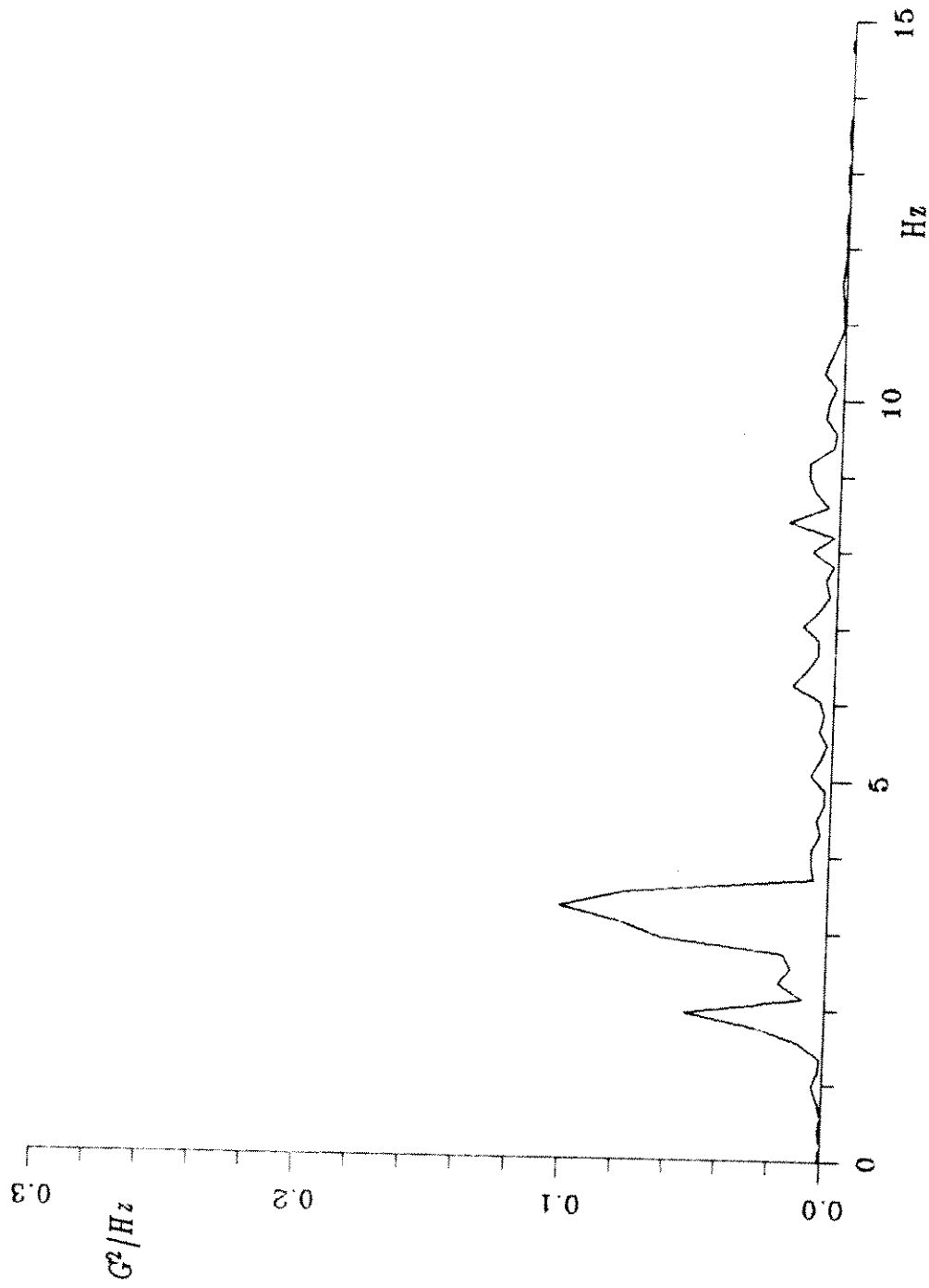


Fig. A.4 Cross-flow acceleration spectrum at L/4 (AL0)
 :Bare cable, ref. vel. 1.05 ft/sec, additional low sheared low tension

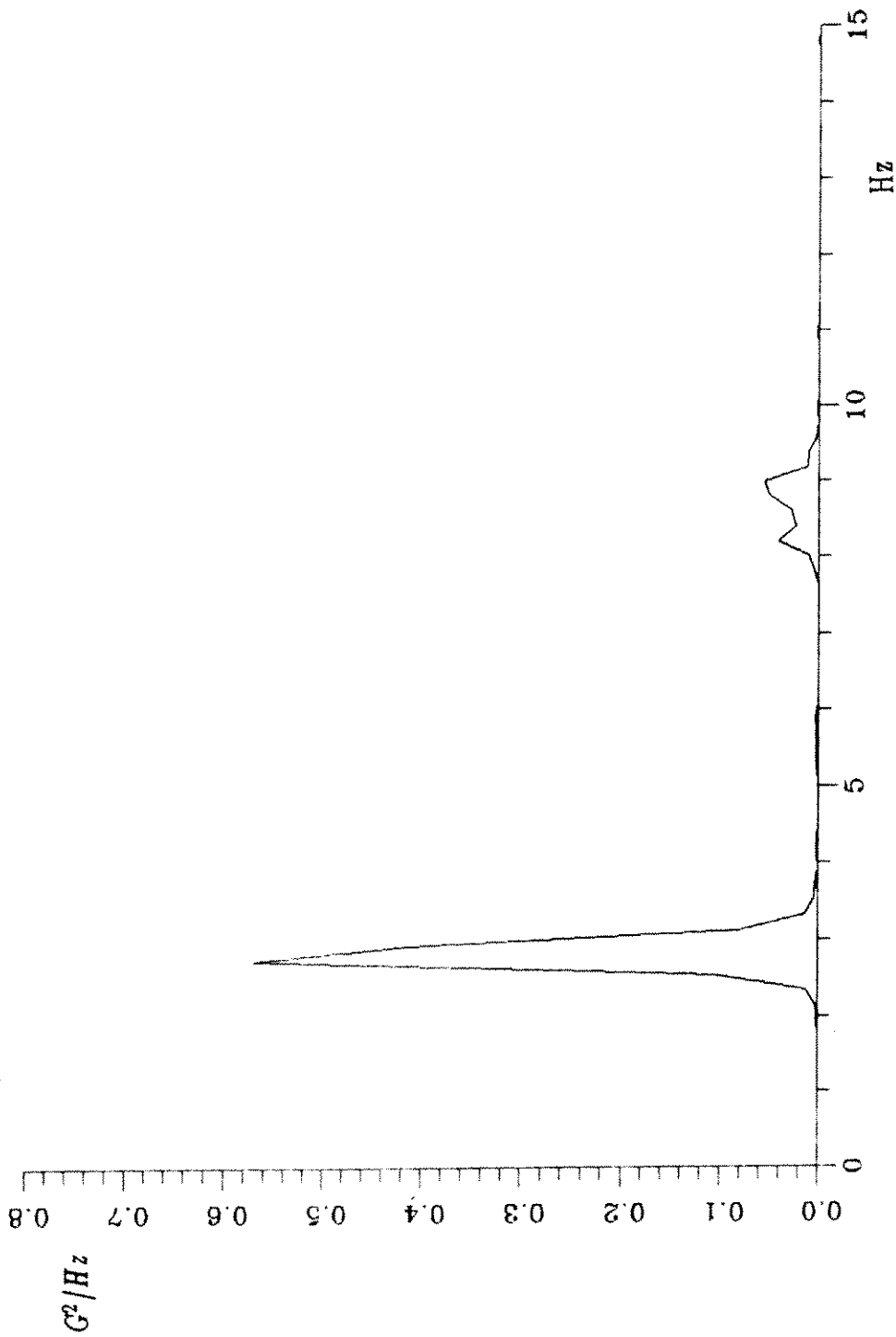


Fig. A.5 Cross-flow acceleration spectrum at L/4 (AL1)
:Single helical, ref. vel. 1.04 ft/sec, additional low sheared low tension

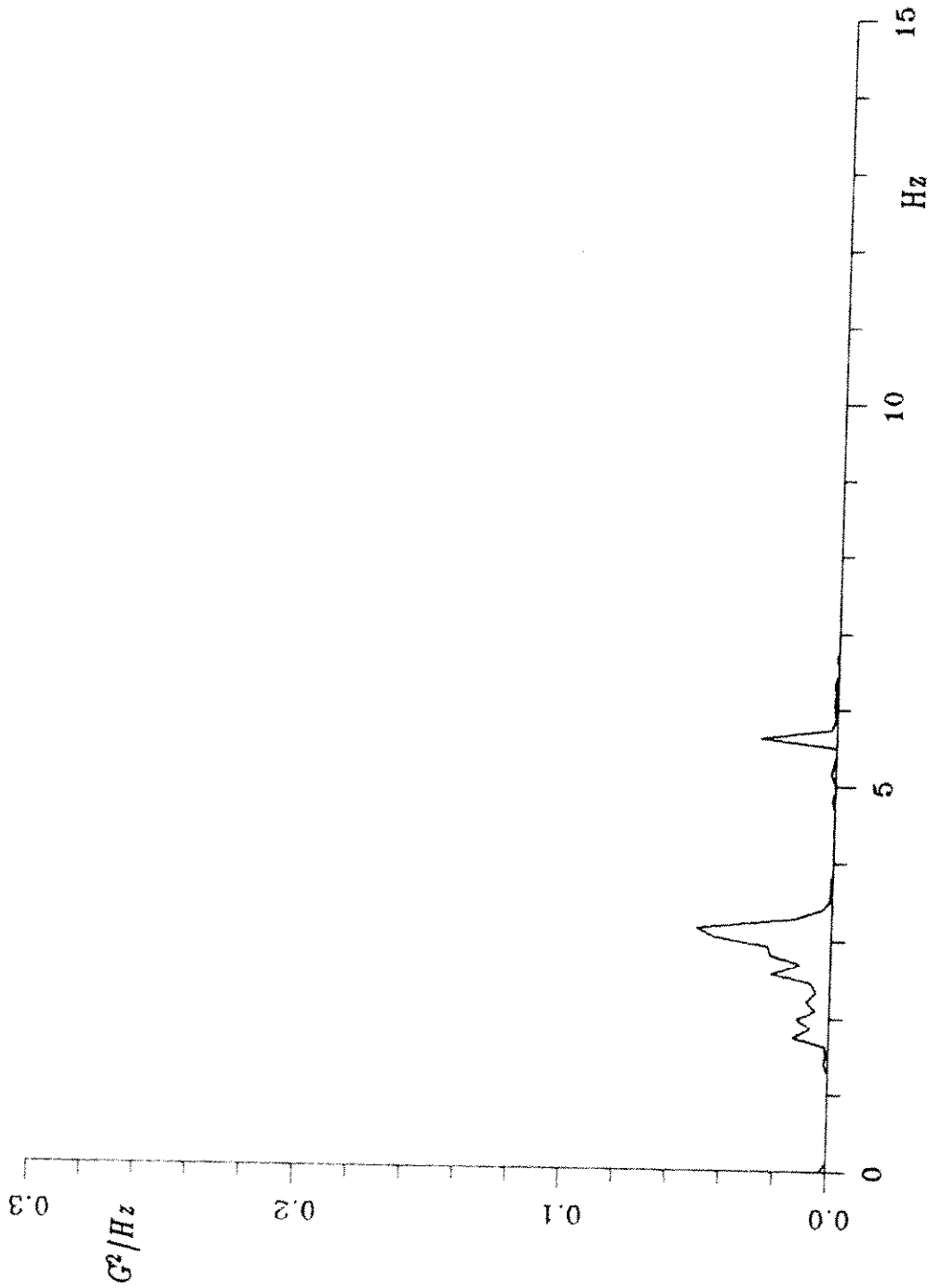


Fig. A.6 Cross-flow acceleration spectrum at L/4 (AL2)
:Triple helical, ref. vel. 1.06 ft/sec, additional low sheared low tension

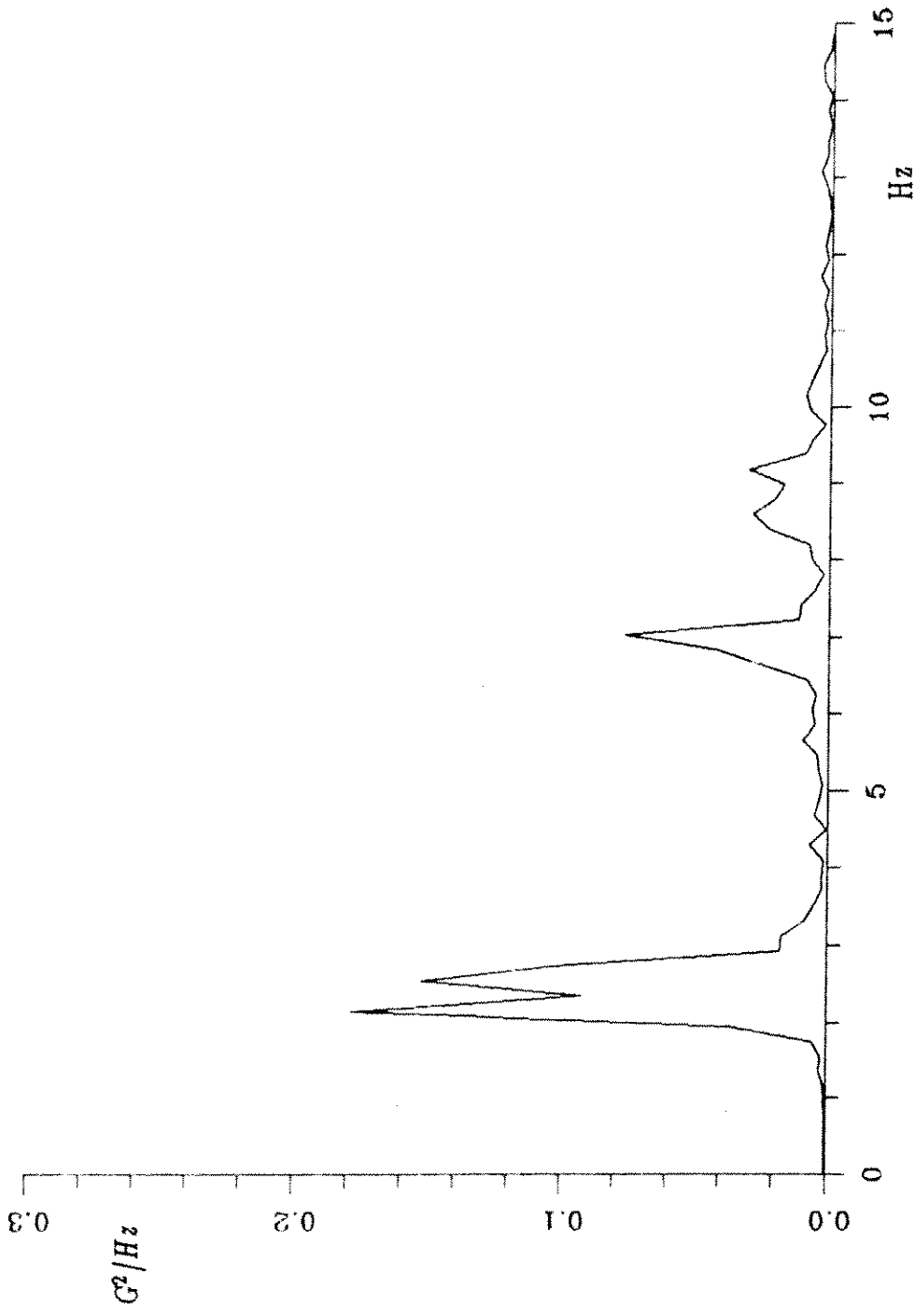


Fig. A.7 Cross-flow acceleration spectrum at L/4 (AH0)
 :Bare cable, ref. vel. 1.54 ft/sec, additional low sheared high tension

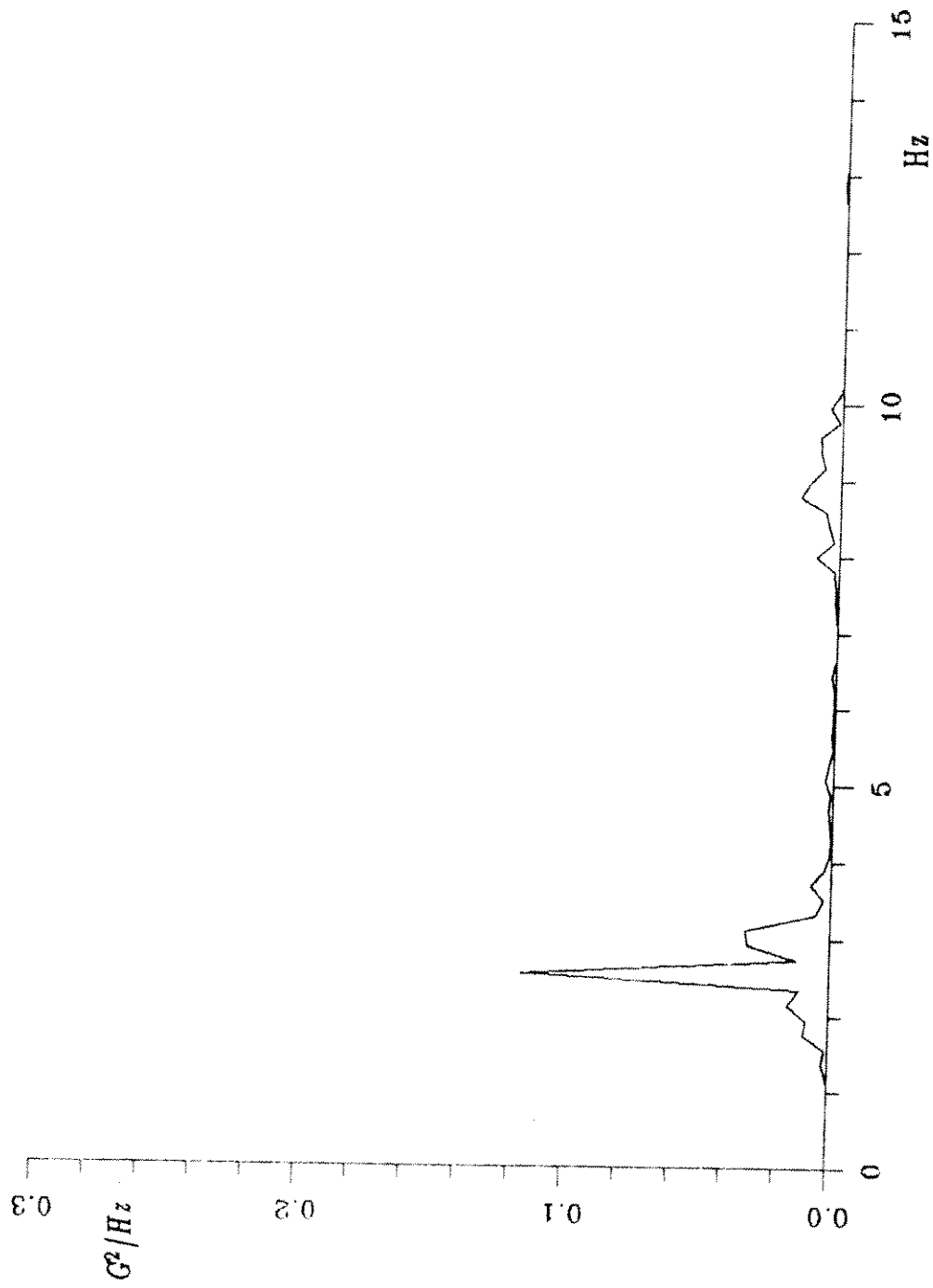


Fig. A.8 Cross-flow acceleration spectrum at L/4 (AH1)
:Single helical, ref. vel. 1.15 ft/sec, additional low sheared high tension

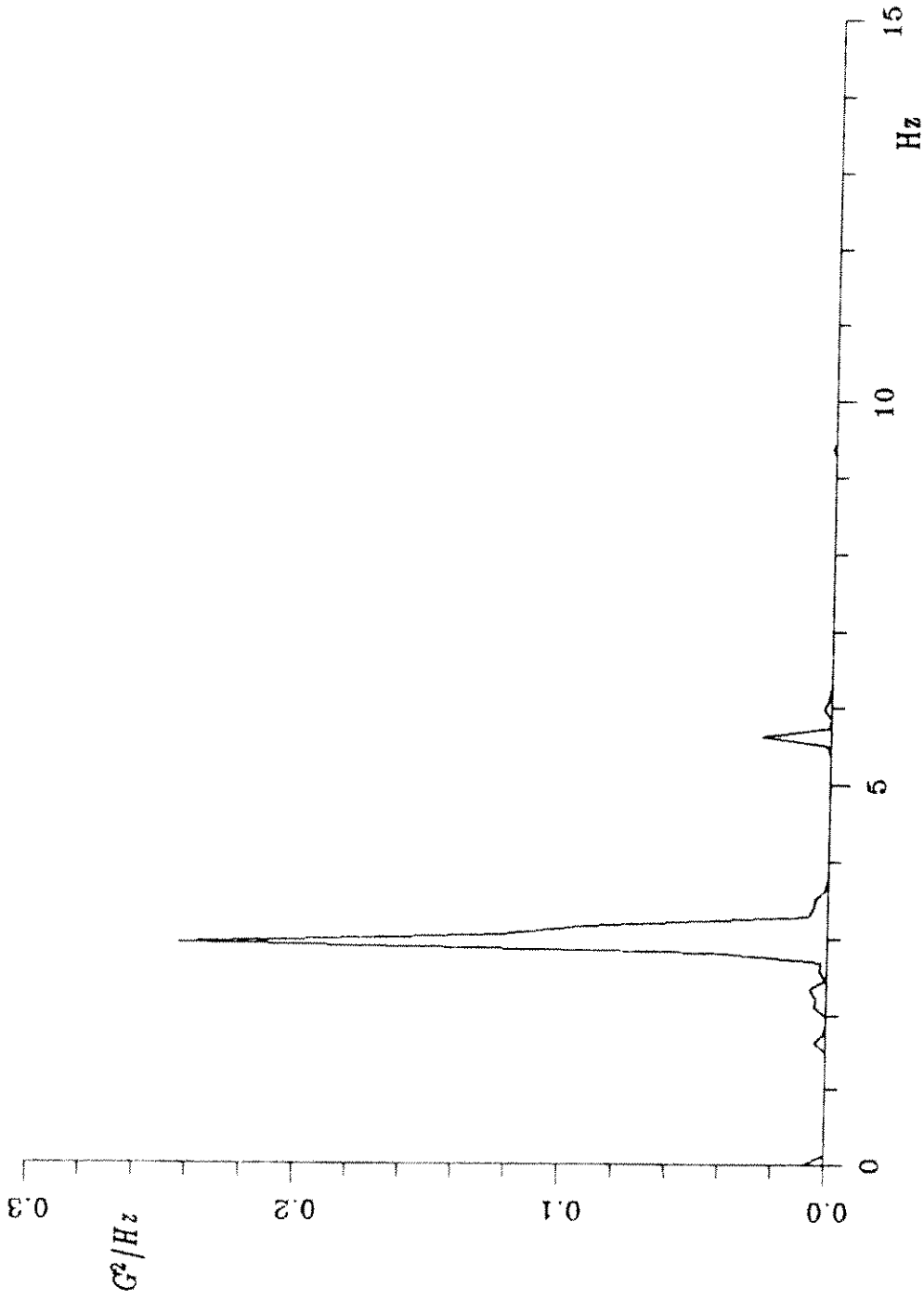


Fig. A.9 Cross-flow acceleration spectrum at L/4 (AH2)
:Triple helical, ref. vel. 1.56 ft/sec, additional low sheared high tension

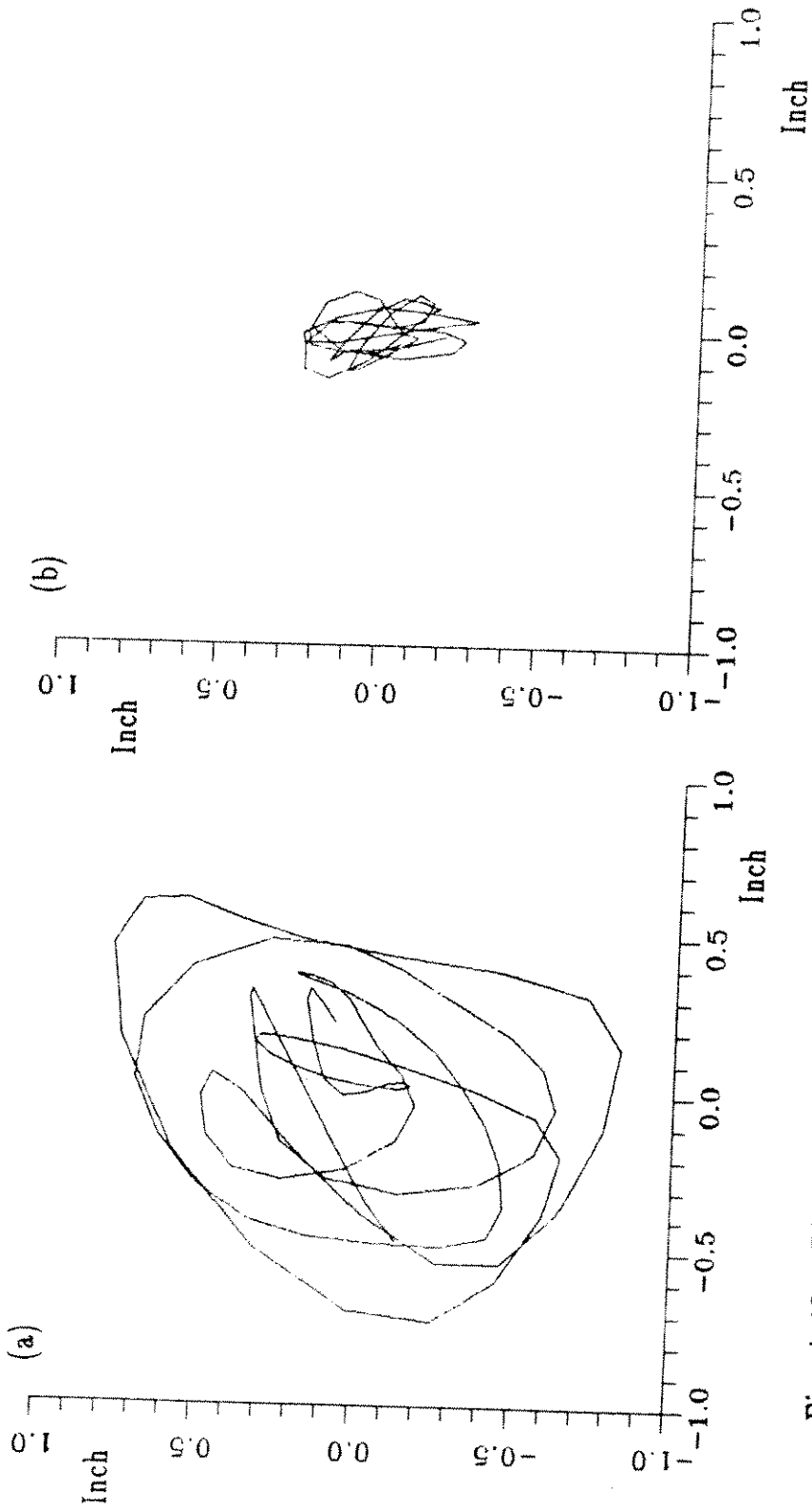


Fig. A.10 Displacement trajectories at L/4 (AL)

- (a) Bare cable, ref. vel. 1.05 ft/sec, additional low sheared low tension
- (b) Triple helical, ref. vel. 1.06 ft/sec, additional low sheared low tension

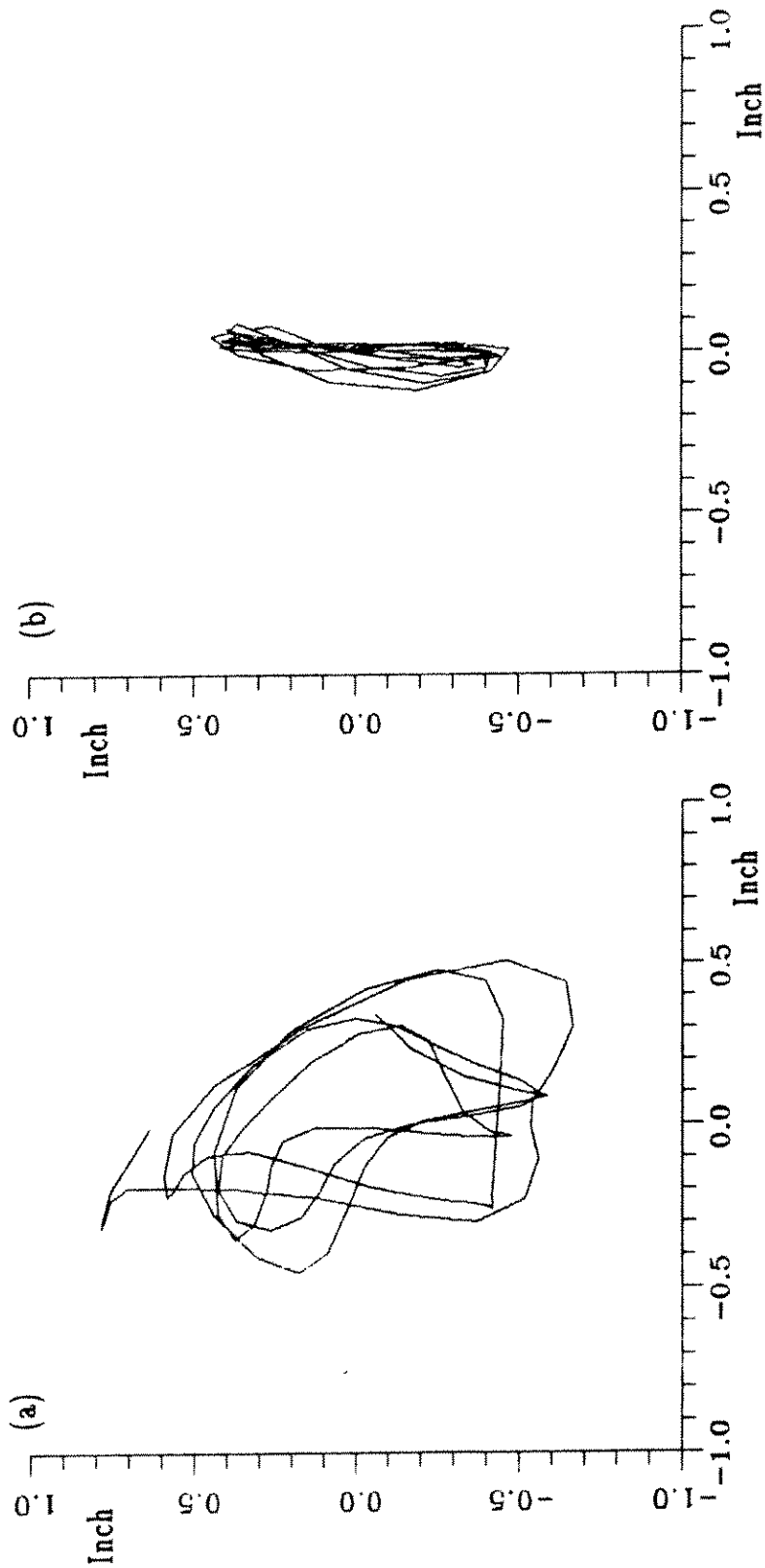


Fig. A.11 Displacement trajectories at L/4 (AH)
 (a) Bare cable, ref. vel. 1.54 ft/sec, additional low sheared high tension
 (b) Triple helical, ref. vel. 1.56 ft/sec, additional low sheared high tension

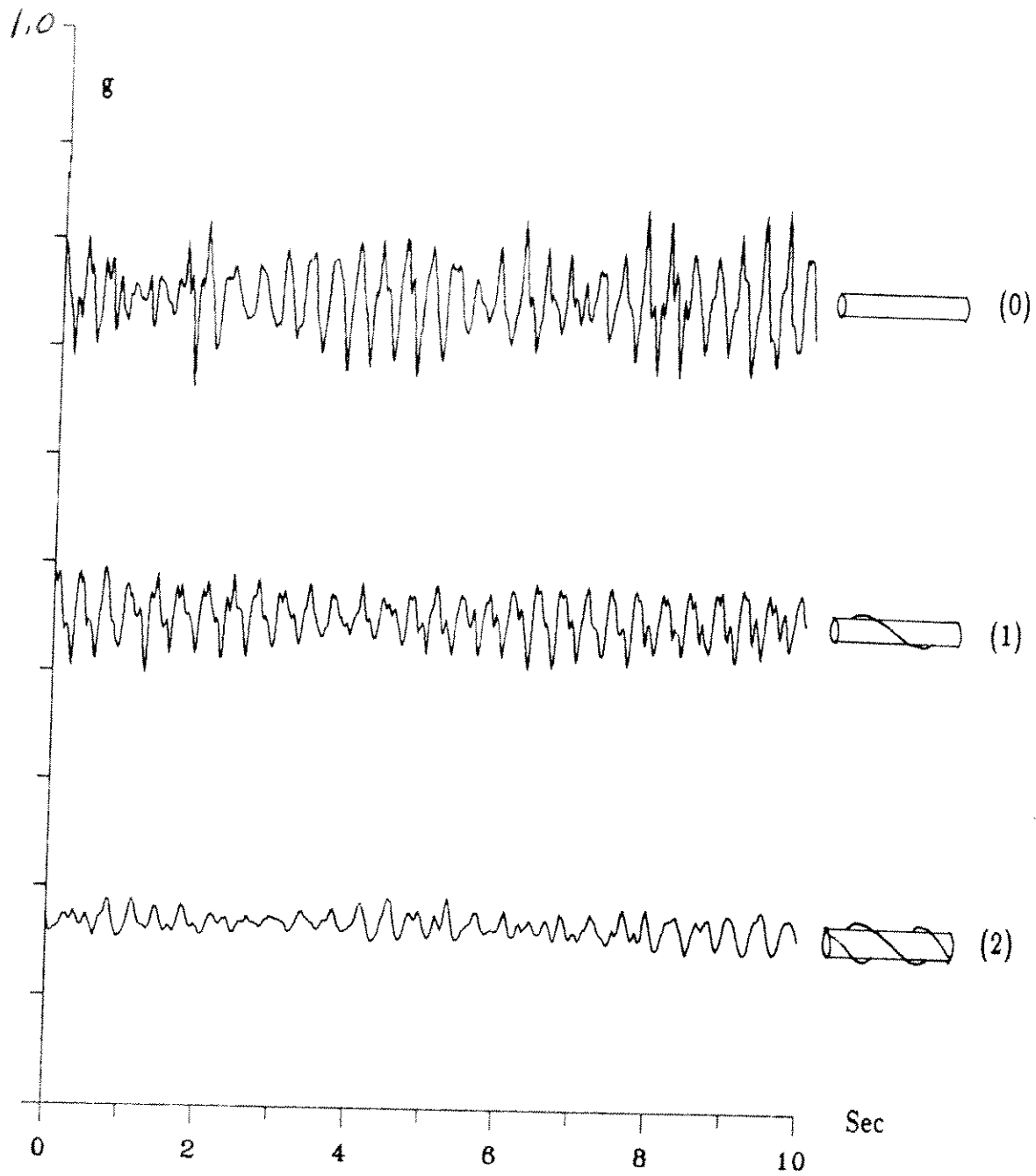


Fig. A.12 Time series cross-flow accel. signals at 13L/16
: Additional low sheared low tension

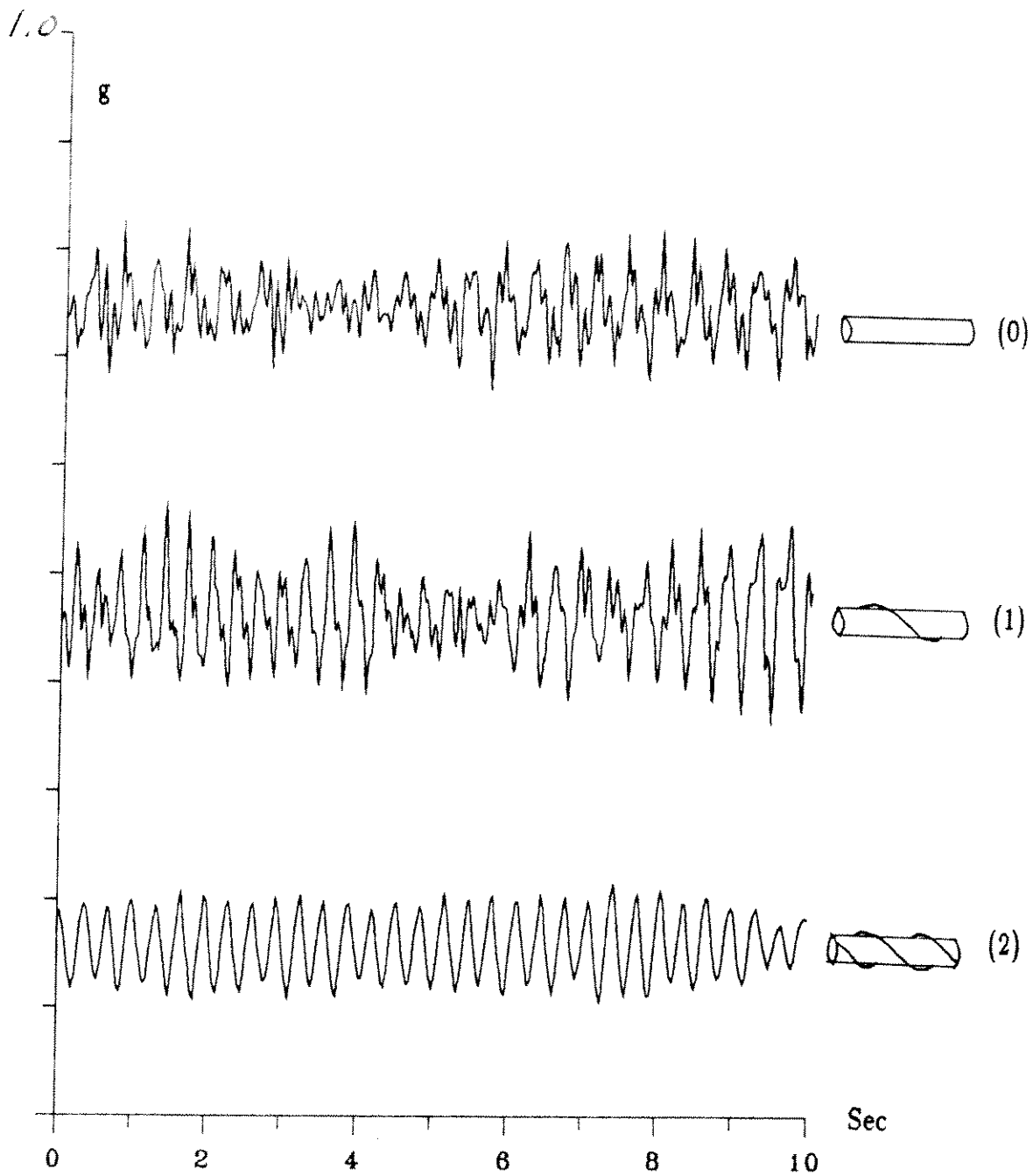


Fig. A.13 Time series cross-flow accel. signals at 13L/16
: Additional low sheared high tension

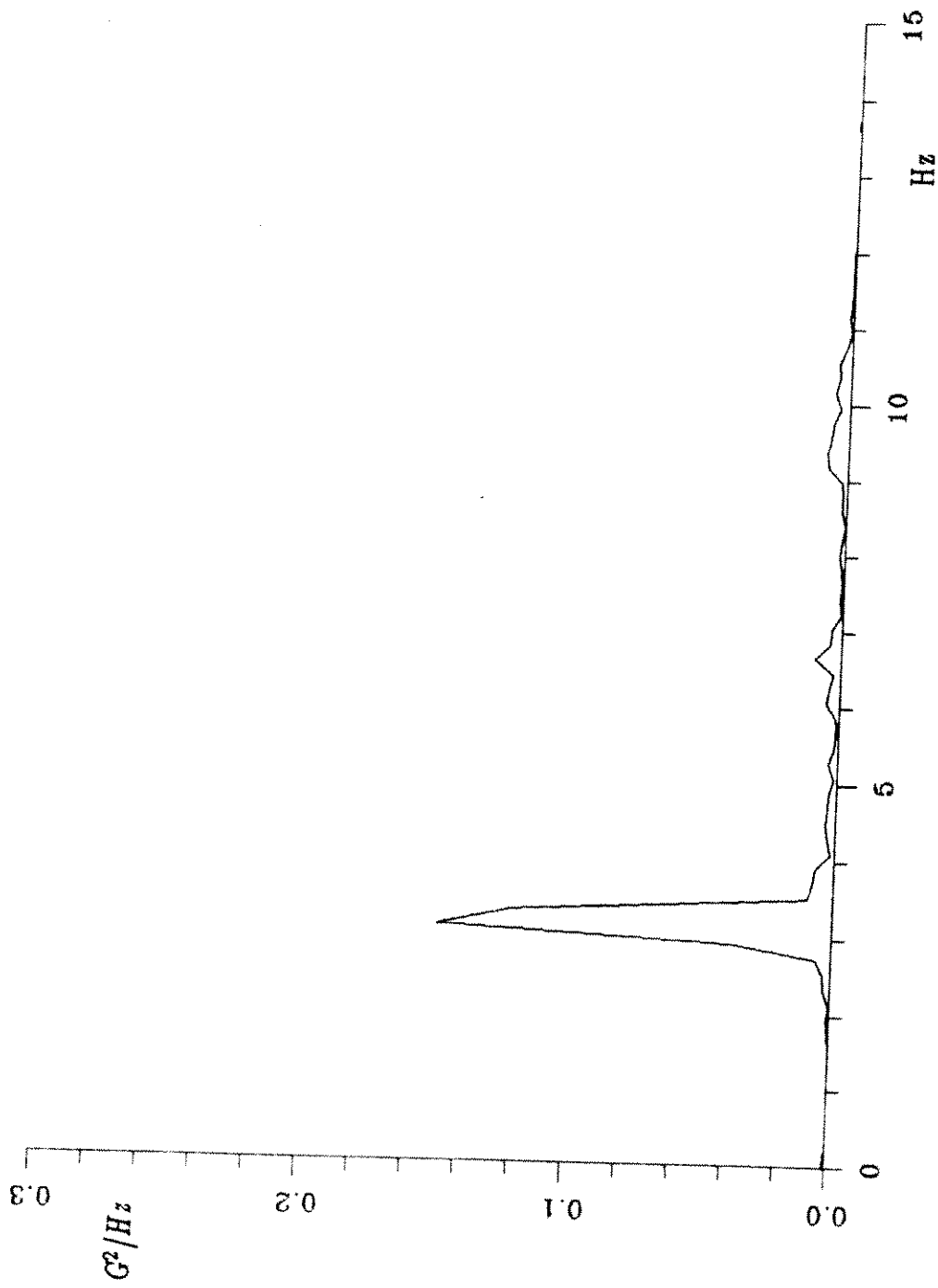


Fig. A.14 Cross-flow acceleration spectrum at 13L/16 (AL0)
 :Bare cable, ref. vel. 1.05 ft/sec, additional low sheared low tension

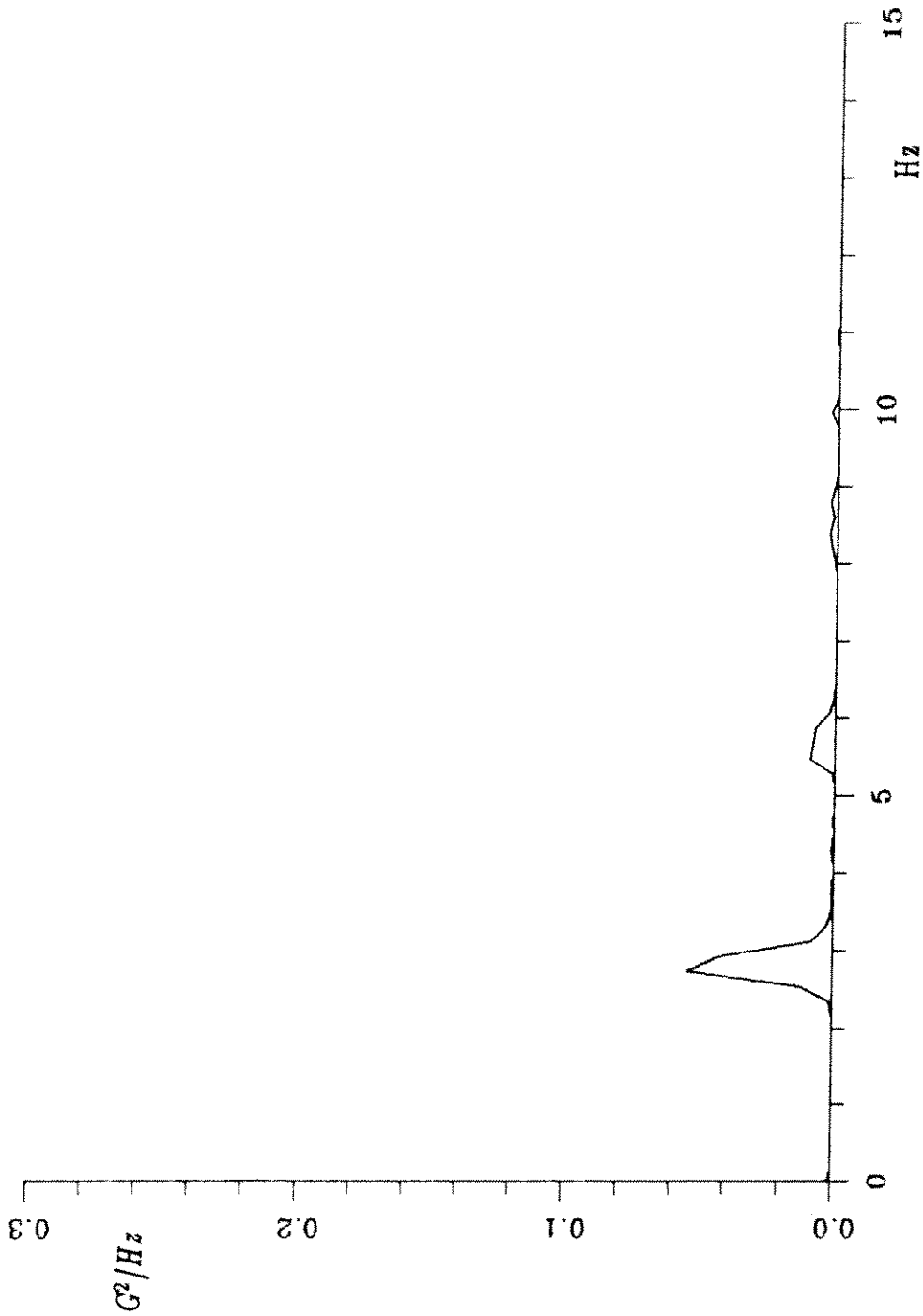


Fig. A.15 Cross-flow acceleration spectrum at 13L/16 (AL1)
:Single helical, ref. vel. 1.04 ft/sec, additional low sheared low tension

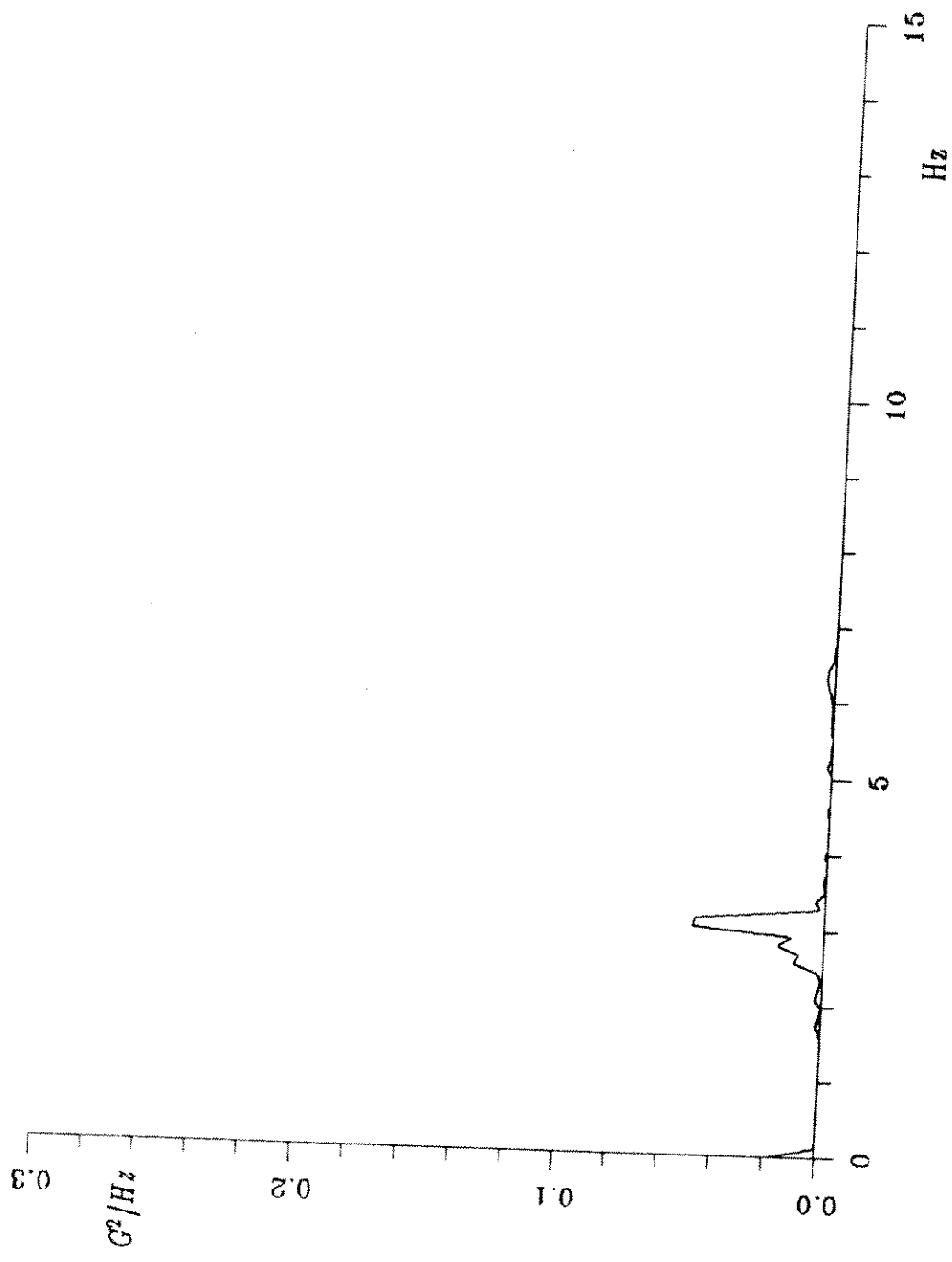


Fig. A.16 Cross-flow acceleration spectrum at 13L/16 (AL2)
 :Triple helical, ref. vel. 1.06 ft/sec, additional low sheared low tension

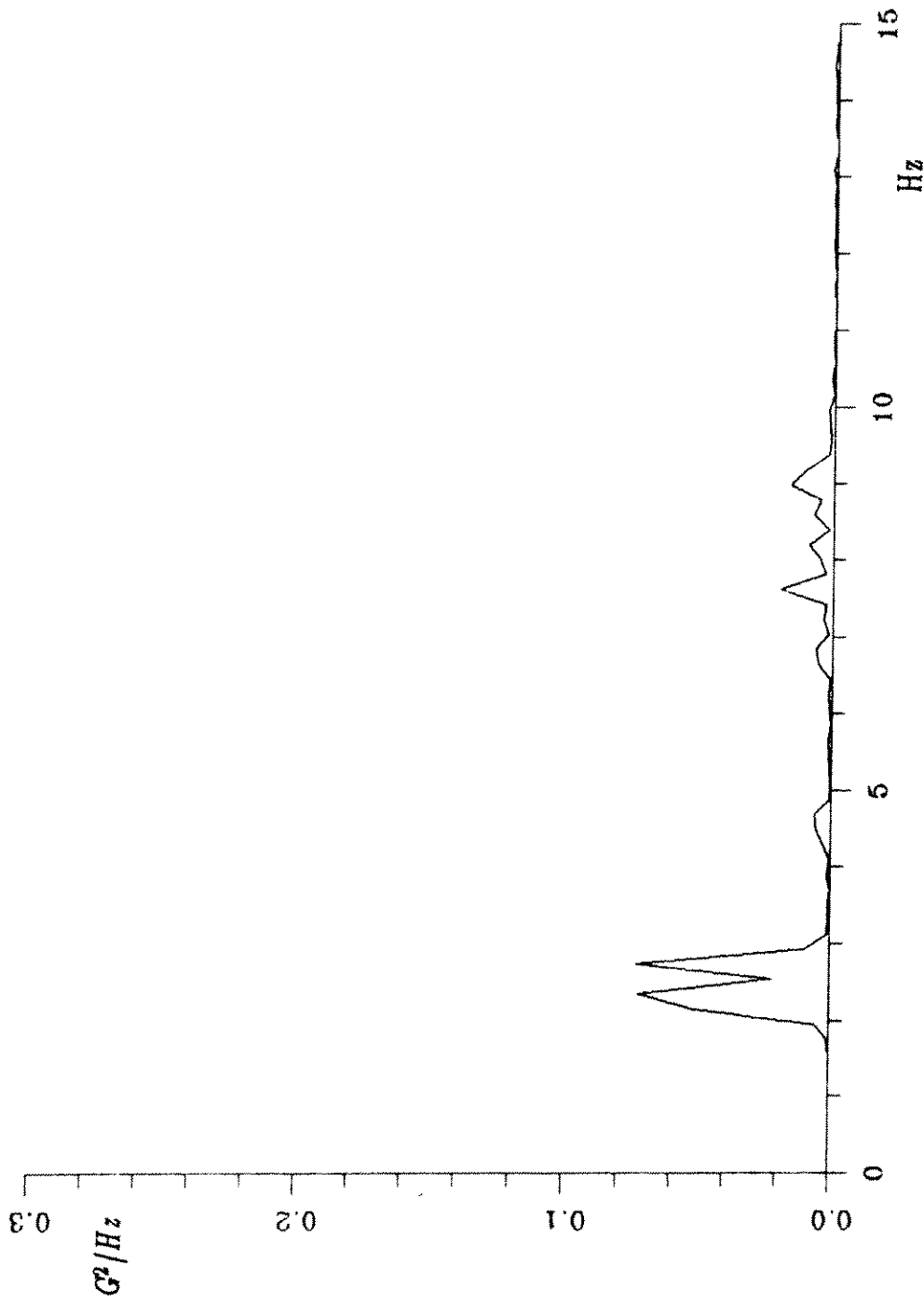


Fig. A.17 Cross-flow acceleration spectrum at 13L/16 (AH0)
:Bare cable, ref. vel. 1.54 ft/sec, additional low sheared high tension

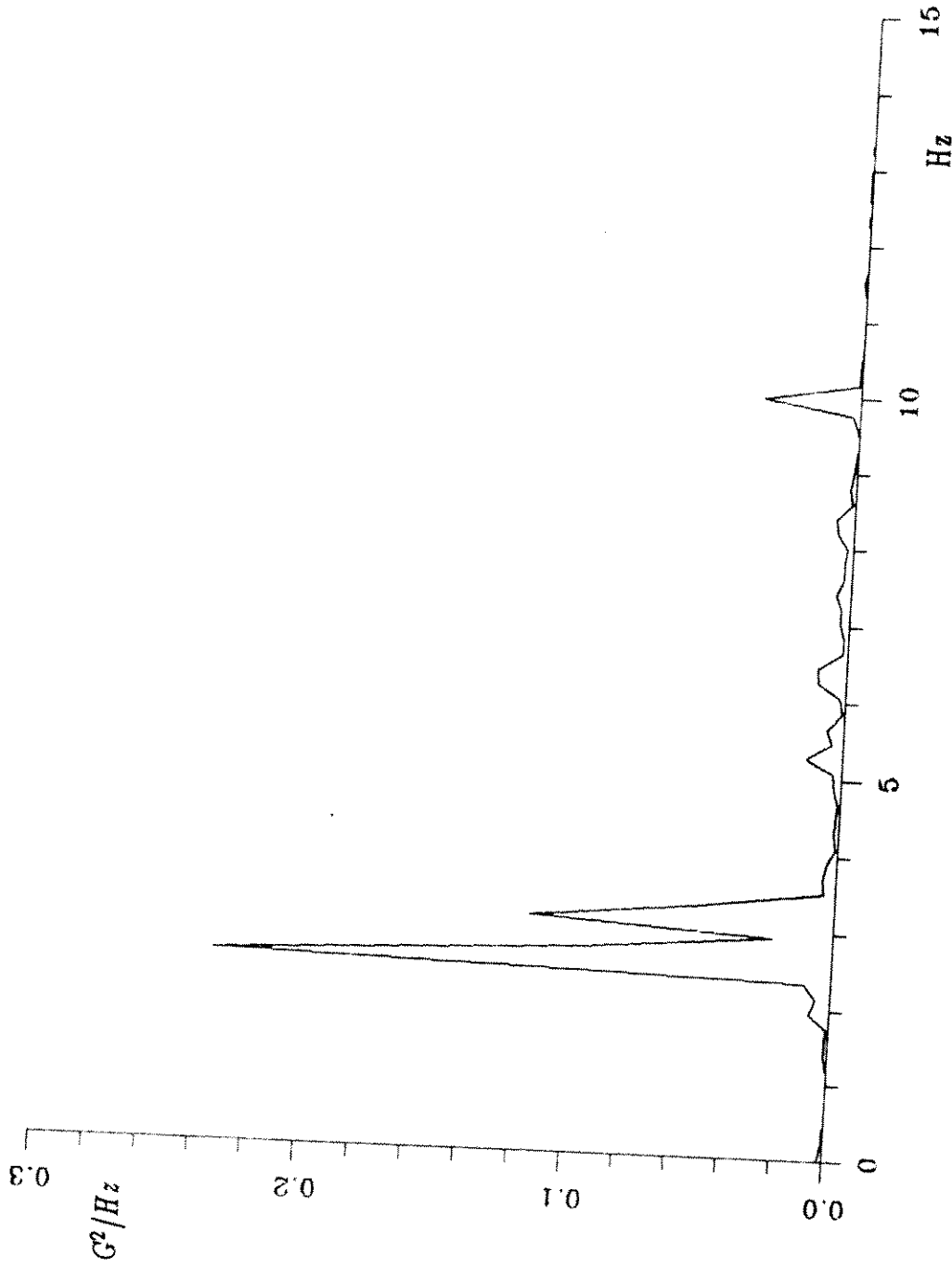


Fig. A.18 Cross-flow acceleration spectrum at 13L/16 (AH1)
:Single helical, ref. vel. 1.15 ft/sec, additional low sheared high tension

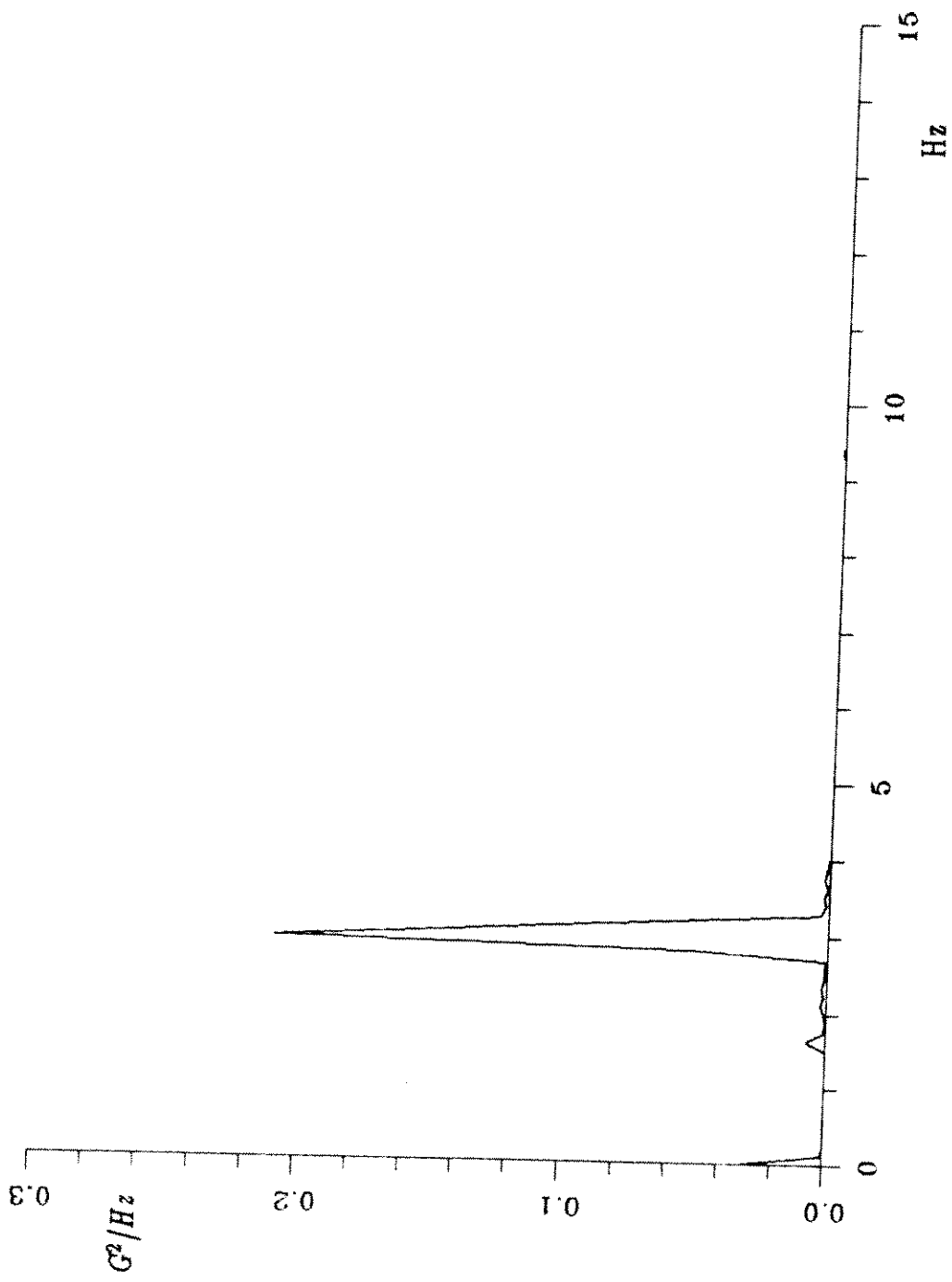


Fig. A.19 Cross-flow acceleration spectrum at 13L/16 (AH2)
 :Triple helical, ref. vel. 1.56 ft/sec, additional low sheared high tension